Valorisation of Thai biomass - Sustainable routes to porous materials and cellulose nanostructures

Jutarat Kavinchan

PhD

University of York

Chemistry

September 2023

Abstract

In this research, the valorisation of Thai biomass specifically rice husk and water hyacinth were used as renewable feedstocks into value-added products such as bio-derived porous materials, cellulose nanostructures for various applications, for example, adsorbents and reinforcing agent in bio-composite films preparation through sustainable routes is reported. Microwave-assisted method has been carried out for pretreatment step, synthesis step and extraction which offers many advantages; energy saving and rapid procedure for processing, where microwave heating is caused by the direct absorption of microwave energy by components of the material as the microwave passes through them.

A range of bio-derived high surface area porous materials include MCM-41, silica nanoparticles and MCM-41 magnetite composite materials were successfully prepared from rice husk as abundant agricultural waste in Thailand under mild conditions through microwave-assisted method with using silicate solution extracted from rice husk. These materials were also obtained from greener method that can be used as a promising material for methylene blue dye adsorption in aqueous solution. Both MCM-41 and MCM-41 magnetite composite materials exhibited type IV behavior, confirming that the products display mesoporous structure which have benefit for adsorption performance. It was found that all materials were fitted with pseudo-second order and Langmuir isotherm. The results also showed that MCM-41 magnetite composite material has the best removal rate of all materials (nearly 100% within an hour), while MCM-41 could remove more than 80% of MB (84.22%) and silica nanomaterial can only remove 65.50% of the methylene blue dye within 60 minutes. Moreover, a sustainable route for extraction of cellulose from water hyacinth to cellulose microfibrils/nanofibrils was carried out under microwave-assisted method without using harsh conditions. Bio-composite films reinforced with cellulose microfibrils/nanofibrils were successfully prepared which possess good mechanical properties (tensile strength) and optical properties for use as food and non-food packaging applications.

List of Contents

List of Tables

List of Figures

Acknowledgements

First of all, I would like to thank my supervisor, Dr. Duncan MacQuarrie for his suggestion and kind support for the opportunity to attend at conference in Germany.

I would like to give special thanks to my lab buddy for help, encouragement and support, especially when I felt like giving up.

I want to particularly thank Prof. Avtar Matharu for his suggestions as IPM. I would also like to thank Dr. Clare Steele-King for her invaluable help with SEM and TEM. Many thanks to technicians' team.

I would like to express my gratitude to the Royal Thai Government and the University of Phayao for PhD scholarship.

Finally, I would like to say thank you so much to my parents for their love and great support throughout of my life.

Declaration

I declare that this thesis is a presentation of original work and I am the sole author. This work has not previously been presented for a degree or other qualification at this University or elsewhere. All sources are acknowledged as references.

Parts of this research has been presented at the following conferences:

1. '7th Green & Sustainable Chemistry Conference', Dresden, Germany on 22/05/2023.
2. 'PhD Student Poster Presentation', University of York, Department of Chemistry, on 24/03/2022.

Chapter 1

Introduction

1.1 Contextualisation

Concerns regarding petroleum depletion and global warming because of climate change which caused by greenhouse gas emission have been great interest in renewable alternative resources rather than fossil fuels.[1,2] A continuously growing world population also need a significant amount food, energy and materials which could be fulfilled through the efficient use of sustainable resources. Nowadays, the world population is 8.1 billion, which is expected to be 9.7 billion by 2050.[3] Currently, crude petroleum is still used as the primary source of energy and materials, which is not renewable and the increasing of greenhouse gas emission, the main cause of climate change is caused by this production.[4,5] Thus, the requirement to find the sustainable alternative resources such as lignocellulosic biomass (agricultural residues, forestry wastes, and grasses, etc.) have shown the remarkable progress and could be the promising feedstocks for biorefinery to convert them to energy, value-added chemical and products.[6–8]

Agricultural wastes are byproducts, and abundantly available waste materials. For example, rice husks are byproducts of rice milling and rice straws are produced by harvesting of paddy, most of the produced rice husks and rice straws is directly disposed of by open field burning that can cause the air pollution.

Waste water hyacinths overgrowth in the river during the rainy season that can also cause the water pollution for other aquatic life by blocking out sun and depleting oxygen content.[9–12] Thus, proper utilization of biomasses that generally refers to agricultural wastes and their residues, food waste, animal waste and aquatic plants can bring immense benefits to both the environment and economy. [12-14]

The continued global development of economic activities is also linked to the increase of generated industrial and agricultural wastes, all of which require appropriate methods or treatments before discharge to natural resources. The water pollution caused by draining of heavy metals and dyes-containing industrial effluents, as well as the air pollution, from

burning of agricultural wastes in open field, have attracted the attention of researchers all over the world. These pollutants are toxic to humans and other living organisms and can cause serious health problems.[15-18] To solve these urgent problems, the utilization of waste materials and byproducts plays a vital role in developing better uses for biomass (avoiding burning) and also for waste water clean-up.

Thus, to explore the valorisation of waste biomass through the sustainable routes, the biorefineries are the sustainable processing of biomass into a wide range of value-added products, chemicals and materials coupled with the concepts of green chemistry and the United Nations (UN) Sustainable Development Goals (SDG) to create sustainable products which are practical steps towards a zero-waste production. Reducing waste not only benefits the environment but also offers numerous advantages for individuals and society as a whole. Additionally, these concepts and goals are blueprint, to combat the climate change by reducing carbon footprint, and to achieve a better and more sustainable future for all generations to come.

1.2 Biorefinery technologies

Biorefinery is defined as processing of biomass as feedstock is converted into a spectrum of value-added products to produce bioenergy, materials and chemicals.[12,19] There is a significant advantage over a petroleum refinery which has a negative effect for environment during the manufacturing processes. There are four generations of biorefineries based on types of feedstocks and the output products. The first generation of biorefineries commonly used crops as feedstocks such as corn or sugarcane to produce biofuels (e.g. bioethanol and biodiesel).[7,20] However, it was not providing sustainable renewable resources for widespread fuel and chemical production because direct competition with food production.[21] The second generation uses lignocellulosic biomass or residues such as agricultural residues, forestry residues and non-edible crops which are non-food competing feedstocks and the third generation considers the use of algae as feedstocks.[12,22,23] The fourth generation is based on the use of genetic engineering to

increase desired traits of organisms used in production.[22,24] In this thesis, agricultural waste and aquatic plant, including rice husk and water hyacinth which are lignocellulosic biomass and residues are used as feedstocks to design a sustainable biorefinery for conversion of agricultural waste into value-added products which will be described later (see 1.3).

1.2.1 Pretreatment step and fractionation

One of the most complicated methods for lignocellulosic biomass conversion is pretreatment step. In lignocellulosic biomass the cellulose is usually coated by hemicelluloses forming as cellulose-hemicellulose complex that can prevent the access of enzymes into the complex structure. Lignin is a complex three-dimensional polymer that acts as an adhesive to bind microfibrils and cross-link wall components.[25-27] Thus, lignocellulosic biomass requires pretreatment in order to remove lignin and hemicellulose, decrease the crystallinity of cellulose, and increase the surface area and porosity of the biomass, all of which makes it accessible to hydrolytic enzymes that further convert cellulose and hemicellulose into fermentable sugars.[28-30]

Fractionation or extraction of lignocellulosic biomass is a vital step where each biopolymer is separated and utilized. This for maximizes the use of different components in biomass, providing the wide spectrum of value-added chemicals.[31]

Generally, there are many different methods for biomass pretreatment which include physical, chemical, physicochemical as well as biological methods, each of which has different advantages and limitations in both technical and economic aspects that allow the different alteration of structural lignocellulosic material according to its further valorisation.[30] In the physical pretreatment step such as shredding and milling, the requirement of energy depends on the final particle size and the crystallinity of lignocellulosic biomass which usually require higher energy than other procedures. Chemical pretreatment which focused on delignification of biomass can decrease the

degree of polymerization and crystallinity of cellulose.[30] In the past decade, alkaline pretreatment has been mostly applied to remove lignin from biomass as well as to improve enzymatic digestibility of the pretreated biomass, however there are a few drawbacks, such as the release of toxic substances, equipment corrosion and the formation of byproducts such as phenol and furans during pretreatment, which inhibit the subsequent fermentation.[27,29,32,33]

Various approaches of fractionation based on chemical or thermal processes, or combinations of both have been investigated for separation of biomass components. Super-critical and near-critical water (namely hot compressed water; HCW or liquid hot water; LHW) is a hydrothermal method which is one of the promising approaches for fractionation. Compared to alkaline/acid pretreatment, HCW technique does not require rapid decompression, does not employ any catalyst or chemicals other than water as a green solvent. It is directly applicable to moist biomass, generates less inhibitory by-products, and can bring about selective hemicellulose elimination without cellulose destruction.[34] Pressure is applied to maintain water in the liquid state at elevated temperatures (160–240 ^{O}C). This process aims to solubilize mainly the hemicellulose, to make the cellulose more accessible and to avoid the formation of inhibitors.[35] During this stage, hemicellulose and lignin are solubilized and released into liquid phase while cellulose remains intact. Moreover, hot compressed water can operate at temperatures higher than 150 ^{O}C and pressures from 0.1 to 25 MPa., the superheated liquid water auto-ionizes into hydronium ions and hydroxide ions which act as a promoter for cleavage of ester bonds of acetyl side chains of hemicelluloses, which results in formation of acetic acid. This then leads to autocatalytic hydrolysis of the hemicellulose and alteration of lignin structure, leading to increased enzyme accessibility to the cellulose fibers.[36] Hence, it can be used for hydrolysis of lignocellulosic materials with advantages of environmental friendliness and simple reaction control and also dehydration of lignocellulosic biomass to produce sugars and furan compounds by addition of catalysts (e.g. WO_3–ZrO_2, TiO_2–ZrO_2, and MgO–ZrO_2).[37]

1.2.2 Thermochemical technology

1.2.2.1 Conventional pyrolysis

Conventional pyrolysis decomposes biomass in the absence of oxygen at temperatures between 300 and 900 °C, generating three primary products; solid (biochar), liquid (bio-oil) and gaseous products. The process conditions which include the downstream steps such as vapor condensation can affect the relative amount of solid, liquid, and gaseous products as well as the properties of bio-oil. Moreover, the feedstock characteristics play an important role in this process.[31] Conventional pyrolysis may also be termed slow pyrolysis, which has been mainly used for the production of char. Slow pyrolysis is characterized by a heating rate less than 10 °C/s and long residence times of gas and solids.[38] This is also named carbonisation, and is usually conducted at atmospheric pressures and temperatures higher than 450 °C to form char or pyrochar. When a slow pyrolysis reaction takes place at low temperatures (typically below 300 ^{O}C), it is known as torrefaction[39], a moderate thermal treatment at temperatures ranging from ~200 to 300 ^{O}C in an inert atmosphere, is used as a pretreatment to upgrade the quality of biomass fuel such as the heating value (energy density) and grindability before it is sent to bio-oil production, gasification or combustion processes.[40-42] Although, this conventional heating is dominant, but it was found that heat losses to the surroundings, non-selective heating and consuming rather high energy are disadvantages.

1.2.2.2 Conventional hydrothermal process

A hydrothermal process is a process that can use wet biomass directly, without prior dewatering. To decrease the use of hazardous and expensive chemicals, water could also be used as the reaction medium, which is environmentally benign, simple, and cost-effective. Starting with the hydrolysis, where the liquid medium reacts with extractives, cellulose or even hemicellulose, breaking ester and ether bonds to yield a variety of products types including oligosaccharides or soluble saccharides and monomers.[31] Hydrothermal carbonisation can change these derivatives to form hydrochar in the range

of 180–250 ^{O}C through further dehydration and condensation reactions.[39] Unlike conventional pyrolysis at higher temperature, hydrothermal carbonisation could be an attractive method to produce both solid and liquid products.[43] Hydrothermal liquefaction at the higher temperature range of 250-375 ^{O}C could produce bio-oil via further hydrolysis of macromolecules, dehydration/decarboxylation, and rearrangement reactions. This has been considered as an environmentally friendly process because all the carbon particulate, gaseous products and liquid fuels are kept in the closed system.[44] Hydrothermal gasification will generate syngas e.g. H_2, CH_4, CO, and light hydrocarbons through stream-reforming, water-gas shift, and methanation reactions which become prevalent as the temperature increases to more than 375 ^{O}C, over the critical point of water. These temperatures would mean a very specialized and expensive vessel and very high energy cost as well.

1.2.2.3 Conventional solvothermolysis

Solvothermolysis is extensively used regarding its relatively lower operating temperature when compared with pyrolysis which assists in the prevention of the formation of tar which normally results from cross-linking reactions.[45] In general, biomass liquefaction through solvothermolysis occurs at moderate conditions (100-200 ^{O}C) in the presence of base or acid catalysts, and the solvents such as ethanol, acetone, ethylene glycol, polyethylene glycol and phenol have been intensively investigated.[46] An increase of carbon content in bio-crude makes the heating value of bio-crude from hydro- or solvothermolysis liquefaction greater than that from pyrolysis. But there are several drawbacks from wastes management and energy consumption.

1.2.2.4 Microwave processing

Microwave heating has long been recognized to be an energy-efficient and rapid procedure for chemical processing, where microwave heating is caused by the direct absorption of microwave energy by components of the material as the microwave passes through them.[47] While dried feedstock is demanded in pyrolysis process, in microwave

pyrolysis this is less critical, and the pyrolysis is performed at lower temperature (180-300 ^{O}C), compared to the conventional pyrolysis (300-900 ^{O}C).[48,49] There is also less need to have a fine powder as MW provide volumetric heating. This saves a lot of energy as milling and etc. are not needed. Microwave hydrolysis is performed in an aqueous medium at a lower temperature (100–250 ^{O}C) compared to microwave pyrolysis which is undertaken between 180 ^{O}C and 300 ^{O}C. As they transform electromagnetic energy into thermal energy, microwave-assisted processes are more rapid and therefore enable shorter conversion times than those provided by conventional heating. [4,49]

1.2.3 Biochemical technology

A biochemical technology is a platform which converts carbohydrate of biomass into other forms of sugars, prior to conversion into other chemicals, for example ethanol and butanol through fermentation, from which high selectivity of products are generated. This approach also benefits from low processing temperature.[12] Typically, to increase the procedure efficiency, this approach normally requires a preprocessing step. Due to the complex structure of lignocellulosic biomass, the pretreatment step plays a crucial role as an early and necessary stage for obtaining potentially fermentable sugars in the hydrolysis step, to alter the recalcitrant structure of lignocellulosic biomass, break down the lignin structure, remove lignin and disrupt the crystalline structure of cellulose for enhancing enzymes accessibility to the cellulose during hydrolysis step.[50,51]

Enzymatic hydrolysis has been well established for decades, and has the advantages of high selectivity and mild operational conditions; nevertheless, the enzyme's cost and its rapid deactivation in the presence of inhibitors from prior chemical or thermal pretreatment steps are the major challenge for industrial implementation.[52] In order to increase the efficiency of enzymatic hydrolysis and subsequent sugar yield from complex lignocellulosic biomass, alkali-pretreatment causes modification of the physicochemical properties by removal of lignin and hemi-celluloses, reduction of cellulose crystallinity, and increased porosity of the materials.[53,54] To convert lignocellulosic biomass into sugar

forms and then convert to bioethanol and other chemicals, various microorganisms have been exploited for ethanol production. *S. cerevisiae* is a prime species that can be frequently used in laboratory and industrial scales because it can produce and tolerate high ethanol concentrations under the optimal condition.[55] The successful strategy to produce lignocellulolytic enzymes can be achieved through microorganism selection and improved fermentation conditions, including screening for effective lignocellulolytic enzyme-producing microbes and developing pre-treatments that alter the cellulose lattice structure and increase enzyme accessibility. Consequently, it is necessary to find the microorganisms that have a high rate of lignocellulolytic enzymes production.

1.3 Scope of Thesis

1.3.1 Project 1: Rice husk

Synthesis of bio-derived mesoporous materials from rice husk for methylene blue adsorption in aqueous solutions

Water quality is a significant concern, where surface water sources are polluted due to the improper discharged from major sources of pollution such as industrial waste and agricultural waste. Discharge of wastewater into rivers has contributed to the contamination of water sources.

To address the water pollution problem, it needs to develop an approach in the management of water resources. A number of strategies have been reported to remove these pollutants such as organic dyes, heavy metals and pesticides from water, including precipitation, coagulation, biological treatment, chemisorption filtration, ion-exchange, photocatalysis, and adsorption.[56-58] Among them, adsorption is commonly used for heavy metals and dyes removal from water because its low cost and simple.[59-63] Many kinds of low-cost biomass adsorbents offered outstanding performances for chemicals and heavy metals removal from water.[62,64-67] However, some of these materials have drawbacks such as weak interaction with metal ions and relatively low capacity.[68-71] Hence, there have been many interested to overcome these disadvantages, for example, the study of

developed porous materials that have been widely used for adsorption due to their large specific surface area and tunable pore sizes that can effectively adsorb metals or dyes on their pores and surfaces as well.[62,68-71]

Over a few decades, silica porous materials have grown significantly. MCM-41 is one of the most promising materials that has been used for various applications, including ion exchange, catalysis, biosensor, drug delivery and adsorption due to its highly uniform pore channels and high surface area.[72-74] Previously, these materials have been prepared by using chemicals as starting materials which have high toxicity that can effect for human health, for example, skin, eye and respiratory tract irritation and specific target organ toxicity (e.g. kidney) and are expensive such as tetraethylorthosilicate (TEOS) by using various methods, including hydrothermal route, solvothermal route and microwave-assisted synthesis for preparing porous materials.[75-78] Both conventional hydrothermal method and solvothermal route require a long reaction time and a high crystallization temperature, whereas microwave-assisted synthesis offers the advantages of homogeneous heating and fast elevation of the temperature of synthesis system to crystallization temperature, instead of the conduction and convection that occur with conventional heating - resulting in more homogeneous nucleation and shorter crystallization times.[79-81] Furthermore, microwave-assisted synthesis also has a lot of benefits: simple, inexpensive, precise control of the reaction, shape and size controlling and environmentally benign due to the significantly lower energy required due to the significant reduction in crystallisation.[82-85]

The high demand for porous silica materials with desired properties which the global market size was valued at USD 11029.22 million in 2022, is expect to expand and reaching USD 15547.42 million by 2028 has led to the development of greener synthesis procedures.[86,87] The most common green synthesis methods use biomasses like agricultural wastes such as rice husk and rice straw, which contributes to production cost reduction, improvement in the environmental problems, turning them into more attractive, valuable, and useful products.[88,89] So, this project will look at valorising Thai

biomass with a view to producing high surface area porous materials via a green method.[90,91]

Currently, many researchers report the extraction of silica from rice husk ash and rice straw ash for synthesis of mesoporous silica materials because the SiO_2 content in the rice husk ash was around 86 – 97% and in the rice straw ash, it was around 70-75%.[92,93] The silica is extracted by alkaline solution such as sodium hydroxide (NaOH) and sodium carbonate (Na_2CO_3) solution, to give an alkaline silicate solution.[94,95] This solution is then mixed with cetyltrimethyl ammomium bromide (CTAB) that is used as template under the optimum condition for synthesis, leading to the MCM-41 materials. These as-produced materials are then characterized.[23,94] Generally, a variety of techniques have been used for characterization of materials including X-ray diffraction (XRD), small-angle X-ray scattering technique (SAXS), scanning electron microscopy (SEM), transmission spectroscopy (TEM), Fourier transform infrared spectroscopy (FT-IR), Ultraviolet–visible spectroscopy (UV/Vis) and thermogravimetric analysis (TGA).[75,76,96]

In this research, the design of high surface area porous materials will be developed using various methods, particularly a “Green method” for enhancing their properties, with low cost, environmentally benign, rapid, less toxic substance releasing. Bio-derived silicate solution from rice husk was used as starting material for the synthesis of high surface area porous silica, MCM-41, and its composite via using microwave-assisted method for more energy saving, which also offer the advantage over the conventional heating because it is due to a sample is being heated up uniformly thus allowing for a faster, more efficient heating but also impacting chemical reactions which proceed more homogeneously and reveal increased reaction rates.[4,84,97] Therefore, the aim of this research project is to prepare high surface area porous materials derived from Thai biomass (e.g. rice husk) with enhanced performance through an economical and sustainable process for environmental remediation.[5,98] These porous materials will be assessed as adsorbents for water purification, specifically looking at toxic chemicals such as methylene blue from textile production.[70,99-101]

1.3.2 Project 2: Water hyacinth

Production of cellulose microfibrils/nanofibrils from water hyacinth for bio-composite films preparation

Cellulose is recognized as one of the most abundant biopolymers locally found in the plant-based fibers. Recently, the development of nano-structured cellulose, also known as nanocellulose, has received a great deal of interest due to its special and unique characteristics.[102-104] Due to nanofibers greatly possessing high toughness, great mechanical performances as well as high specific surface area, they have potential in a range of applications.[105] Basically, nanocellulose can be categorized into two main types: cellulose nanocrystals and nanofibers.[106-109] Nanocellulose can also be obtained from cellulose fibers through several treatment methods such as traditional treatment like a wet chemistry route with acids, conventional heating or/and enzymatic treatment. The production of nanocellulose has been produced by a two-step process.[110,111] In the first step, the pretreatment process of native cellulose biomass is done which yields treated cellulose fibers.[111,112] While in the second step, pretreated cellulose fibers are converted into nanocellulose using various routes, for example, acid hydrolysis, high-pressure homogenisation, micro grinding, micro fluidization, high intensity ultra-sonication, electrospinning, and steam explosion.[11,113-116] Cellulose nanofibers demonstrate the entangled networks with high aspect ratio which are typically composed of structurally ordered aggregates of elementary fibers having a diameter less than 100 nm and a length up to several micrometers.[11,117] Cellulose nanofibers have now emerged as a promising candidate for use in many potential applications such as packaging films, food stabilizer, coating materials, and reinforcing fillers.[118-123]

Practically, there are several mechanical isolation technologies usually employed to isolate nanocellulose from various biomass feedstocks, for example, ultrasonication, high-pressure homogenizer and etc.[124,125] Cryocrushing is used to isolate the fine cellulose nanofibers from micron-sized fibers. The bleach fibers in the form of an aqueous

suspension are immediately frozen by liquid nitrogen and subsequently crushed by simultaneous shear and impact forces using either motor or mechanical forces in order to release the individual nanofibers.[126] In addition, high intensity ultrasonication applying a frequency of 20-50 kHz is widely utilized to disrupt the cell wall of plants in which the elementary nanofibers are tightly embedded. Based on its actions, the ultrasonication typically generates the ultrasound waves producing cavitation bubbles, high pressure, hydromechanical forces which are transferred directly to the swollen fibers, thus facilitating cellulose defibrillation.[12,127,128] Furthermore, high-pressure homogenizer is one of the most practical techniques also used to isolate the fine cellulose nanofibers from micron-sized fibers, which the aqueous suspension was defibrillated continuously through an integration chamber to meet high shear and impact forces, resulting in ease of scale-up production.[113,124,129,130]

Over the last decades, cellulose nanofibers have been isolated from a variety of sources, for example, woods, crops, and agricultural wastes. However, fewer studies have been greatly interested in aquatic weeds such as water hyacinth which is commonly found in river or canal.[9,11,117] Water hyacinth is a rapid growth weed that has significant negative impacts on eco-systems, so it has been considered as an invasive aquatic plant in Asia since 1902. In addition, water hyacinth is composed of high cellulose content, which is approximately 60 wt%, compared to other plants (corncob (~45%), bamboo (~47%), sugarcane bagasses (~40-50%), etc.).[131-135] The dried water hyacinth mainly comprises low lignin (3-7%) and high amount of cellulose (19-60%) and hemicellulose (29–40%), which can be easily hydrolyzed to reducing sugars and then fermented to bioethanol by effective yeasts. [9,136] Due to its abundant availability and high carbohydrate contents, water hyacinth highly satisfies the requirements as a potential substrate for bioethanol production and value-added chemicals as well.[50,105] Furthermore, a process for cellulose nanocrystals production from water hyacinth would also be of interest in various applications such as biomedical applications, flexible electronics photodetectors, water treatment, etc.[116,137-139] In this project, the design of greener method will be developed

for cellulose nanocrystals production from water hyacinth and enhancing their properties with a low cost for various applications.[118,140-143]

In this study, a design route for extraction cellulose from water hyacinth to cellulose microfibrils/nanofibrils has been developed using various methods, focusing on developing a "Greener route" for enhancing their properties. Microwave-assisted hydrothermal pretreatment method was used to provide defibrillated celluloses for more energy saving and rapid reaction time without using any chemicals was studied. Moreover, various pretreatment methods with mild conditions include the alkaline-pretreatment, bleaching step (chlorine and chlorine-free bleaching method), and acid hydrolysis were also investigated. Therefore, the aim of this research project is to produce cellulose microfibrils and nanocelluloses from water hyacinth with low cost alongwith an attempt to develop a greener procedure for production of cellulose microfibrils/nanofibrils materials using mild conditions for applications such as films preparation for food packaging. Attempts have been made to improve the mechanical properties of bio-composite films.[121,144]

1.4 Research Aims

1.4.1 Aims of project 1: Synthesis of bio-derived mesoporous materials from rice husk for methylene blue adsorption in aqueous solutions

1. To produce bioderived adsorbents from rice husk (Thai biomass) with low cost for application
2. To develop a greener procedure for synthesis of high surface area porous material
3. To study the mechanism of methylene blue adsorption, adsorption kinetics, adsorption isotherms and thermodynamic parameters

1.4.2 Aims of project 2: Production of cellulose microfibrils/nanofibrils from water hyacinth for bio-composite films preparation

1. To produce cellulose microfibrils and cellulose nanofibrils from water hyacinth (Thai biomass) with low cost
2. To characterise cellulose microfibrils and cellulose nanofibrils materials
3. To study the application for bio-composite films preparation and and improve their properties

1.5 Green Chemistry and the United Nations (UN) Sustainable Development Goals (SDG)

Comprehensive assessment of a process or product's sustainability (or "greenness") requires quantifying environmental and human health impacts. To move towards sustainability, it is necessary to consider by the twelve principles of green chemistry which were developed by Paul Anastas and John Warner (1998), which are based on the minimization or non-use of toxic solvents in chemical processes and analyzes, as well as, the non-generation of residues from these processes.[145] These represent an early conception of what would make greener chemical, process, or product.

The principles are as follows:

1. Prevention:
   Prevention of waste generation is better than clean up or to treat waste after it has been creatred.
2. Atom Economy:
   Synthetic methods should be designed for maximisation of resource efficiency, with minimisation of chemical use not incorporated into the final product.
3. Less Hazardous Chemical Syntheses:
   Wherever practicable, synthetic steps should be taken to use chemicals with little or no toxicity to human health and the environment.
4. Designing Safer Chemicals:

Chemical products should have minimal toxicity whilst satisfying their chemical/material requirements.

5. Safer Solvents and Auxiliaries:

   The use of auxiliary substances (e.g., solvents, separation agents, etc.) should be made unnecessary wherever possible and innocuous when used.

6. Design for Energy Efficiency:

   Energy requirements should be minimized, reducing environmental impact and improving economic viability. If possible, synthetic methods should be conducted at ambient temperature and pressure.

7. Use of Renewables. Feedstock should be renewable rather than depleting at whatever time technically and economically practicable.

8. Reduce Derivatives:

   Unnecessary derivatization (use of blocking group, protection/deprotection, temporary modification of chemical/physical processes) should be minimized or avoided if possible, as such steps necessitate additional reagents and can produce waste.

9. Catalysis:

   Catalytic reagents are superior to stoichiometric reagents.

10. Design for Degradation:

    Chemical products should be designed so that at the end of their function they break down into innocuous degradation products and do not persist in the environment.

11. Real-time analysis for Pollution Prevention:

    Analytical methodologies need to be developed to allow for real-time, in-process monitoring and control prior to the formation of hazardous substances.

12. Inherently Safer Chemistry for Accident Prevention:

    Substances and the form of a substance used in a chemical process should be chosen to reduce the potential for chemical accidents, together with releases, explosions, and fires.

Nowadays, we all face big challenges in the modern world. The 2030 Agenda for Sustainable Development, adopted by all United Nations Member States in 2015, provides a shared blueprint for peace and prosperity for people and the planet, now and into the future. An urgent call for action by all countries include developed and developing countries- in a global partnership which recognized to end poverty and other deprivations must go hand-in-hand with strategies that improve health and education, reduce inequality, and spur economic growth – all while tackling climate change and working to preserve our oceans and forests.[146]

It is very important that we need to achieve goals for improving sustainability by the combination of green chemistry principles with the UN SDGs which focus on the targets to fight with the urgent global problems especially for the climate change.[146] There are the 17 Sustainable Development Goals (SDGs) which offer the most practical and effective pathway to tackle the causes of poverty, violent conflict, human rights abuses, climate change and environmental degradation as can be summarized in **Fig. 1**.

Fig. 1 The list of 17 Sustainable Development Goals

Many SDGs goals may be linked to green chemistry principles, for example, SDG6 (Clean water and sanitation) which is closest as using a greener procedure for synthesis of high surface area porous material for methylene blue adsorption (which is toxic substance in textile industries). As we know that water scarcity remains a concern in many parts of the world. Agriculture and untreated wastewater are major threats to water quality. Efforts are needed to improve farming practices and wastewater treatment, especially in regions with high population growth. So wastes water treatment is one of the keys for to get Goal 6 which also linked with waste prevention (principle 1, waste prevention).

SDG12 (Responsible consumption and production) which relating to implement policies that support a shift towards sustainable practices and decouple economic growth from resource use and to shift towards a more sustainable and circular approach to consumption and production. This goal may link with many green chemistry principles include 3 (Avoid hazardous substances), 4 (Designing Safer Chemicals), 5 (Safer Solvents), 6 (Energy Efficiency), 7 (Use of renewable feedstocks) and 10 (Biodegradation). These green chemistry principles were taken out into consideration throughout the whole thesis which will be discussed later. In addition, SDG14 (Life below water) that can be linked with the aim of project 2 which using water hyacinth for production of cellulose microfibrils/ cellulose nanofibrils. Because these blooms of water hyacinths lead to oxygen depletion resulted in the negative effects for ecosystems, local communities, fisheries and tourism.

It is necessary to note that the scope of these green chemistry principles go beyond concerns over hazards from chemical toxicity and include energy conservation, waste reduction, and life cycle considerations, for example, the use of more sustainable or renewable feedstocks (rice husk and water hyacinth) and designing for end of life or the final disposal of the product. In this project, waste biomass (rice husk) was used as starting materials for synthesis of the high surface area porous materials and water hyacinth was used for production of cellulose microfibrils/nanofibrils via a greener method such as microwave-assisted method and to develop a procedure for synthesis these materials and

also a production of cellulose microfibrils/nanofibrils by using chemicals with little or no toxicity to the environment under the microwave-assisted method that it is environmentally benign due to much reduced energy requirements. Moreover, this study was not only the use of renewable feedstock but also environmentally and economically practicable.

Generally, lignocellulosic biomass including agricultural byproducts and weeds in Thailand are abundant which offer a suitable feedstock for biorefinery. Green and sustainable integrated biorefinery will play a crucial role in this century for utilisation of these residues to convert into a range of value-added products such as alternative or sustainable materials like high surface area mesoporous materials and bio-composite films in this research. Efficient pretreatment or fractionation which is a prior step for breakdown and further conversion of lignocellulosic biomass into value products remain one of the biggest challenges in biorefineries.

Several technologies including pretreatment/fractionation, thermochemical and biochemical technologies have been used for many decades, each of them has different advantages and limitations in both technical and economic perspectives as well as the environmental impact. In the conventional method, the use of organic solvents and toxic chemicals for processing still need to be addressed. The major key challenges to the success of sustainable biorefineries are development of processes to maximise biomass conversion efficiency and minimize waste (close-to-zero-waste), combined with using an alternative greener approach (microwave-assisted method) or either greener chemicals (deionized water or mild condition) for conversion of unvalued wastes into a range of valuable products that should be fulfilled for an integrated biorefinery to be highly successful in the future.

1.6 Lignocellulosic biomass

Cellulose is one of the main constituents of lignocellulosic biomass, is usually a polysaccharide chain of D-glucose linked by β-(1, 4)-glycosidic bonds (**Fig. 2**), in which

every monomer unit is corkscrewed at 180^{O} compared to its neighbors.[147,148] Cellulose fibers are linked together by a number of hydrogen bonds- resulting in its insolubility in water and organic solvents.[149] The generated cellobiose units are linked together to produce a crystalline structure of cellulose known as elementary fibrils.[150,151] These latter are bundled together to produce micro-fibrils, which in turn formed macro-fibrils or cellulosic fibers. The intra- and intermolecular chemical groups impart cellulose its specific properties such as hydrophilicity, chirality, ease of chemical functionalization, insolubility in most aqueous solvents, and infusibility. Cellulosic chains have a degree of polymerization of ~10000 AGUs and 15000 units, in wood- and cotton-derived cellulose, respectively.[48,152]

Cellulose characteristics are closely dependent on the degree of polymerization as well as the polymeric chain length. Typically, native cellulose is composed of both ordered (crystalline) and disordered (amorphous) domains.[129,153] Its crystallinity depending on the natural source as well as the extraction process. The amorphous regions have low density compared to the crystalline ones and are prone to react with other molecular groups.[154] In addition, cellulose has relatively high strength, high stiffness, low density, and good thermal stability. Therefore, it is a promising candidate for reinforcing biocomposites.[124,155]

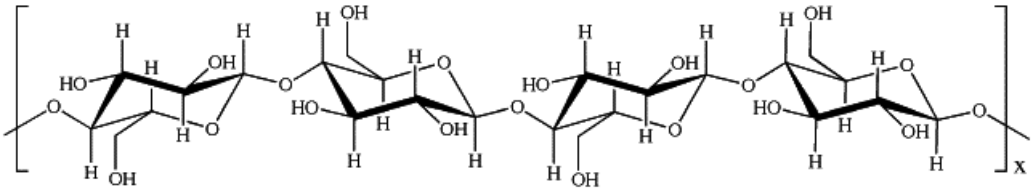

Fig. 2 Cellulose structure repeating β (1,4)-bound D-glucopyranosyl units

Hemicellulose (Fig. 3) consists of branched chains of polymers including, pentoses, hexoses and sugar acids. Hemicellulose includes some important monomer which are

glucose, xylose, mannose, galactose, arabinose, and glucuronic acid. Hemicelluloses are also sugar polymers. Unlike cellulose, which is made only from glucose, hemicelluloses consist of glucose and several other water-soluble sugars produced during photosynthesis. Unlike cellulose, these monosaccharides include pentoses (xylose, rhamnose, and arabinose), hexoses (glucose, mannose, and galactose), and uronic acids (i.e., 4-o-methylglucuronic, D-glucuronic, and D-galactouronic acids. In hemicelluloses the degree of polymerisation is lower – they are composed of shorter molecules than cellulose. This coupled with their less regular structure and branching makes them much more easily hydrolysable.[141,156-159]

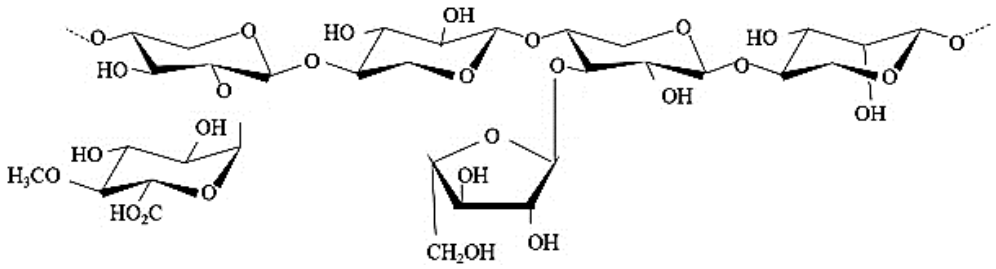

Fig. 3 Hemicellulose structure

Lignin is a polyphenolic material and one of the main components in the plant cell wall. Typically, lignin from various types of biomasses consists of three aromatic alcohols: p-coumaryl alcohol, coniferyl alcohol, and sinapyl alcohol.[87,160,161] Phenoxyl radials generated from these three monolignols (Fig. 4) are randomly polymerized to produce a biopolymer with a three-dimensional network. The proportion of aromatic alcohols depends considerably from species to species, particularly with regard to the type and quantity of linkages in polymer and the number of methoxy groups present on the aromatic rings.[162-164]

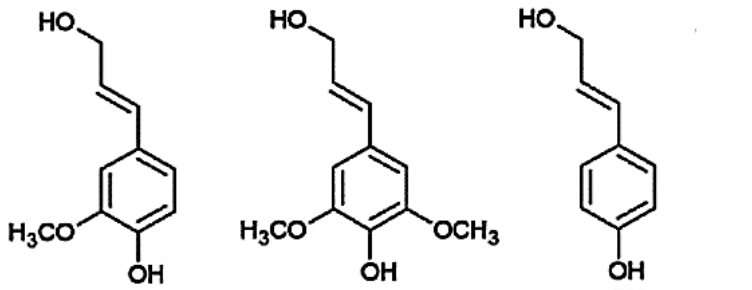

Fig. 4 Lignin is being formed by the oxidative polymerization of three main monolignols (coniferyl alcohol, sinapyl alcohol and p-coumaryl alcohol)

1.6.1 Rice husk

Rice (*Oryza sativa*) is currently the world's second most vital staple food crop particularly in Asia, after wheat. Rice husk is the main byproduct of industrial processing of rice, and is a widely used byproduct as biomass in energy production.[165-167] A large amount of biomass from rice is generated worldwide, particularly in the major rice production countries in Asia such as China, India, Vietnam, Indonesia and Thailand.[168-170]

Rice husk is generated at around 0.20-0.33 ton per ton of rice harvested which imply that 20-33% of rice husk is a by-product produced during the dehusking process at rice milling sites.[171,172] Rice husk (RH), which is a byproduct of rice milling, has received specific attention owing to its abundance, around 120 million tons of which is produced annually.[89,173] Rice husk consists of cellulose, lignin and silica the concentration of cellulose ranges from 35-50 wt% and silica ranges from 15-28 wt%, respectively.[172,174] Rice husk has a high ash content, ranging from 10-20% is predominantly composed of 87-97 wt% silica, which has a very high surface area, is highly porous and lightweight that can offer it valuable for industrial use.[95,174] The valorisation of rice husk to produce bioenergy with substantially lower CO_2 emissions as well as silica or bio-derived chemicals could be sold at higher unit prices have been more interested due to silica has a wide range of

industrial applications such as a filler for coatings, reinforcing agent in rubber and plastic and sodium silicate solution extracted from rice husk can be used as a precursor for Si-based materials.[174-176] Insufficient modes of treatment and management of rice husk has created an intensive interest amongst researchers to study it for technological and scientific interventions.[172,177-179]

1.6.2 Water hyacinth

Water hyacinth (*Eichhornia crassipes*) is a tropical monocotyledonous aquatic species of the Pontederiaceae family (pickerelweeds) that is native to the Amazon region of Brazil and Ecuador.[9,117] Water hyacinth is listed as one of the world's most invasive and recalcitrant weeds because of its availability in huge quantities, extraordinary adaptive ability, and remarkable growth rate. It is a type of lignocellulosic biomass whose cellulose content is as much as 60%, followed by 17% for lignin, 8% for hemicellulose, and 15% for other impurities.[10,180] Typical structure and characteristics of water hyacinth can be seen in Fig. 5.

The water hyacinth population has become a national issue in Thailand because it blocks waterways and also has a negative impact on biodiversity in rivers and lakes, and each year, the Thai government spends a large amount of money to solve this problem.[9,11,180,181] After it is gathered from areas of open water, water hyacinth typically ends up in landfill or is used as a fertilizer or animal food. Generally, natural fibers consist of cellulose, hemicellulose, and lignin. Lignin and hemicellulose are amorphous while cellulose is semicrystalline.[9,113,117,182] As in other aquatic plants, water hyacinth requires less lignin to stiffen its body, and the less availability of lignin in its cell walls is the main characteristic of its evolution from a terrestrial to an aquatic existence.[9,27] The high cellulose content from water hyacinth means that it could be an economically viable feedstock for cellulose nanocrystals.[131,139,181]

In addition, the use of water hyacinth as the feedstock adds economic value to the plant while tackling the waterway clogging problems.[11,116]

(a) (b)

Fig. 5 (a) Water hyacinth (Eichhornia crassipes)[183] (b) dried water hyacinth stems

1.7 Production of high surface area porous materials

High surface area porous materials have received considerable attention in many areas due to their unique physical and chemical properties as well as their applications in various fields such as waste removal, degradation of different pollutants such as dyes and toxic metals, catalyst and catalyst support.[184-186] Additionally, mesoporous silica nanomaterials gained a raised interest, due to its extensive multi-functionality, based on its high specific surface, uniform and tunable pore size, high pore volume, and facile functionalization.[68,94,100] In this research, high surface area porous material will be studied for application.

1.7.1 MCM-41

The Mobil Composition of Matter No. 41 (MCM-41) material has a hexagonal-ordered structure with mesopores with sizes of 3–5 nm and possess the high surface area of 1000 m^2/g as well as having a relatively high pore volume. These properties, along with the fact that the pores are generally straight, with little curvature, give it excellent mass transport properties, making it a promising material for application especially for adsorption.[187-189]

The preparation of MCM-41 was first reported by scientists of the Mobil Company in 1992 which is about the project of the company to find materials with pores larger than that presented by zeolites.[190,191] The synthesis of the MCM-41 involves few processes and the resulting structure of the material significantly depends on the conditions, for example, the type of silica precursor, the ratio of cetyltrimethyl ammomium bromide (CTAB)/Si and the reaction time and type of hydrothermal treatment step.[191-195] Typically, the synthesis of MCM-41 is based on the condensation of silica precursors, typically sodium silicate or tetraethylorthosilicate (TEOS), in the presence of cationic surfactants under basic conditions. The standard preparation of MCM-41 consists of mixing a silicate precursor, usually TEOS, with a cationic surfactant i.e., a CTAB at pH=11.[196,197]

In the first stage, the hydrolysis of the alkoxide takes place. The cationic surface is present in the form of cylindrical micelles, and its positive head group attracts the negative charges of the silica species, which are thus concentrated around the micelles forming a tubular array of silica structure or silicate highly ordered mesoporous system.[78,192] Then, the silanol groups polymerize by condensation, forming three-dimensional structures linked by siloxane bonds (Si-O-Si).[194,198] The size and the morphology of materials depend on various factors such as temperature, rate of addition and agitation.[75,76,190,199] In the final step, the surfactant will be removed from the inside of pores by calcination to produce molecular sieves with narrow pore size distributions with high ordered mesoporous structures.[195,200]

The synthesis of MCM-41 from TEOS is limited because of expensive TEOS and high amount of the CTAB was required in the preparation step thus the alternative precursors, including sodium silicates have generated great interest as sodium silicate solutions are very cheap and readily available as they are precursors in glass manufacture.[94,195] They can also be prepared from agricultural wastes such as rice husk and fly ash which are beneficial as eco-friendly and low-cost alternative silica precursors.[73,74,201,202] Fig. 6 illustrates the preparation of MCM-41.

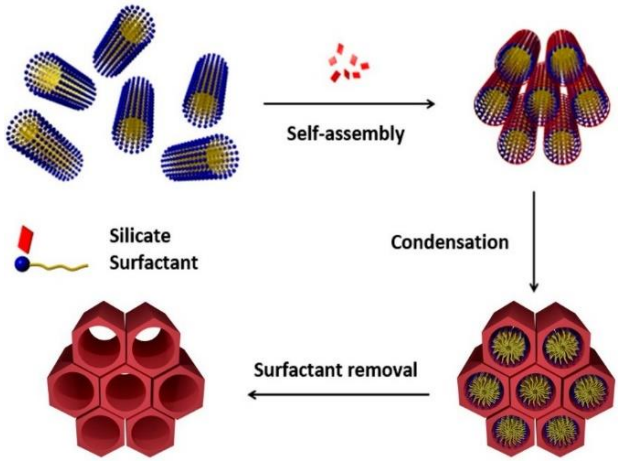

Fig. 6 Schematic illustration of the preparation of MCM-41[175]

1.7.2 Silica

Silica particles have many applications in industries as filler material in composites, raw material for the electronic components, catalysts, drug delivery systems, thermal insulators, chromatography and adsorption.[92,203] Many techniques have been used for silica synthesis such as flame spray pyrolysis, micro-emulsion technique and sol gel method. Among them, sol gel method is the common technique for the synthesis of silica nanoparticles because this process can control the particle size and shape by systematically tailoring the synthesis conditions.[94,95,100,204,205]

The possible formation mechanism in sol gel method involves two steps: (1) a colloidal suspension "sol" is first prepared wherein particles are suspended in the liquid (2) whereas the second step involves the development of a 3D polymeric network, which results in the formation of "gel". The production of silica nanoparticles at low temperature by using silica precursors i.e., tetraethyl orthosilicate (TEOS).[206]

However, sodium silicate solution is also used as precursor as well.[83] The possible mechanism of silica particles formation can occur after acidic treatment. To control the

structure of SiO_2 powder synthesized from rice husk, the structure of SiO_2 can be controlled by acid and/or alkali leaching (e.g., HCl, HNO_3, H_2SO_4, NaOH and NH_4OH).[207]

Rice husk (RH) is one of the promising silica sources of materials due to its abundance. Leaching of RH with acids including HCl is performed for the removal of metallic impurities prior to thermal treatments.[208,209] Typically, the as-obtained silica derived from rice husk was added to NaOH to produce sodium silicate solution, which was then treated with a variety of acid solutions in the presence of ethanol to produce silica particles. [210,211]

1.7.3 MCM-41 magnetite composite material

Among the various types of nanomaterials, magnetic nanoparticles have received great attention because of their high surface area, small size, biocompatibility, non-toxicity, strong magnetic properties and easy of separation and recovery using an external magnet.[212,213] Due to their unique properties, magnetic nanoparticles have been used in various applications such as drug delivery and catalysis.

Mesoporous materials and magnetic nanoparticles and have attracted significant attention due to their outstanding features in the context of green chemistry.[184] However, magnetic nanoparticles are very unstable in acidic and basic media. To solve this problem, mesoporous silica like MCM-41 have been used for the stabilization of this magnetic material.[214]

Mesoporous silica is very noticeaby and widely applied in chemical processes due to its notable features such as tunable physical and chemical properties, easy preparation, high surface area, low cost, high flexibility, and high availability.[90,91,174,175] So, recently magnetic mesoporous silica materials have been considered as effective adsorbent for water remediation because they have advantages of both magnetic nanoparticles and mesoporous silica such as simple recoverability and easy separation.[99,184,215-218]

1.7.4 Application of high surface area porous materials for methylene blue dye adsorption in aqueous solution

Methylene blue (MB) is a heterocyclic aromatic chemical compound with the chemical formula $C_{16}H_{18}ClN_3S$. This compound can be used in medicine, biology and chemistry. It is also very widely utilized in dyeing cottons, coloring paper, coating paper of stocks, wools, etc. The chemical name according to International Union of Pure and Applied Chemistry (IUPAC) is 7-(dimethylamino) phenothiazin-3-ylidene]-dimethylazanium chloride.[65,93] The structure of MB was shown in Fig.7.

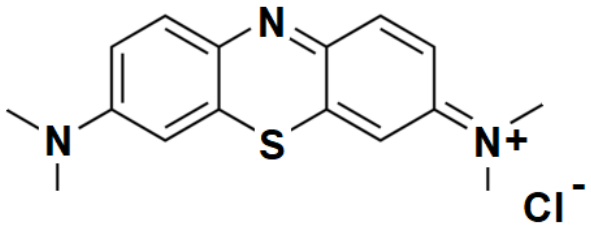

Fig. 7 Methylene blue dye structure

MB can cause some harmful effects even though it is not strongly hazardous. Various treatment processes have been reported to remove dyes from wastewater, for example, photodegradation, coagulation–flocculation, chemical oxidation, membrane filtration, and adsorption. Adsorption has received the most attention and is the most commonly applied process of water remediation because of its simplicity of design, low cost, insensitivity to toxic substances, and efficiency in treatment.[60,65,93]

1.8 Production of defibrillated celluloses

Cellulose is one of the most abundant biopolymers on earth, occurring in wood, cotton, and other plant-based materials and serving as the dominant reinforcing phase in plant structures. Cellulose comprises glucose monomer building blocks which are linked together with β-(1-4)-glycosidic linkages to form a linear polymer.[147]

1.8.1 Cellulose microfibrils and cellulose nanofibrils

In this thesis, processes for cellulose microfibrils and cellulose nanofibers production from water hyacinth have been studied for applications. The cellulose strands bundle together binding to each other via hydrogen bonding of the hydroxyl-groups and thus form microfibrils (in micron range) which are ordered (crystalline) and disordered (amorphous region).[219] This renders cellulose as hydrophobic and water insoluble which make it difficult to process.

Typically, nanocellulose can be categorized into two major classes, (1) nanostructured materials (cellulose microcrystals and cellulose microfibrils) and (2) nanofibers (cellulose nanofibrils, cellulose nanocrystals, and bacterial cellulose).[154,220] This nanomaterial endows useful features such as high surface area-to-volume ratio, high tensile strength, low coefficient of thermal expansion, hydrogen-bonding capacity, biocompatibility, eco-friendliness, renewability, and lack of toxicity.[103,221]

Cellulose microfibril, or microfibrillated cellulose or cellulose nanofiber or nanofibrillar cellulose, commonly obtained by chemical and mechanical treatment, presents an entangled network structure with flexible, longer, and wide nanofibers (1–100 nm in width and >10,000 nm in length), and lower crystallinity with respect to cellulose nanocrystal.[220,222]

Nano-fibrillated cellulose is often done using the TEMPO-mediated oxidation method. Its nanoscale is about 5–60 nm in diameter and many microns in length which consists of cellulosic domains i.e., crystalline and amorphous domains.[223,224] Generally, several resources of native biomass, such as corn husk, rice straw, soft and hardwoods.[225] Normally, cellulose nanocrystal (CNCs) are needle-shaped and highly crystalline. They can be produced from cellulose pulp by acid hydrolysis process; through this process amorphous fibrils are dissolved to maintain the crystallinity.[137,153,226] The dimension of the yielded cellulose nanocrystal is around 3-35 nm in diameter and 20–100 nm in

length.[153,227] Cellulose nanocrystals have been employed to reinforce a wide range of polymer matrixes.[145,159] Both thermoplastic polymers and thermosets have been reinforced with CNCs to produce high-quality and cost-effective materials. The application of CNCs to wound healing was recently reported is many investigations, and promising achievements have been reached owing to their useful properties as well as their ability to be functionalized.[228-230] Fig. 8 illustrates a hierarchical structure of cellulose, nanocellulose production via acid hydrolysis and bionanocellulose cultured from cellulose-synthesizing bacteria.

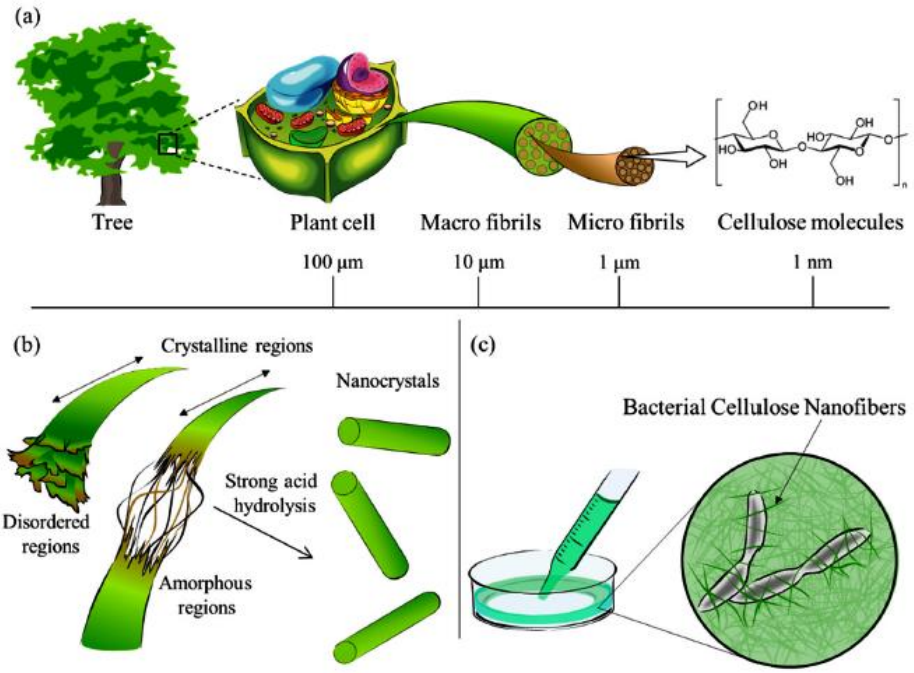

Fig. 8 (a) Cellulose contained in plants has a hierarchical structure from the meter to the nanometer scale (b) A schematic diagram of the reaction between cellulose and strong acid to obtain Nanocellulose and (c) Bionanocellulose cultured from cellulose-synthesizing bacteria [159]

Cellulose has a crystalline structure while lignin and hemicellulose are amorphous as can be seen plant cell wall structure and microfibril cross-section in **Fig. 9**.[110] Cellulose nanocrystals are unique nanomaterials derived from the natural polymer, i.e., cellulose. The advantages of cellulose nanocrystals include high surface-area-to-volume ratio, low density, lightweight, and environmentally benign.[231-233] The physical appearance of cellulose nanocrystal is rod-like or ribbonlike particles of 3-50 nm in diameter and 50-1000 nm in length. Consequently, cellulose nanocrystal can potentially be used in a variety of applications, such as reinforcing agents in high-performance nanocomposites, personal care products, filtration media, paints and coatings and absorbent products.[10] Moreover, the significant application of nanomaterials in the areas of packaging industries, health and hygienic sector and cosmetics. In the aspect of techno-economically feasibility, nano-cellulose-based materials may prove to be outstanding, environmentally friendly, and mitigate effluent load.[120,121,223]

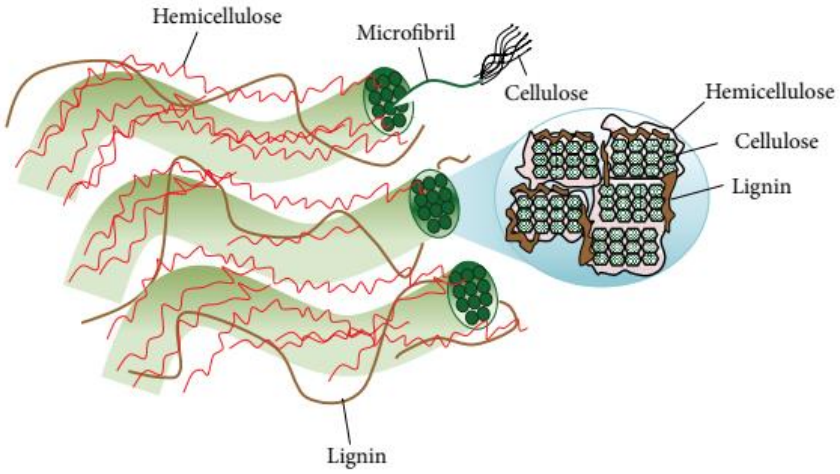

Fig. 9 Plant cell wall structure and microfibril cross-section [108]

1.8.2 Extraction of defibrillated celluloses

Cellulose microfibril (CMF) has great potential to be used as a bio-based structural-reinforcing cost-efficient material. In general, the fabrication of cellulose microfibril does

not require acid hydrolysis, which would be the next step required for converting microfibrils to cellulose nanowhiskers or cellulose nanofibrils.[10,158,234] Over the last few years, new surface modification techniques and mechanical processes have been introduced to address these problems.[222,225]

1.8.2.1 Alkaline treatment

Alkaline treatment is the procedure to remove hemicellulose and other impurities as well as to dissolve noncellulosic constituent through the mechanism of strong base hydrolysis of highly branched hemicellulose and the depolymerization of part of the lignin.[217,218] Moreover, the presence of wax, natural fats and pectin along with hydroxyl groups which may hide reactive sites (-OH groups of fibers) and represents a hydrophobic blockage for fiber bonding and wetting with the polymer matrices would also be eliminated by alkali treatment, resulting in breaking down of the composite fiber bundle into smaller and thinner fibers.[218,235] Cellulose is extracted by exposing ground fibers to sodium hydroxide, which favorably and efficiently increases the accessibility of the cellulose.[218,236] The alkali treatment could increase amount of cellulose exposed on the fiber by decreasing the outer non-cellulosic layer composed of materials such as hemicelluloses, lignin, pectin, wax, oils and other impurities contained in the raw fibers.[237]

1.8.2.2 Bleaching treatment

Bleaching treatment is an important step to remove lignin in fibers – a process which is also called delignification. Bleaching is a chemical processing before or after the removal of hemicellulose to remove colored lignin.[238,239] Oxidizing agents, such as hypochlorite and peroxide, were commonly used as bleaching agents.[240]

After alkaline treatment, the alkali treated-fibers are mainly bleached by boiling the fibers with sodium chlorite ($NaClO_2$) solution under acidic condition.[222] The acidic condition is created by acetate buffer solution which is made up of NaOH and glacial acetic acid and diluted with distilled water. In the presence of acidic buffer solution, sodium chlorite

would break down into chlorine dioxide (ClO_2) under the presence of buffer salts which help to liberate the chlorine dioxide from sodium chlorite during the bleaching step.[240] This ClO_2 would be able to oxidize with lignin which is left in the fibers by attacking the aromatic ring of the lignin, the loss of lignin could result in further fibrillation of the alkali-treated fibers.

As well as sodium chlorite, sodium hypochlorite (NaOCl) is one of the better oxidizing agents, it is also possible to render the removal of lignin efficiently. Chlorine-free techniques have been developed for bleaching step. This procedure is more environmentally benign than the conventional methods and also effective that have been used chlorine oxidizing chemical for bleaching step.[239]

1.8.2.3 Acid hydrolysis

Various technologies have been discovered for the isolation of nanocellulose from pretreated cellulose fibers as can be seen in **Fig. 10**. Regarding the isolation of crystalline cellulosic region, in the form of microcrystalline cellulose, acid hydrolysis is most widely used for the extraction of nanocellulose from biomass fibers because it requires shorter reaction time than other processes.[115] It is easily hydrolyzed into the disordered regions of cellulose.[106] The hydrolysis treatment is generally followed by neutralization, washing and drying processes. The acid hydrolysis processes with HCl and H_2SO_4 from various cellulosic sources to produce nano-fibrillated cellulose.[22,115,158] In this step, sulfuric acid is widely employed for the acid hydrolysis.

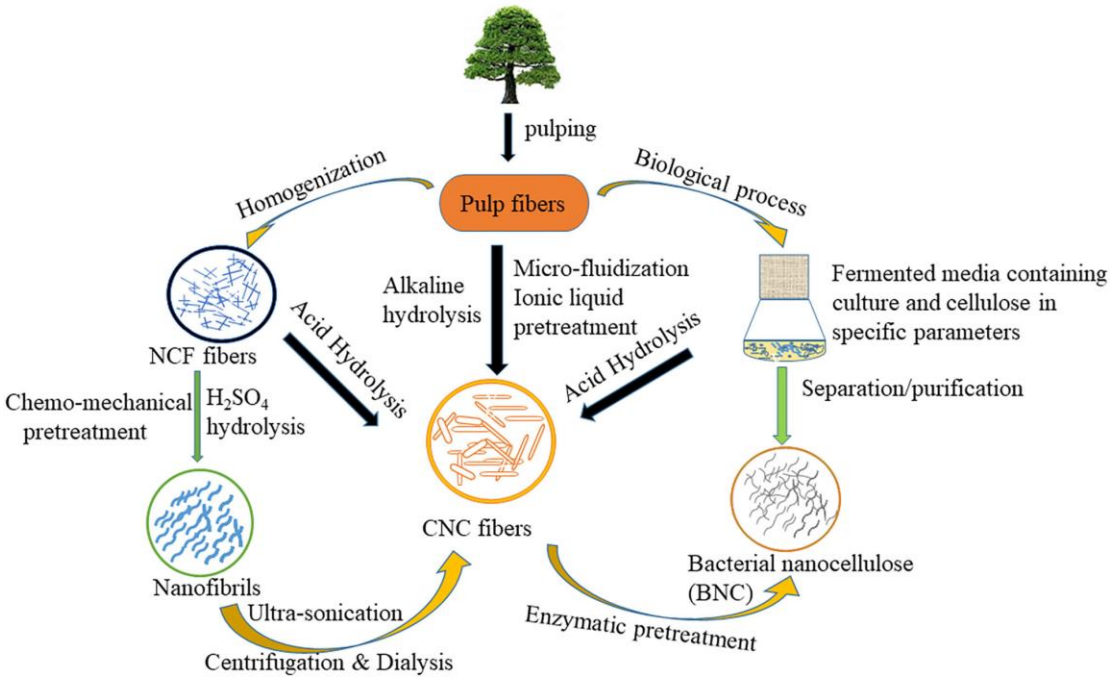

Fig. 10 The schematic illustration of nanocellulose production [223]

1.8.3 Application of cellulose microfibrils and cellulose nanofibrils

Recently, cellulose microfibrils and cellulose nanofibrils and its applications have been great interest in both research and industrial areas due to its unique properties such as excellent mechanical properties (good tensile strength), high surface area and rich hydroxyl groups for modification.[107,137,226]

The production of nano-scale cellulose fibers and their application in composite materials has gained increasing attention due to their stiffness and high strength combined with low weight, biodegradability and renewability.[241,242]

Due to its high surface area and abundant of hydroxyl groups, nanocellulose can be used for surface modification. The most common method is direct chemical modification or covalent attachment with hydroxyl groups of nanocellulose surface as well as using the hydroxyls for the modification of grafted polymers and nanocomposite materials.[109,243] One of the main applications from the surface modification of nanocellulose is the

fabrication of amphiphobic surface. Amphiphobic surface is the surface which can repel both polar and non-polar liquids. This anti-wetting property relates to the special surface with self-cleaning, anti-bacterial, anti-reflective, corrosion resistant properties, etc.[241,244] Moreover, in addition to its excellent mechanical property, nanocellulose film is transparent, optically clear, and foldable. Such transparent films can be applied to electronic devices, solar cells, flexible displays, flexible circuits instead of the conventional film.[121,144,241,244-247]

1.8.3.1 Bio-composite films preparation

Recently, bioplastics are considered for developing eco-friendly packaging materials but there are some limitations such as poor mechanical and barrier properties.[248] However, these properties can be improved by blending with some polymers or adding some nanofillers with biopolymers which is one of the most effective methods of creating new biomaterial with desired properties.[249] The as-prepared modified films produced through biopolymer blending usually exhibit unique properties such as improvement of mechanical properties.[144]

Polyvinyl alcohol (PVA), a water-soluble crystalline polymer, as a biodegradable polymer, has extensive prospects in the fields of food packaging film materials, textile, artificial organs, biomedical fields and etc.[121,152,250-252] PVA is normally used in composites to lower the cost of the product without any compromise or minimal compromise of its properties and its hydrophilic composition, which consists of hydroxyl groups in the PVA structure, is also beneficial in many applications. Blending can improve the properties of biodegradable polymers for packaging purposes, continuous improvement especially in applications where properties such as water vapor permeability, mechanical properties and biodegradation is necessary. [238,253-255] Some studies were also carried out to explore the material improvement of biofilms via chemical or physical crosslinking.[255-258] Nanocellulose possesses valuable characteristics such as renewability and

biodegradability with satisfactory mechanical properties when incorporated in a polymer matrix.[102,126,259]

Chapter 2

Synthesis of bio-derived porous materials from rice husk for methylene blue adsorption in aqueous solutions

2.1 Silica extraction

Rice husk is an abundant agricultural material which has a high silica content. This research reports on the purity of silica extracted from rice husk through acid pretreatment under the conventional method and a microwave-assisted method. Then, the preparation of silicate solution from silica derived from rice husk which can be used as starting materials for synthesis of MCM-41 and its composite materials discussed in latter section that has been gaining more and more interest when they were made to use for MB adsorption in aqueous solution.

2.1.1 Comparison of yields of silica extracted from rice husk after pretreatment by conventional method and microwave-assisted method

Rice husk contains mineral trace elements such as calcium, potassium, iron, sodium, copper, zinc, aluminum, magnesium and so on, the levels of which depend on many factors, for example, the harvest area and fertilizer.[260,261]

The composition of rice husk, pretreated rice husk via conventional and microwave heating and silica extracted from rice husk after calcination was investigated by X-ray fluorescence (XRF). It was found that raw rice husk, collected from local farm in Chiang Mai province, Northern Thailand, has a high content of silica of 72.64 wt% and other oxides including, CaO (25.35%), K_2O (1.09%) and Fe_2O_3 (0.92%). After an acid pretreatment step using conventional method and microwave-assisted pretreatment, the purity silicas were produced (>99%). The conditions for pretreatment step were carried out via conventional heating and microwave-assisted method as can be seen in Table 1.

Fig. 11 shows the raw rice husk, the pretreated rice husk and the as-obtained silica derived from rice husk. The as-obtained white silica powders with high purity were produced after calcination and the purity of silica was very high 99.70% after pretreatment via microwave-assisted method at 80 ^{O}C for 50 min compared to conventional heating for pretreatment step at 100 ^{O}C for 24 h (99.96%).

Rice husk Ground rice husk After pretreatment After calcination

Fig. 11 Rice husk, ground rice husk, pretreated rice husk and the as-obtained silica after calcination

Table 1 The conditions for silica extraction from rice husk

Techniques	Conditions
Conventional heating (Cov.)	100 ^{O}C for 3 h
Conventional heating (Cov.)	100 ^{O}C for 24 h
Microwave heating (MW)	80 ^{O}C for 30-50 min

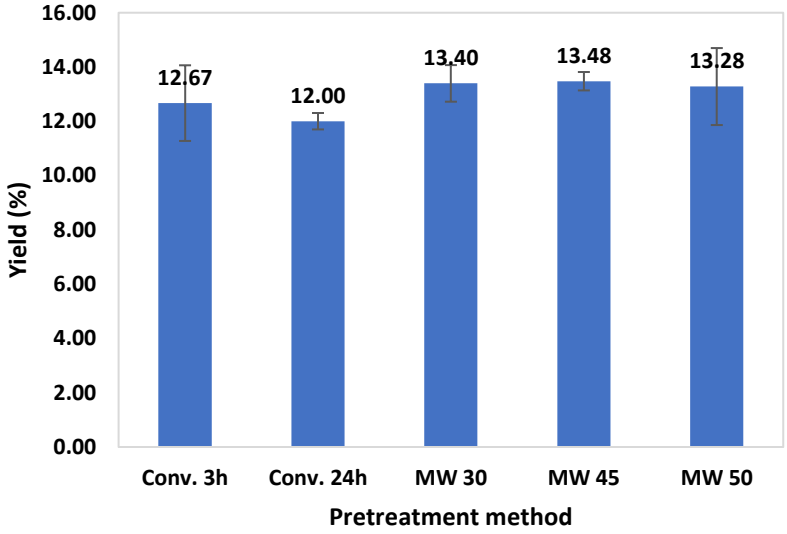

Fig. 12 Yield of silica extracted from rice husk by conventional pretreatment and microwave-assisted pretreatment method

After calcination, silicas derived from rice husk treated by microwave-assisted method (13.28-13.48%) have higher yield than silicas treated by conventional method (12.00-12.67%). Due to its simplicity and speed of the microwave-assisted method, the pretreatment step under microwave irradiation was selected for silica extraction from rice husk.

Fig. 12 shows the highest yield of silica (13.47%) obtained from the microwave-assisted method (80 ^{O}C for 45 min) so this pretreatment method was used for silica preparation in the next step.

Table 2 The composition of raw rice husk, pretreated rice husk via conventional and microwave heating and silica extracted from rice husk after calcination analyzed by X-ray fluorescence (XRF)

Component	Raw RH	Conventional method		Microwaved-assisted pretreatment		
		3 h	24 h	30 min	45 min	50 min
SiO_2	72.64	98.16	99.96	99.53	99.61	99.70
CaO	25.35	1.84	0.04	0.47	0.39	0.30
K_2O	1.09	-	-		-	
Fe_2O_3	0.92	-	-		-	

As can be seen in **Table 2** the as-obtained silica materials after calcination have high purity of SiO_2 (>99%). The impurities of K_2O and Fe_2O_3 in raw rice husk were removed and only trace metal oxide of CaO was found. Due to acid pretreatment method using HCl was effective way for removal of alkaline oxides and other impurities to obtain for highly pure of SiO_2.[261-263]

The N_2 adsorption-desorption isotherm of silicas from rice husk as well as pore size distribution are also shown in **Fig. 13** and **Fig. 14** which reveal the mesoporous structure of SiO_2.[92] As can be seen in **Table 3**, the as-obtained SiO_2 materials possess relatively high Brunauer-Emmett-Teller (BET) surface area of 309-334 $m^2 g^{-1}$ which higher than the BET surface area of as-obtained silicas from conventional pretreatment (219-221 $m^2 g^{-1}$). It

should be noted that microwave-assisted pretreatment has advantage not only for rapid reaction time but also provides direct heating to the bulk reaction mixture led to high uniform of homogenous phase of silica materials were obtained from the process.[264] Moreover, the as-obtained silicas from this work are also greater than the previous reports by Azat *et al*. (120 $m^2 g^{-1}$).[262]

Table 3 Porosity properties of silica obtained from conventional pretreatment at 100 ^{O}C for 3 and 24 h and microwave-assisted pretreatment at 80 ^{O}C for 30-50 min

Method	Time	BET Surface area ($m^2 g^{-1}$)	Pore volume ($cm^3 g^{-1}$)	Average pore diameter (nm)
Conventional pretreatment	3 h	219	0.15	3.70
	24 h	221	0.28	3.75
Microwave-assisted pretreatment	30 min	309	0.30	3.91
	45 min	311	0.31	3.99
	50 min	334	0.33	3.97

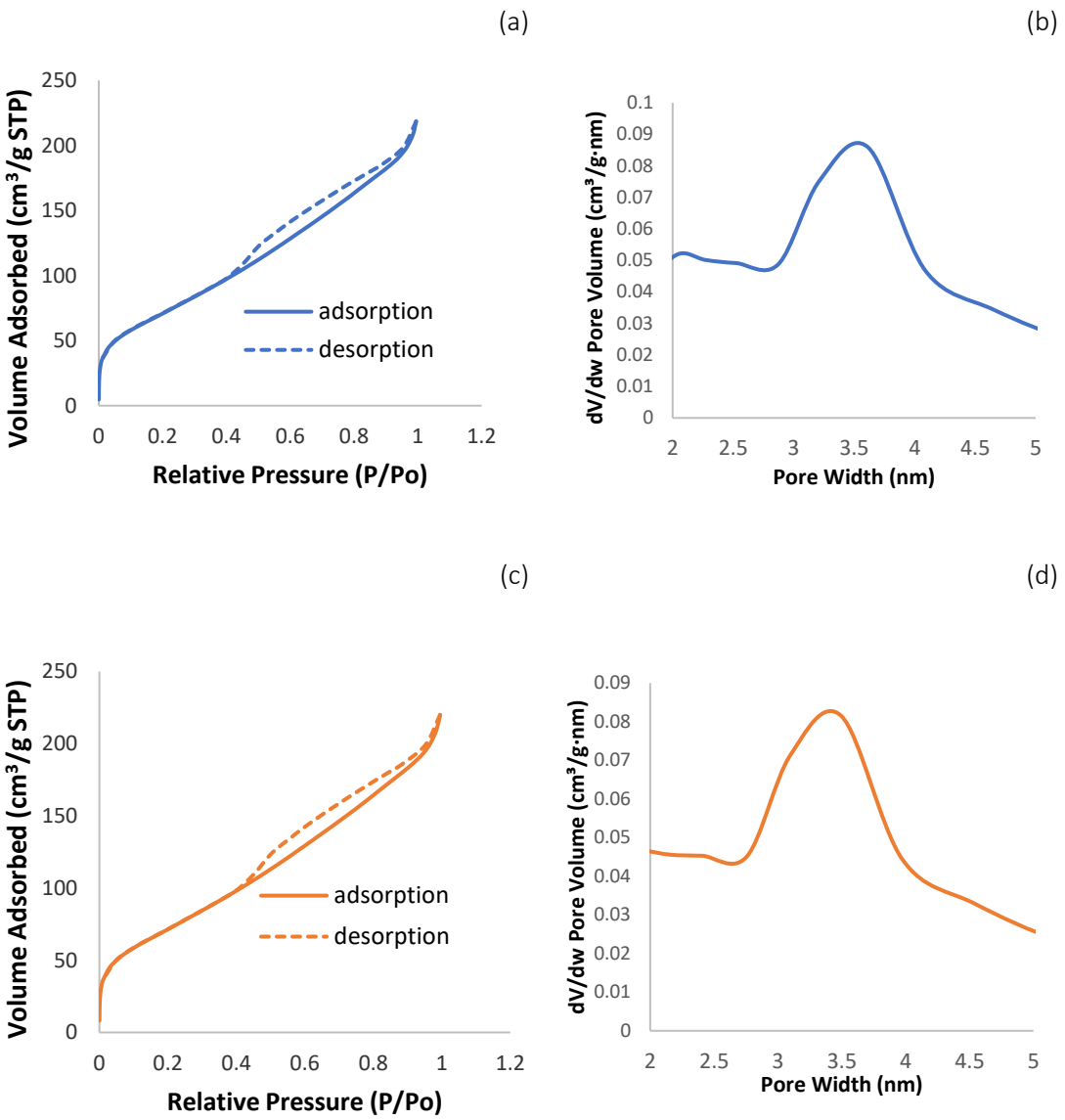

Fig. 13 The N_2 adsorption-desorption isotherm and BJH pore size distribution of silicas from rice husk via conventional pretreatment at 100 ^{O}C (a-b) for 3 h, and for (c-d) 24 h

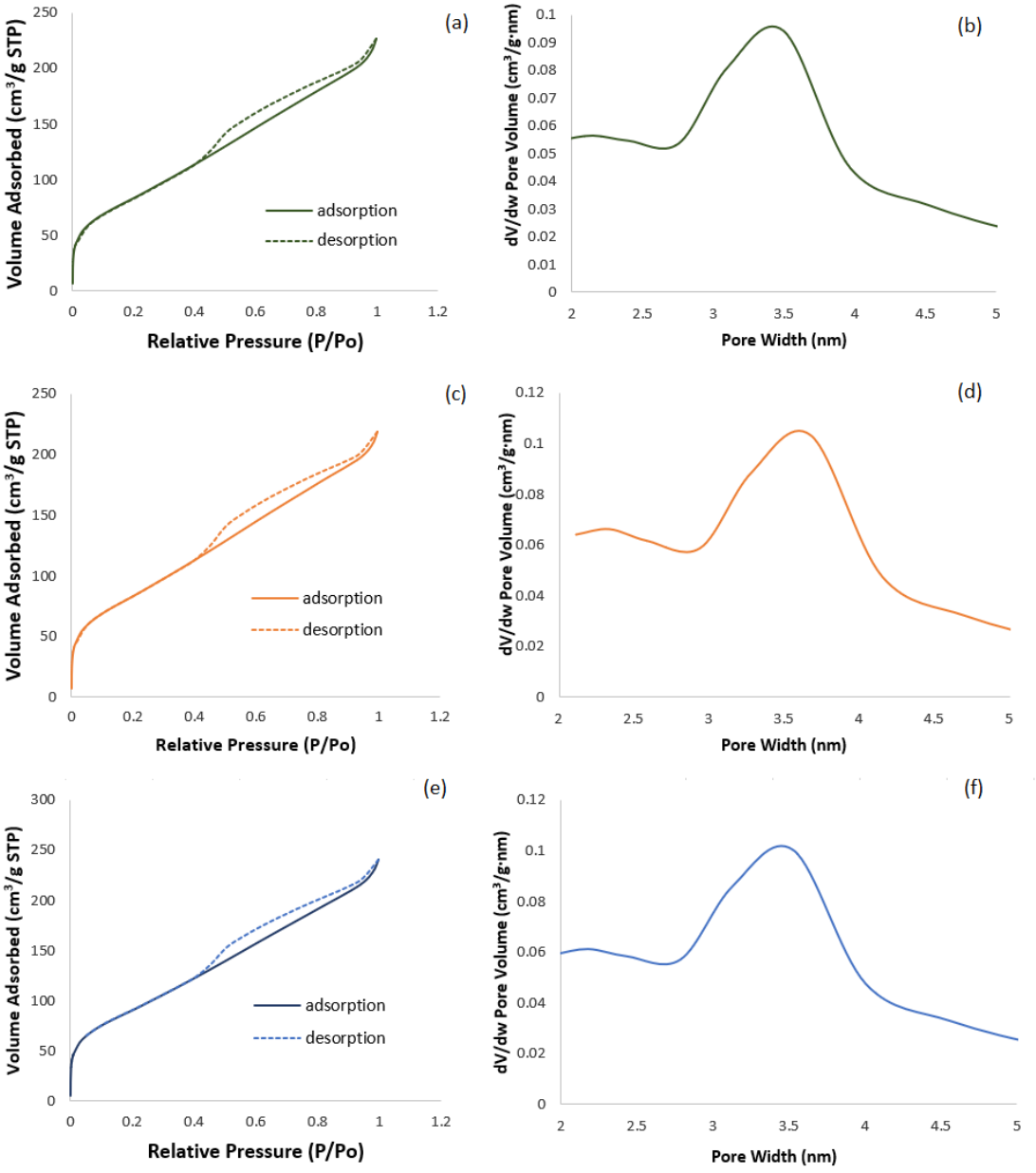

Fig. 14 The N_2 adsorption-desorption isotherm and BJH pore size distribution of silicas from rice husk via microwave-assisted pretreatment at 80 ^{O}C for (a-b) 30 min, (c-d) 45 min, and (e-f) 50 min, respectively

The surface chemistry of the as-obtained silica materials was investigated by FTIR. FTIR spectra of silica derived from rice husk shown in **Fig. 15** which illustrates that band at 1074–1090 cm^{-1} was attributed to asymmetric Si-O-Si stretching vibration (siloxane

group) and band at 963 cm^{-1} which can be assigned to the symmetric Si-OH stretching vibrations of silica materials.[94,263-265]

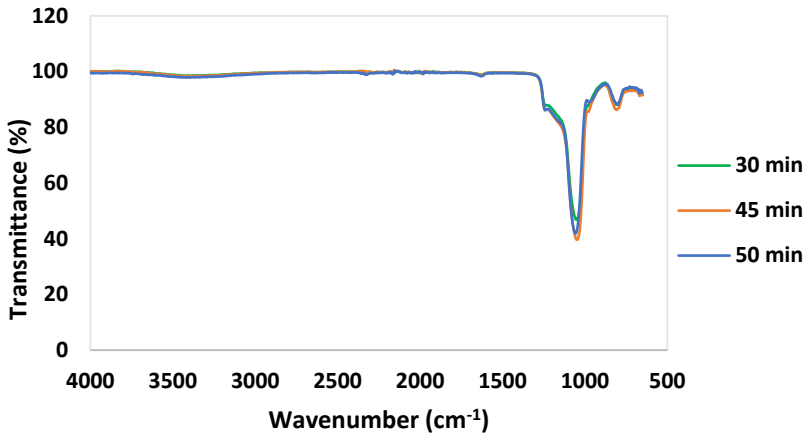

Fig. 15 FTIR spectra of silica derived from rice husk via microwave-assisted pretreatment at 80 ^{O}C for 30-50 min

2.2 Preparation of silicate solution

In this research, highly pure silica can be prepared from rice husk can be prepared as discussed in the previous section. This part represents the preparation of silicate solution from silica derived from rice husk which can be used as starting materials for mesoporous materials such as MCM-41 and its composites in the next step.

The first step to prepare sodium silicate solution is adding 1M NaOH solution (solid-to-liquid ratio = 2:10) and subsequently heating at 80 ^{O}C until it completely dissolved as a clear solution like the commercial silicate solution.

This concentration of the resulting solution was determined before using it as a starting material for mesoporous materials preparation. In this step, the concentration of silicate solution derived from rice husk was calculated by calibration curve of commercial silicate solution by using FT-IR technique. This method was slightly modified from the literature as reported elsewhere.[94]

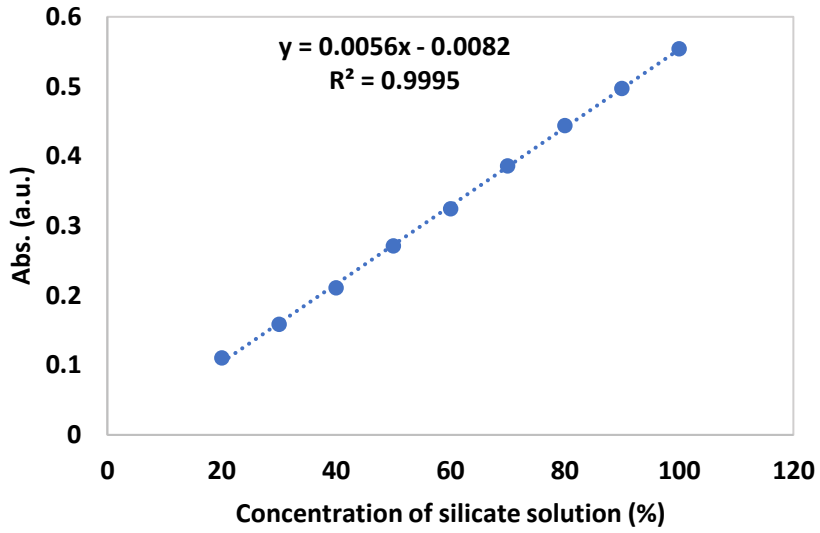

Fig. 16 Calibration curve of commercial silicate solution

Fig. 16 shows FT-IR calibration curve of commercial silicate solution (various concentration from 20-100%) at 963 cm^{-1}, the calculated concentration of silicate solution derived from rice husk is found to be 73.42% (close to the peaks shown in Fig. 18)

In this study, the attempt to prepare the higher concentration of resulting silicate solution was investigated but it was found that the precipitation of silica could occur so it should be noted that this concentration could be the optimum concentration for using as a starting material for the next step.

To investigate the functional groups of the resulting silicate solution compared to the commercial silicate solution. From these results, it was found that FTIR spectra of the resulting silicate solution derived from rice husk exhibits the same characteristic peaks of the commercial silicate solution shown in Fig. 17 and Fig. 18.

FTIR analysis provides evidence for the presence of Si-O-Si in sodium silicate solution. All sodium silicate solutions represent the strong broad bands at 1000 cm^{-1} corresponding to the stretching vibrations of Si-O-Si.[89,94,266] The peak at 1640 cm^{-1} corresponding to the OH bending mode vibrations of water.[177] Broad peaks at 3000–3600 cm^{-1} were attributed to

the OH stretching vibrations of water.[177] It should be noted that this result confirmed that the resulting sodium silicate solution derived from rice husk can be used as starting materials for the preparation of sustainable mesoporous MCM-41 materials as can be discussed in the latter part.

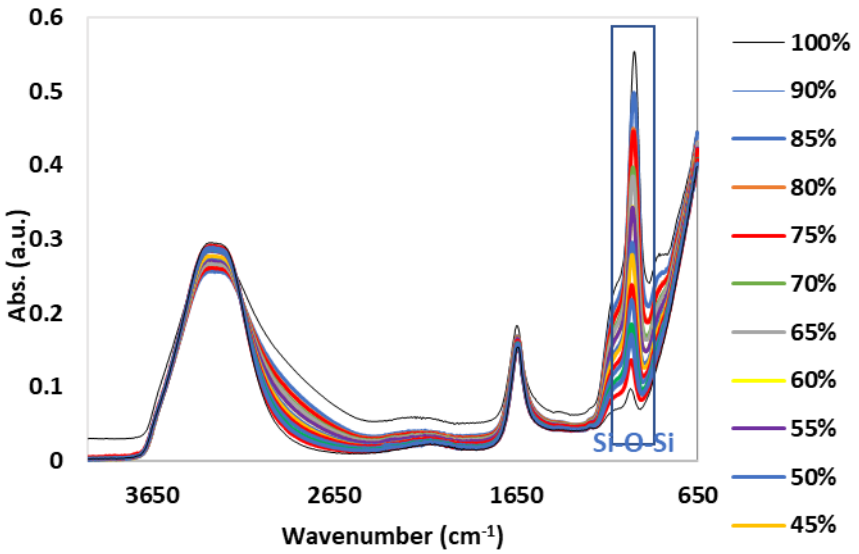

Fig. 17 FTIR spectra of commercial silicate solution at various concentration (45-100%)

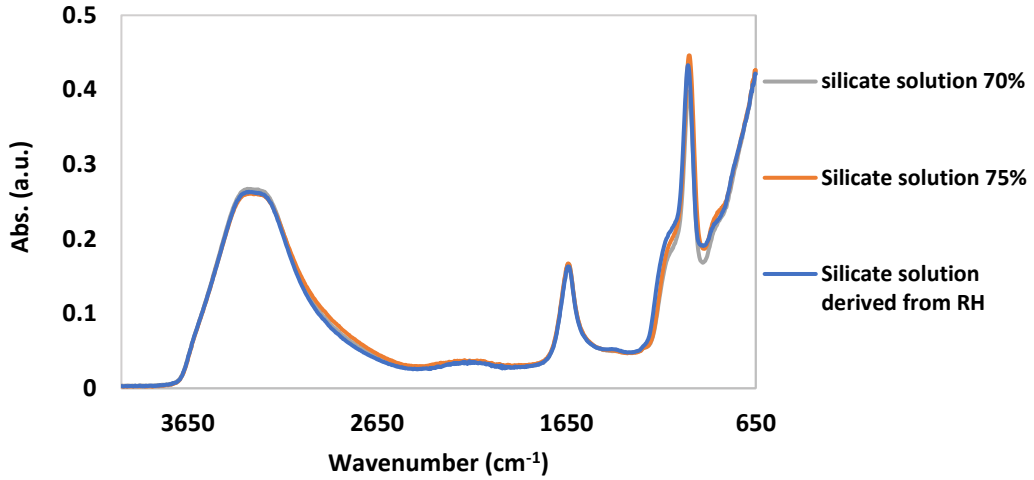

Fig. 18 FTIR spectra of commercial silicate solution (70-75%) and silicate solution derived from rice husk via microwave-assisted pretreatment

2.3 Synthesis of MCM-41 mesoporous materials

In this work, the synthesis of high surface area mesoporous MCM-41 derived from rice husk was studied. The resulting silica from the previous part was converted to sodium silicate by dissolution in NaOH solution and bio-derived sodium silicate solution was used as starting material for synthesis of MCM-41 though conventional method and microwave-assisted method compared with as-prepared MCM-41 synthesised using commercial silicate solution by conventional method. The comparison of various conditions was investigated, including the silica source, methods, and ratio of CTAB:Si. Finally, this MCM-41 derived from rice husk which possess the high surface area of mesoporous material will be used for application as the adsorbent for MB adsorption in the latter section.

2.3.1 Conventional method using commercial sodium silicate solution

The preparation of MCM-41 using commercial sodium silicate solution was investigated which can be denoted as S method. In this work, the resulting silica from the previous

part was converted to sodium silicate by dissolution in NaOH solution and bio-derived sodium silicate solution was used as starting material because it is cost-effective and less toxic than TEOS. Moreover, this starting material was prepared from rice husk (agricultural waste) which is abundant and renewable.

The porosity properties of the as-prepared high surface area mesoporous MCM-41-S produced from commercial sodium silicate solution through the conventional method were determined by the N_2 adsorption-desorption analysis.

The N_2 adsorption-desorption isotherm of MCM-41-S synthesised using commercial silicate solution, denoted as MCM-41-S, has a type IV classification confirming that the products display mesoporosity typical of MCM-41 (**Fig. 19**). This isotherm shows a Type B or H4 hysteresis loop where the desorption branch remains above the adsorbed branch over a wide range of p/p_o. This is associated with narrow mesopores open at both ends.[74,76,212] BET surface area, pore diameter and pore volume derived from the N_2 adsorption–desorption measurements (**Table 4**) show that MCM-41 synthesised from commercial silicate solution possesses high surface area of 1164 $m^2 g^{-1}$ with relatively high value of pore volume (0.99 $cm^3 g^{-1}$).

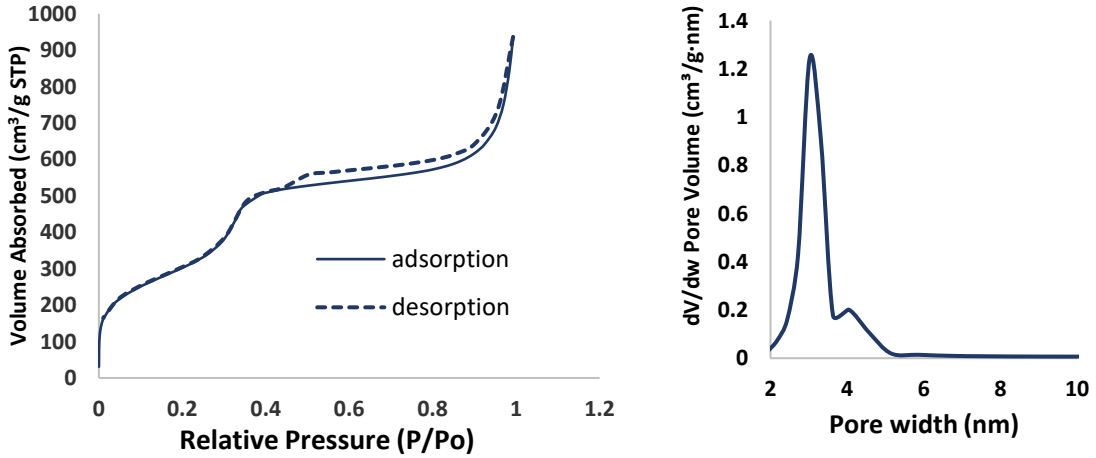

Fig. 19 The N_2 adsorption-desorption isotherm and BJH pore size distribution of MCM-41-S synthesized using commercial sodium silicate solution

Table 4 Porosity properties of MCM-41-S synthesized from commercial sodium silicate solution

Sample	BET Surface area ($m^2 g^{-1}$)	Pore volume ($cm^3 g^{-1}$)	Average pore diameter (nm)
MCM-41-S	1164	0.99	3.42

2.3.2 Comparison of MCM-41 synthesised using sodium silicate solution derived from rice husk via conventional method and microwave-assisted method

This part represents the porosimetry data from N_2 adsorption-desorption analysis of MCM-41 prepared from sodium silicate solution derived from rice husk via conventional method, denoted as MCM-41-C, and via microwave-assisted method, denoted as MCM-41-MW, respectively.

As shown in Fig. 20 and Fig. 21, the N_2 adsorption-desorption isotherms both have a Type IV classification confirming that the products display mesoporosity expected of MCM-41. Both isotherms show a Type B or H4 hysteresis loop, which is typical for mesoporous solid.[188,202,267] BET surface area, pore diameter and pore volume derived from the N_2 adsorption–desorption measurements (Table 5) show that MCM-41 synthesised from silicate solution derived from rice husk also possesses high surface area of 946 $m^2 g^{-1}$ for MCM-41-C (Fig. 20) and 1082 $m^2 g^{-1}$ for MCM-41-MW (Fig. 21). Moreover, both materials possess the high value of pore volume of 0.99 $cm^3 g^{-1}$ and 0.86 $cm^3 g^{-1}$ for MCM-41-C and MCM-41-MW, respectively.

As MCM-41-MW has high surface area and large pore volume which is a benefit for using as adsorbent and it can be prepared through microwave-assisted method in hydrothermal treatment step (30 min) which used shorter reaction time than conventional heating (4

h) thus this material will be used as sustainable adsorbent and investigated for MB adsorption in the next section.

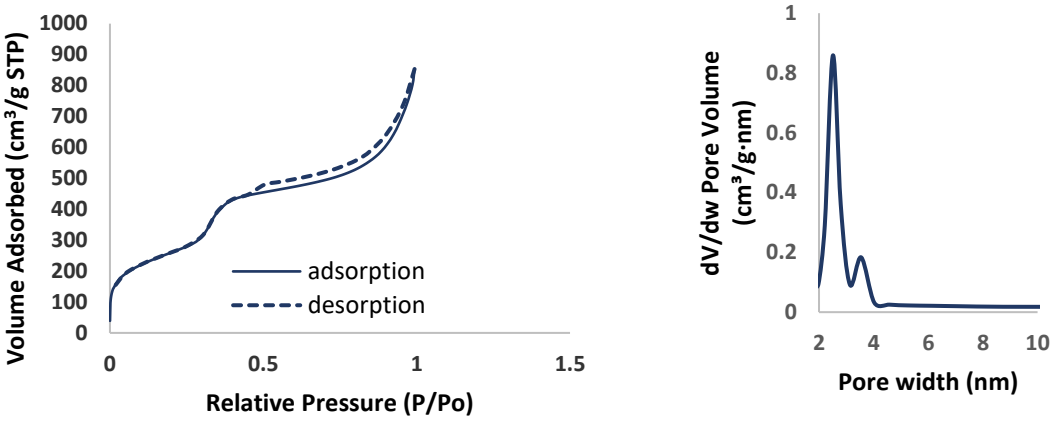

Fig. 20 The N_2 adsorption-desorption isotherms and BJH pore size distribution of MCM-41-C synthesized using sodium silicate solution derived from rice husk by using conventional method (hydrothermal step at 100°C for 24 h)

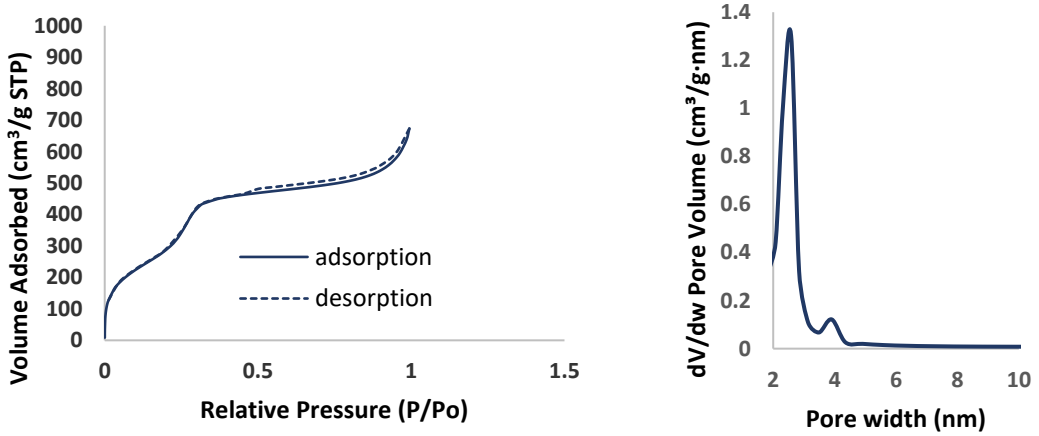

Fig. 21 The N_2 adsorption-desorption isotherms and BJH pore size distribution of MCM-41-MW synthesized using sodium silicate solution derived from rice husk by using microwave-assisted method in hydrothermal step at 100°C for 30 min

Table 5 Porosity properties of MCM-41 synthesized using sodium silicate solution derived from rice husk

Sample	Molar ratio CTAB:Si = 0.5:1	BET Surface area ($m^2 g^{-1}$)	Pore volume ($cm^3 g^{-1}$)	Average pore diameter (nm)
MCM-41-C	Conventional method	946	0.99	4.19
MCM-41-MW	MW-assisted method	1082	0.86	3.18

The as-obtained materials were structurally characterized by FTIR and SAXS measurements. The characteristic of surface chemistry of all materials was characterized by FTIR spectrometry. The FTIR spectra of the MCM-41 samples are shown in **Fig. 22**. Both peaks around 1229 cm^{-1} and 1084 cm^{-1} were attributed to the asymmetric stretching of Si-O-Si groups. The symmetric stretching modes of Si–O–Si groups are observed at 799 cm^{-1}. [75,187] Broad peaks at 3000–3600 cm^{-1} were attributed to Si-O-H stretching vibrations – caused by the absorbed water molecules on the surface and also by silanols (SiOH).[187,268,269]

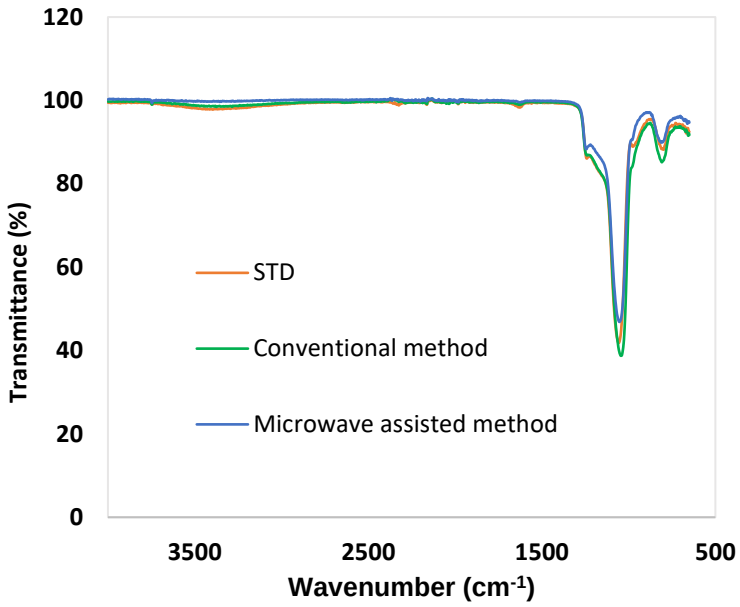

Fig. 22 FTIR spectra of MCM-41-STD, MCM-41-C and MCM-41-MW

Moreover, the structural properties of the as-prepared MCM-41-S, MCM-41-C and MCM-41-MW can be confirmed by SAXS measurements. MCM-41, as expected, exhibited hexagonally arranged mesopores of 3–4 nm.[270] All samples display typical diffraction peaks, confirming the ordered structural arrangement of pores which shown that all materials have characteristic peaks of MCM-41 mesoporous materials.[270,271]

SAXS data shows the four characteristic diffraction peaks of MCM-41 at 2.45° and 4.10 ° as major reflections, along with low intense at 4.73°, correspondence with the indexed reflection of (100), (110), and (200) planes, belonging to *P6mm* space group of MCM-41 mesoporous materials as can be seen Fig. 23. [77,202,272]

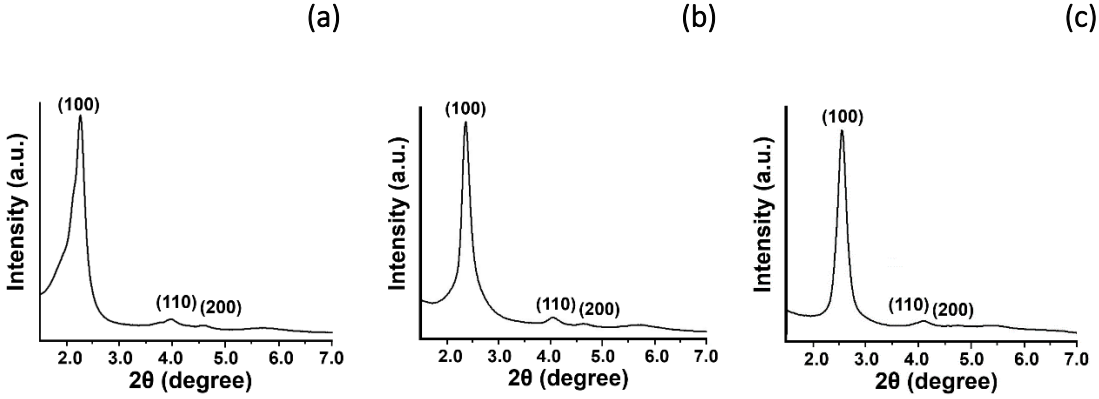

Fig. 23 SAXS patterns of (a) MCM-41-S, (b) MCM-41-C, and (c) MCM-41-MW

The morphology and size of as-synthesised materials were investigated by SEM and TEM. SEM images (**Fig. 24**) reveal the homogeneous phase of as-synthesised materials. The small size of nanostructures can be seen forming the agglomeration which could be confirmed by TEM.[201] These images show the pore structure of MCM-41 which can be seen from the honey-comb structure of MCM-41.[74,202] This suggested that the characteristic structural element of MCM-41 is the hexagonal packing of the pores. The possible formation of ordered mesoporous structure of MCM-41 could be explained by the schematic illuatrated in **Fig. 25**.

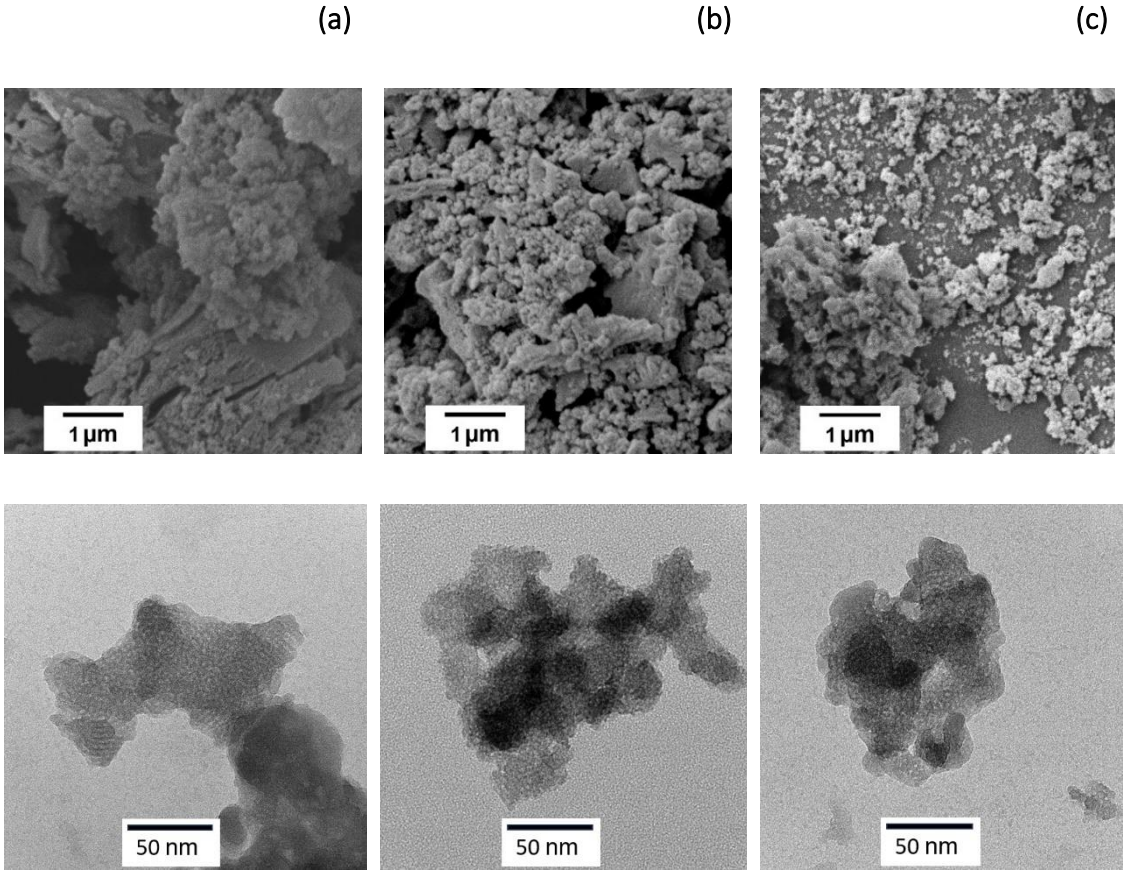

Fig. 24 SEM and TEM images of (a) MCM-41-S, (b) MCM-41-C and (c) MCM-41-MW

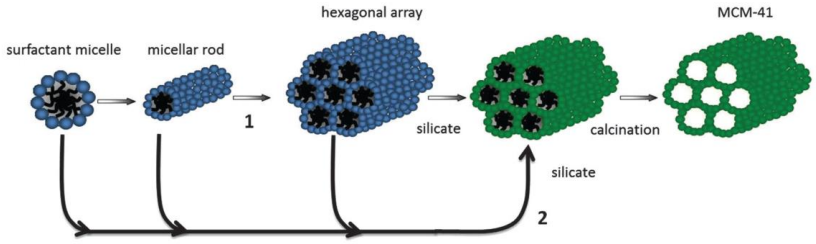

Fig. 25 Schematic illustration for the preparation of MCM-41

(1) preformation of surfactant micellar rods, and (2) formation of surfactant–silicate rods to form MCM-41[199]

2.3.3 Microwave-assisted method using sodium silicate solution derived from rice husk with varying ratios of CTAB:Si

The effect of CTAB:Si ratio on the properties of the resultant materials were investigated and discussed in this part. The textural properties of MCM-41 samples determined by N_2 adsorption-desorption analysis using various molar ratio of CTAB:Si (0.02-0.2:1) are shown in **Fig. 26**. BJH pore size distribution of MCM-41 synthesized using sodium silicate solution derived from rice husk was also represented in **Fig. 27**. N_2 adsorption-desorption isotherms have a Type IV classification confirming that the products display mesoporosity of MCM-41. All isotherms show a Type B or H4 hysteresis loop. BET surface area, pore diameter and pore volume derived from the N_2 adsorption–desorption measurements shown in **Table 6**. The results show that the as-synthesised MCM-41 materials exhibit high surface area. The ratio of CTAB:Si of 0.2:1 produced the highest BET surface area with uniform of mesoporous structure. The increasing of BET surface area was found with the same trend as the increase of CTAB:Si ratio. Whereas, as the CTAB ratio drops to its lowest value, the as-produced materials move away from the typical MCM-41 structure and develops a different pore structure. The decrease of CTAB:Si resulted in the decrease of pore volume. This could suggest that the optimum ratio of CTAB:Si is found to be at least 0.2:1 due to the insufficient amount of CTAB not being able to form the proper surfactant

micellar rods, thus resulting in undesirable materials. Overall pore volume also seems to decrease with reduces CTAB amounts.

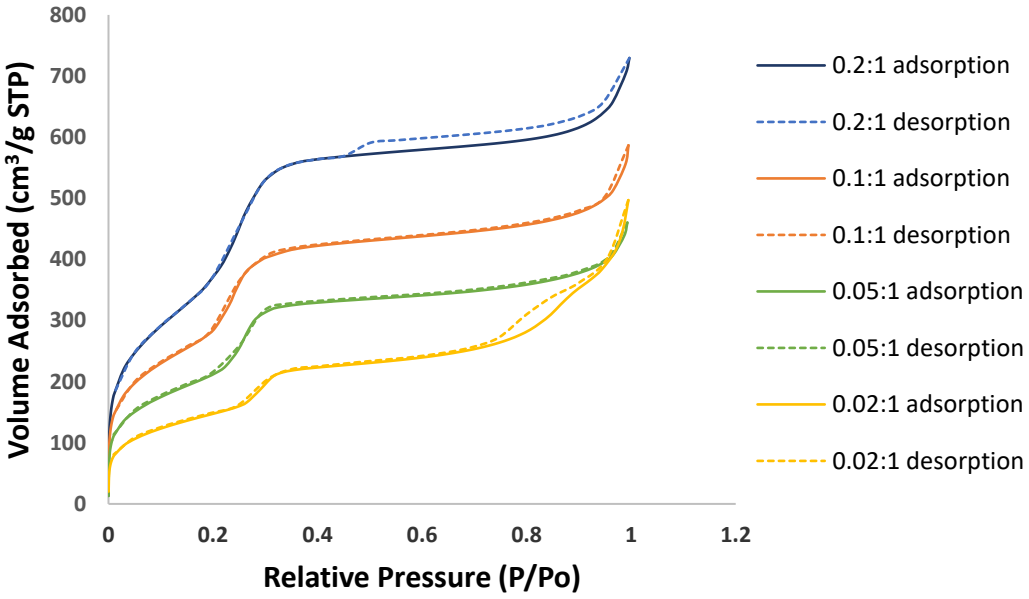

Fig. 26 The N_2 adsorption-desorption isotherms of MCM-41 synthesized using various molar ratio of CTAB:Si (0.02-0.2:1) from silicate solution

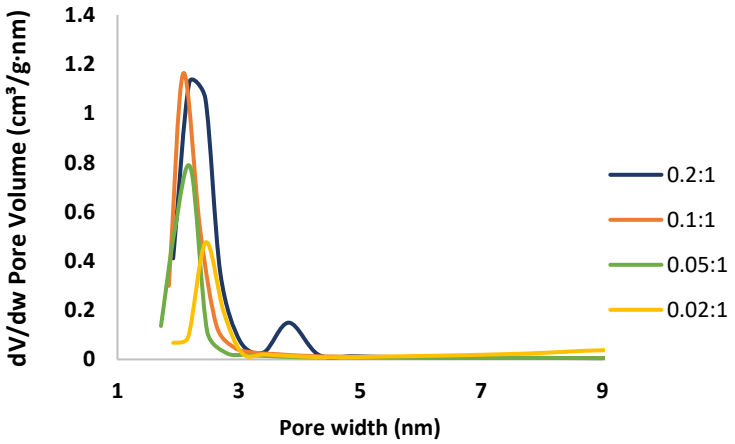

Fig. 27 BJH pore size distribution of MCM-41 synthesized using sodium silicate solution derived from rice husk (molar ratio of CTAB:Si = 0.02-0.2:1)

Table 6 Porosity properties of MCM-41 synthesized using sodium silicate solution derived from rice husk via microwave-assisted method

Ratio CTAB:Si	BET Surface area ($m^2 g^{-1}$)	Pore volume ($cm^3 g^{-1}$)	Average pore diameter (nm)
0.2:1	1372	0.72	2.82
0.1:1	1028	0.74	2.88
0.05:1	776	0.59	0.88
0.02:1	540	0.56	4.14

SEM images reveal the morphology of all as-synthesised materials represented in Fig. 28. Both of as-synthesized products at ratio 02:1 and 0.1:1 represent small size of homogeneous phase which correspondence with the relatively high value of BET Surface area of 1372 $m^2 g^{-1}$ and 1028 $m^2 g^{-1}$, respectively. Some of irregular shapes were found in both the as-synthsized products at the ratio of 0.05:1 and 0.02:1 resulted in the decrease of BET surface area of those samples (776 $m^2 g^{-1}$ and 540 $m^2 g^{-1}$).

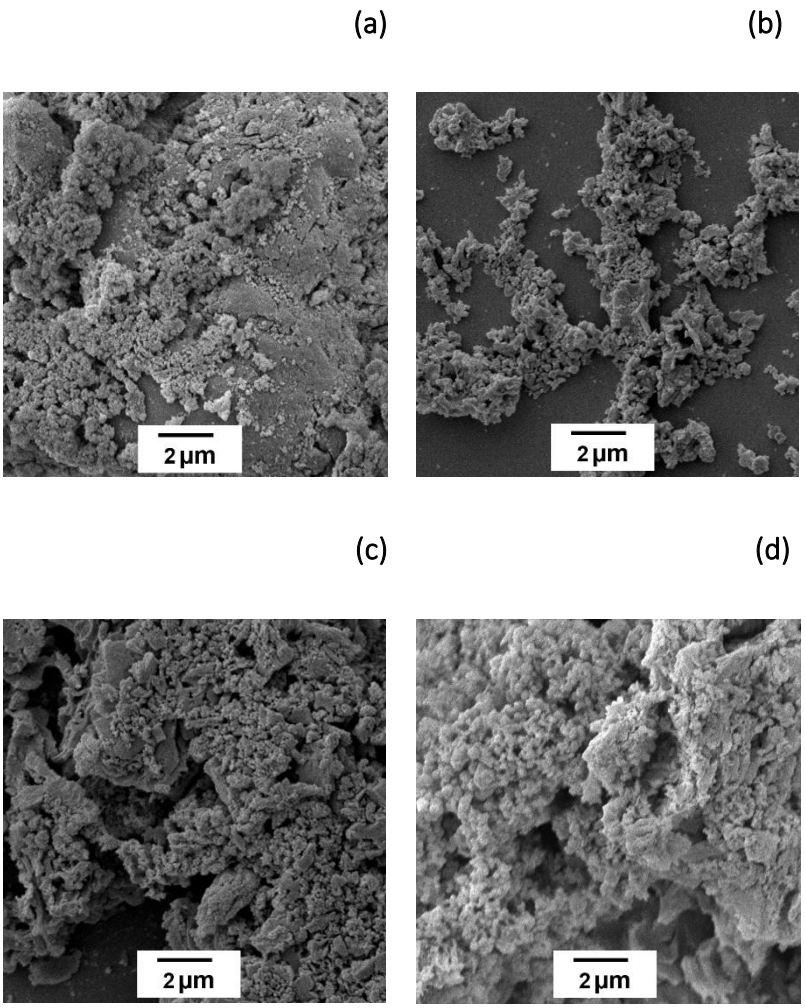

Fig. 28 SEM images of MCM-41 synthesized using various molar ratio of CTAB:Si at (a) 0.2:1 (b) 01:1 (c) 0.05:1 (d) 0.02:1 using sodium silicate solution derived from rice husk

TEM images illustrate the morphology and size of all as-synthesised materials as can be seen in Fig 29. Both of as-synthesized products at ratio 02:1 and 0.1:1 show small size of homogeneous phase — in good accordance with the BET Surface area and average pore diameter value of 2.82 nm and 2.88 nm, respectively. Whereas, TEM images of products synthesized at 0.05:1 and 0.02:1 represent some of irregular shape of structure which might be caused by the insufficient amount of CTAB in the synthesis step and could not

be formed properly surfactant micellar rods as a template for MCM-41 preparation. Also, with less surfactant, maybe some of the silica forms without a template, so is amorphous phase. These might lead to the mix phases of MCM-41 and silica were form — in accordance with some irregular shapes were found in TEM images with the decrease of surface area.

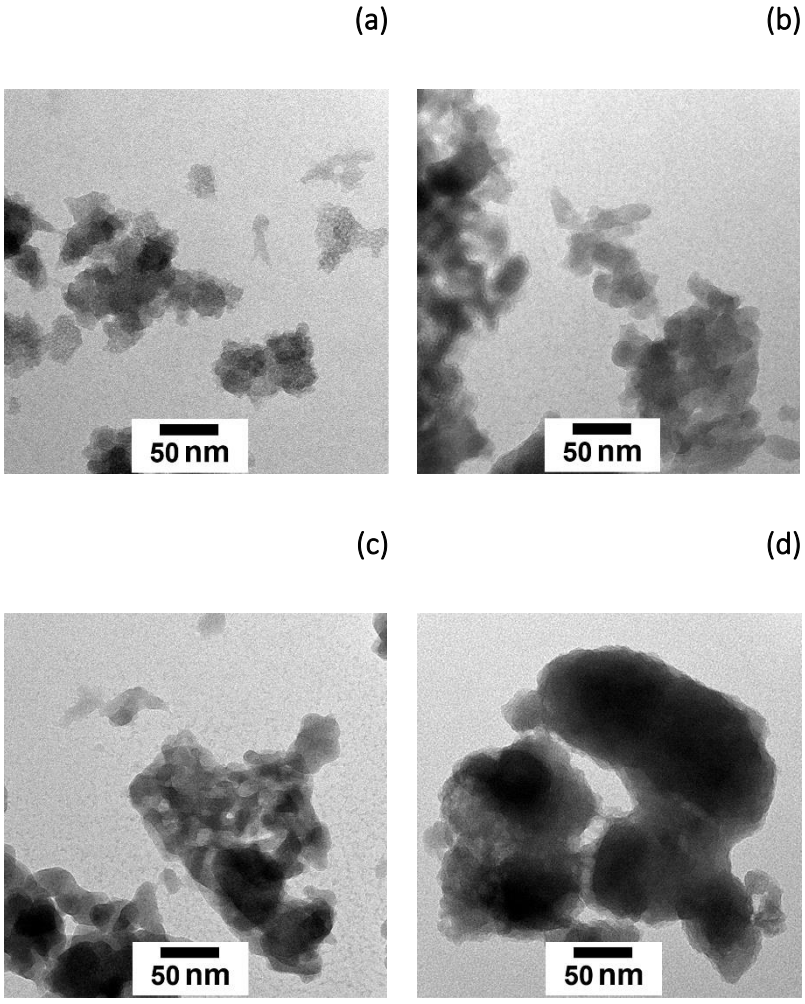

Fig. 29 TEM images of MCM-41 synthesized using various molar ratio of CTAB:Si at (a) 0.2:1 (b) 01:1 (c) 0.05:1 (d) 0.02:1 using sodium silicate solution derived from rice husk

2.4 Synthesis of silica particles via acid precipitation

Silica derived from rice husk in the previous section possess the BET surface area in the range of 309-334 $m^2\ g^{-1}$ and average pore volume around 0.3 $cm^3\ g^{-1}$. This section investigated in more detail about the acid precipitation method for improving the surface area as well as the pore volume of the resulting materials.[273]

2.4.1 Comparison of different methods

The comparison of acid precipitation (H_2SO_4 and HCl) under the sonication assisted method and simple wet chemical method without using any template were reported for the as-obtained silica material. Different methods and acid conditions and the results data of BET surface area, pore volume and pore diameter of materials are shown in **Table 7**. The N_2 adsorption-desorption isotherms of all material also illustrated in **Fig. 30**.

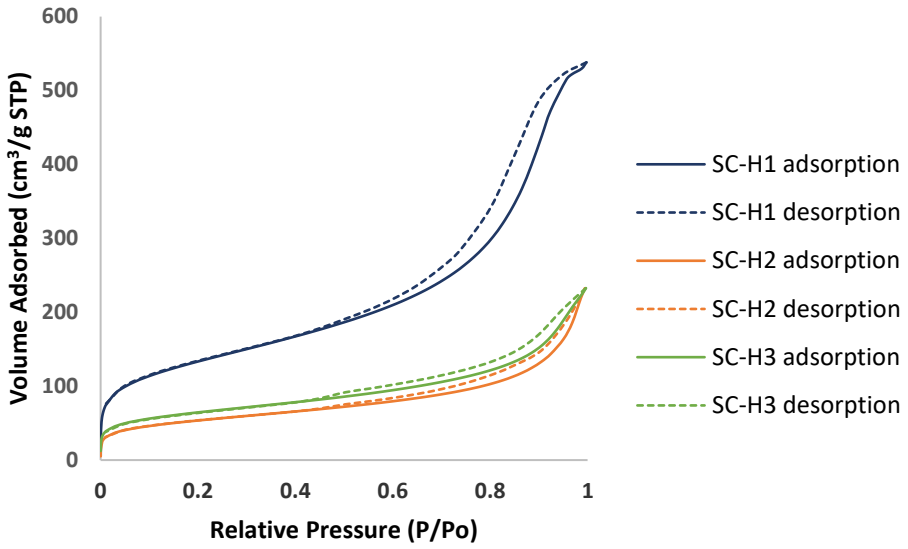

Fig. 30 The N_2 adsorption-desorption isotherms of SC-H1, SC-H2 and SC-H3 synthesised via acid precipitation from sodium silicate solution derived from rice husk

Table 7 Porosity properties of silicas via acid precipitation from sodium silicate solution derived from rice husk

Material	Method	BET Surface area ($m^2 g^{-1}$)	Pore volume ($cm^3 g^{-1}$)	Average pore diameter (nm)
SC-H1	H_2SO_4 precipitation by sonication	479	0.75	6.28
SC-H2	HCl precipitation by simple wet chemical method	395	0.23	4.72
SC-H3	H_2SO_4 precipitation by simple wet chemical method	229	0.26	4.60
SC-H4	HCl precipitation by sonication	-	-	-

Note*** SC-H4 condition can produce only the gel rather than a precipitate

It was found that the product produced by using H_2SO_4 under the sonication assisted method (SC-H1) has highest surface area (479 $m^2 g^{-1}$) and pore volume of 0.75 $cm^3 g^{-1}$. The as-obtained SiO_2 materials using HCl and H_2SO_4 for precipitation have pore volume of 0.23 $cm^3 g^{-1}$ and 0.26 $cm^3 g^{-1}$ and also provided the BET surface area of 395 $m^2 g^{-1}$ and

229 $m^2 g^{-1}$, respectively. In contrast, the precipitation of silica by HCl using the sonication assisted method can produce only the gel rather than a precipitate.

In this work, SC-H1 material which precipitated by H_2SO_4 under the sonication assisted method could be selected for using as adsorbent for methylene blue removal. The as-obtained silica material from this study has higher BET surface area than BET surface area of 164 m^2g^{-1} for SiO_2 nanoparticles which synthesized from rice husk reported by Wang *et al.*[263] and 245 m^2g^{-1} for SiO_2 nanoparticles which synthesized from rice husk reported by Adam *et al.*[274]

The characteristic of surface chemistry of silica was determined by FTIR spectroscopy. **Fig. 31** shows the FTIR spectra of silicas prepared via acid precipitation from sodium silicate solution derived from rice husk. The band at 1090 cm^{-1} was attributed to asymmetric Si-O-Si stretching vibration and band at 999 cm^{-1} which can be assigned to the symmetric Si-OH stretching vibrations of silica materials. [209,265]

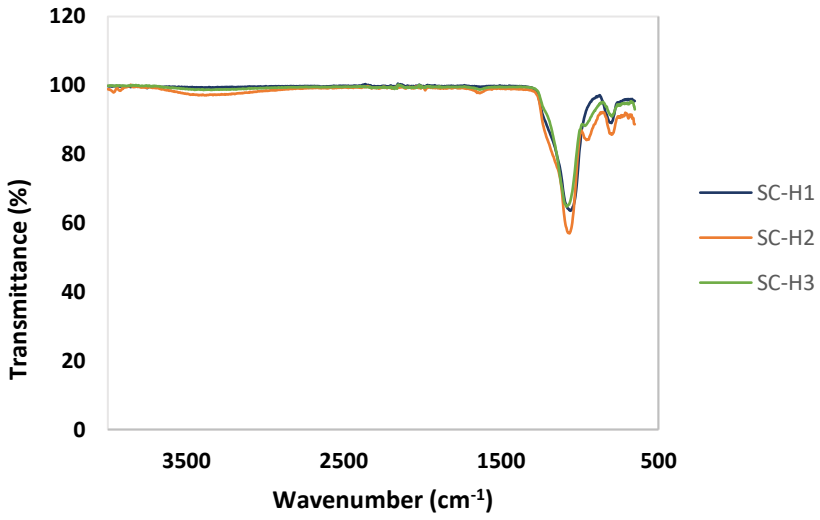

Fig. 31 FTIR spectra of SC-H1, SC-H2 and SC-H3 synthesised via acid precipitation from sodium silicate solution derived from rice husk

To investigate the morphology of SC-H1, SEM and TEM characterization are represented in Fig. 32. SEM image reveals that some irregular shapes of silica was produced with relatively high surface area of 479 $m^2 g^{-1}$ -in corresponding with TEM image with small size in the range of 20-50 nm. This suggests that it can be used as adsorbent for MB removal.

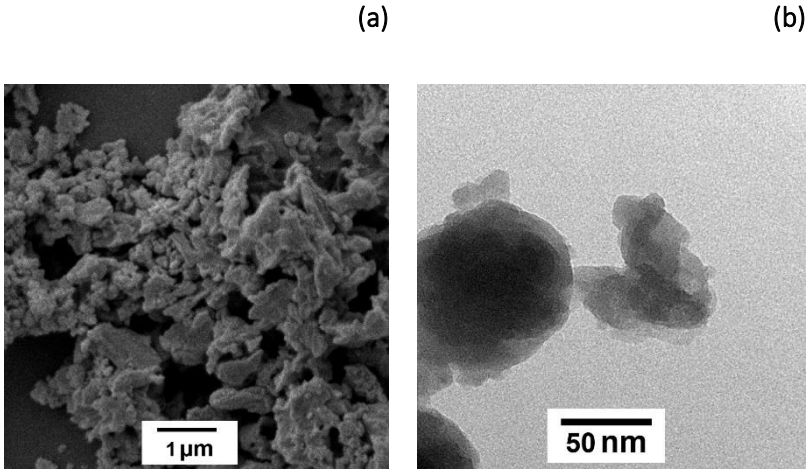

Fig. 32 SEM (a) and TEM (b) images of SC-H1 synthesised via acid precipitation from sodium silicate solution derived from rice husk

2.5 Synthesis of MCM-41 magnetite composite materials

2.5.1 Comparison of different methods

This part represents the as-synthesised MCM-41 magnetite composite materials (CM series) using sodium silicate solution derived from rice husk. MCM-41 magnetite composite materials were prepared using various ratio of CTAB:Si include 0.5:1, 0.2:1 and 0.02:1 were denoted as CM1, CM2 and CM3, respectively.

Magnetite has strong magnetic properties, is low-cost and small particle size. Composite materials would then possess high surface area which can be easily separated from solutions by magnetic separation procedure.[216,275] The specific surface area from BET measurement is 497 $m^2 g^{-1}$ and 534 $m^2 g^{-1}$ for CM1 and CM2 composite materials which reveals the relatively high surface area with the pore volume of 0.55 $cm^3 g^{-1}$ and 0.44 cm^3

g^{-1} as can be seen in **Table 8**. The N_2 adsorption-desorption isotherm of composite materials exhibited type IV behavior (**Fig. 33**), typical for mesoporous MCM-41 materials with uniform porosity <4 nm. The BJH pore size distribution also represented in **Fig. 34**. For this study, N_2 adsorption-desorption isotherm of CM1 material is characteristic of capillary condensation in the pores which is also indicative of the existence of mesopores, indicating that the mesoporous structure could be retained.[214] From results could be also indicate that the reduction on porosity on changing CTAB quantities is the same as was seen for the previous system (section **2.3.3**) so magnetite has no influence these results. In addition, pore volume and pore size of CM1 possess rather higher value than CM2 and CM3, this suggests that it could be a good candidate for using as adsorbent for the next part.

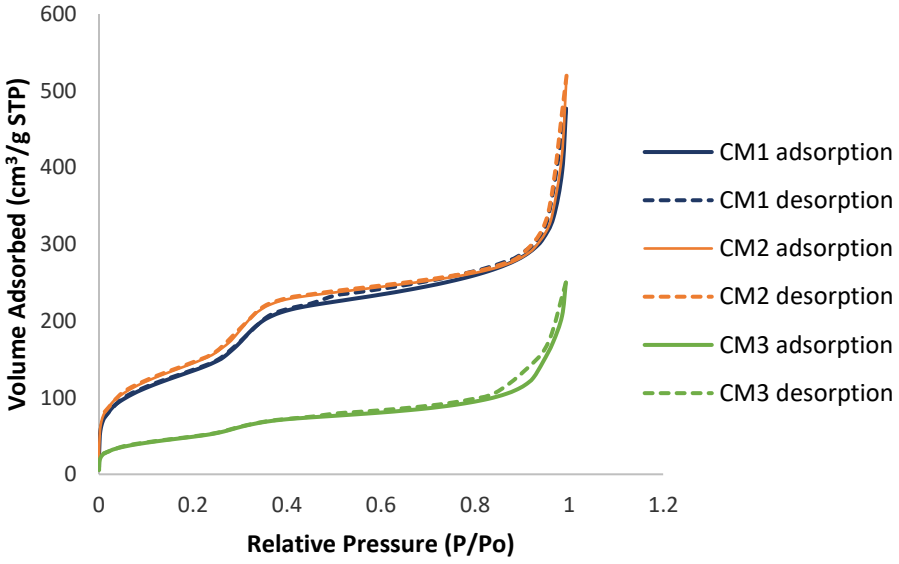

Fig. 33 The N_2 adsorption-desorption isotherms of CM1, CM2 and CM3 materials

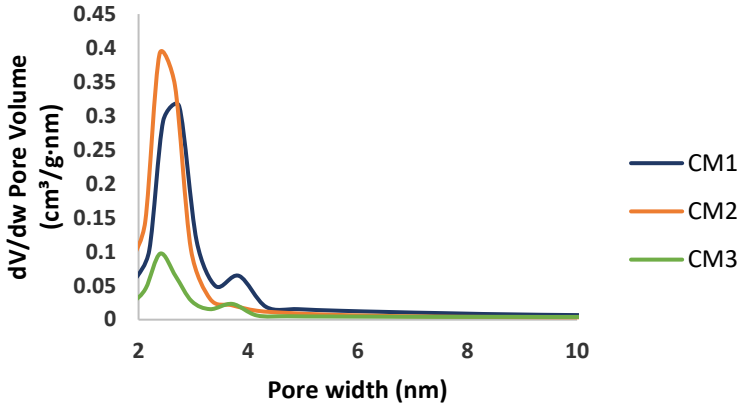

Fig. 34 BJH pore size distribution of CM1, CM2 and CM3 composite materials

Table 8 Porosity properties CM1, CM2 and CM3 composite materials

Sample	Molar ratio of CTAB:Si	BET Surface area ($m^2 g^{-1}$)	Pore volume ($cm^3 g^{-1}$)	Average pore diameter (nm)
CM1	0.5:1	497	0.55	3.58
CM2	0.2:1	534	0.44	3.32
CM3	0.02:1	180	0.20	4.54

To investigate the functional groups of these materials. FTIR spectra of synthesized MCM-41 magnetite composite materials are shown in Fig. 35. These spectra represent of wavenumber in the region between 650 and 4000 cm^{-1}. All materials showed a strong band at around 1060 cm^{-1} due to the Si–O stretching vibration, which is characteristic for this kind of siliceous materials.[94,209] Moreover, a peak at 820 cm^{-1} was attributed to the

Si–O bending vibration.[187,276] The characteristic peak of Fe_3O_4 could be shown at 580 cm^{-1} which is in accordance with the stretching mode of Fe – O bonds of magnetite and a band at 652 cm^{-1} is assigned to stretching vibration of Fe-O-Fe.[184,215,277]

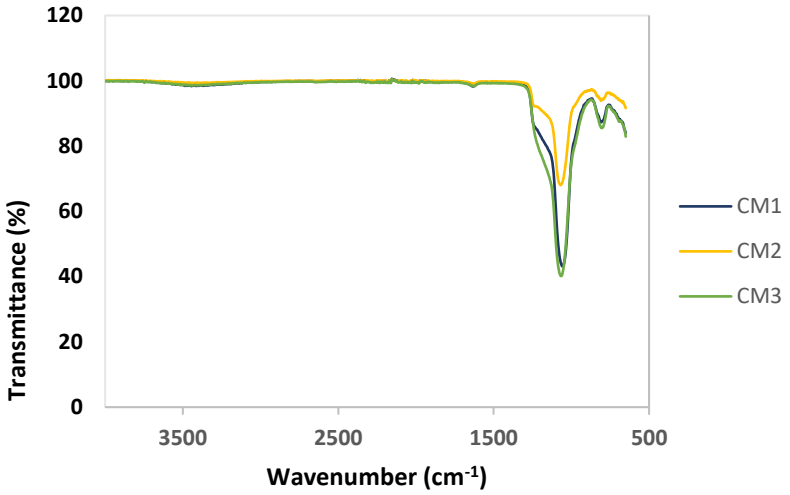

Fig. 35 FTIR spectra of CM1, CM2 and CM3 composite materials

As previous data from N_2 adsorption-desorption isotherm of CM1 material possesses the typical mesopore structure, SAXS pattern in **Fig. 36 (a)** confirmed that CM1 has 2D hexagonal ordering. The reflections can be indexed of (100), (110), (200) and (210) planes, respectively. To confirm that CM1 is a composite material of magnetite nanomaterial. XRD spectra of CM1 and the as-prepared Fe_3O_4 shown in **Fig. 36 (b,c)**. Both as-obtained CM1 and the as-synthesised Fe_3O_4 also reveals the characteristic peaks of Fe_3O_4 at 30.0°, 35.45°, 43.08 °, 53.40°, 57.02° and 62.57° which corresponding to the (220), (311), (400), (422), (511) and (440) planes, respectively.[184,215,216] CM1 exhibits the broad band at around 2θ = 22° which corresponding to silica material. [92,212]

It should be noted that CM1 composite material has the characteristic of both mesoporous MCM-41 and Fe_3O_4 materials meaning it could be a good candidate for MB adsorption in the application section because its high surface area and high ordered

mesopores should make it not only beneficial for adsorption but its magnetic property also benefits via an easy as easy separation by external magnet after water purification.

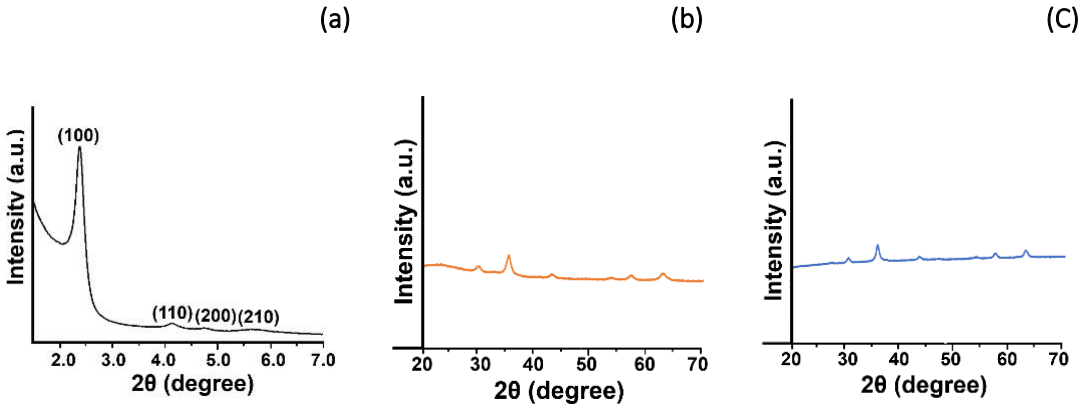

Fig. 36 SAXS pattern and XRD spectra of (a) CM1 composite material and XRD spectra of (b) CM1 composite material and (c) as-prepared Fe_3O_4

SEM and TEM images of CM1 composite material (**Fig. 37**) represent the morphology and size of structure. The homogeneous phase of the as-synthesised CM1 as well as the pore structure of MCM-41 can be observed at the end of structure by TEM characterization. The smaller size of nanostructure suggests that MCM-41 can grow as mesoporous structures. In turn this suggests that the as-prepared MCM-41 could form of those mesoporous structure at the edge of magnetite materials as can be seen from TEM image.

(a) (b)

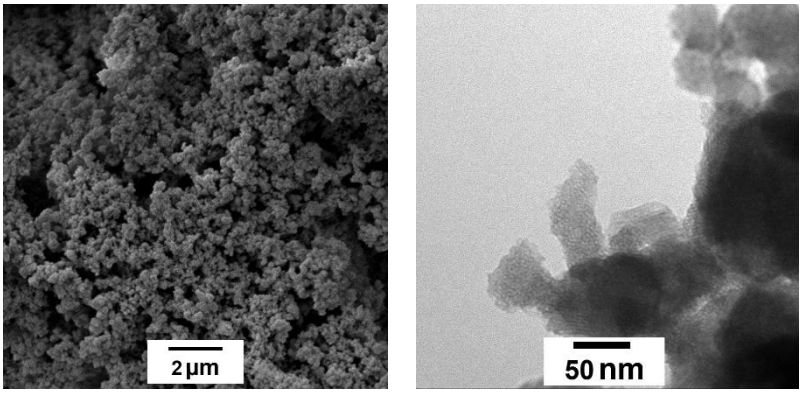

Fig. 37 SEM (a) and TEM (b) images of CM1 composite material

2.6 Application for MB dye adsorption in aqueous solution using as-synthesised mesoporous materials as adsorbent

The remediation of wastewater from dyes is a challenge. Wastewater discharged by the dye industries, which contains harmful organic pollutants can cause water pollution and contaminated groundwater due to its slow rate of biodegradation. Therefore, it needs to be treated before discharging into natural water resources. The adsorption removal is an effective way due to its high adsorption capacity, high selectivity, fast kinetic and cost-effective.[278,279]

The bio-derived high surface area porous materials from rice husk, including MCM-41-MW, SC-H1 and CM1 synthesised in the previous section were selected to study for MB adsorption. This section describes the removal efficiency, kinetic, isotherm and thermodynamic study of these materials. This work was curtailed due to time lost during Covid. In this section the CM1 composite material was used as adsorbent to study the removal efficiency along with MCM-41-MW and SC-H1 derived from rice husk because it has the magnetic property as mentioned before in the previous part so it is beneficial for easy separation from water as represented in Fig. 38.

(a) (b)

Fig. 38 (a) CM1 composite after MB removal and MB standard solution (b) CM1 composite material can be easily separated from solution

2.6.1 Removal efficiency

An ideal adsorbent for water treatment should show a rapid uptake of pollutants and reach equilibrium in a short time. Fig. 39 illustrates that methylene blue dye uptake increased quickly in the first 10-30 minutes and then proceeded slowly after 45 minutes until the equilibrium was achieved.[280] CM-1 composite material shows the best removal rate of all materials (nearly 100% within an hour), while MCM-41 could remove more than 80% of the methylene blue dye (84.22 %) and silica material can only remove 65.50% of the methylene blue dye within 60 minutes.

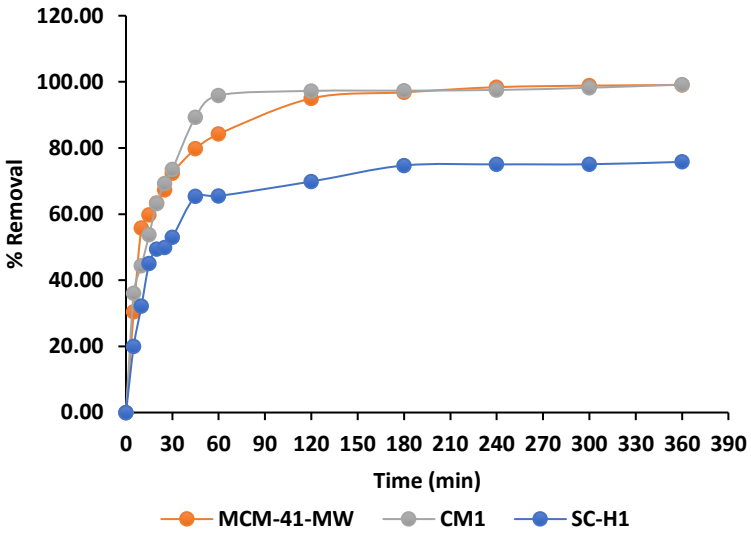

Fig. 39 Removal rate of methylene blue dye solution by using of methylene blue dye solution using MCM-41-MW, SC-H1 and MCM-41 composite

CM-1 composite material not only displays the highest removal efficiency of all material but it also can be easily separated from solution because of its magnetic property thus this material is a good candidate for using as adsorbent for MB adsorption. As a control experiment, magnetite material alone was studied for MB adsorption. The results reveal that Fe_3O_4 could not remove MB from aqueous solution due to its small BET surface area (49 $m^2 g^{-1}$) and pore volume (0.13 $cm^3 g^{-1}$).[66] On the other hand, CM1 composite material has an excellent efficiency of MB removal due to it can be well dispersed in the aqueous solution compared to the mesoporous MCM-41 and silica material, this could be suggested that the MB molecules can be adsorbed onto this material faster than others.

2.6.2 Kinetic study

The investigation of adsorption kinetics is very important to observe the nature of adsorption process. A study of adsorption kinetics provides useful information about the rate and mechanism of methylene blue dye adsorption onto adsorbent (Fig. 40).

An efficient adsorbent should have rapid dye uptake when it is used for wastewater treatment. In this section, MB adsorption kinetics was investigated using the pseudo-first-order model and the pseudo-second-order model.[60,279,281,282] The R^2 and the calculated parameters of the kinetic models including, the equilibrium adsorption amount at equilibrium (q_e), the rate constant of the pseudo first order (k_1), and the rate constant of pseudo second order (k_2) are summarized in **Table 9**.

The R^2 of MCM-41-MW, SC-H1 and CM1 materials were calculated to be 0.9993, 0.9990 and 0.9990-using the pseudo second order model, it can be concluded that the adsorption kinetic process of MCM-41-MW, SC-H1 and CM1 materials were fitted with pseudo second order as can be seen in **Fig. 41**. Moreover, the greater value of R^2 for the pseudo-second-order model of all materials than the value of R^2 for the pseudo-first-order model (R^2 = 0.9766, 0.7853 and 0.7018 for MCM-41-MW, SC-H1 and CM1), indicates that the adsorption kinetics of all materials were fitted with the pseudo-second-order model. [60,201,282-284]

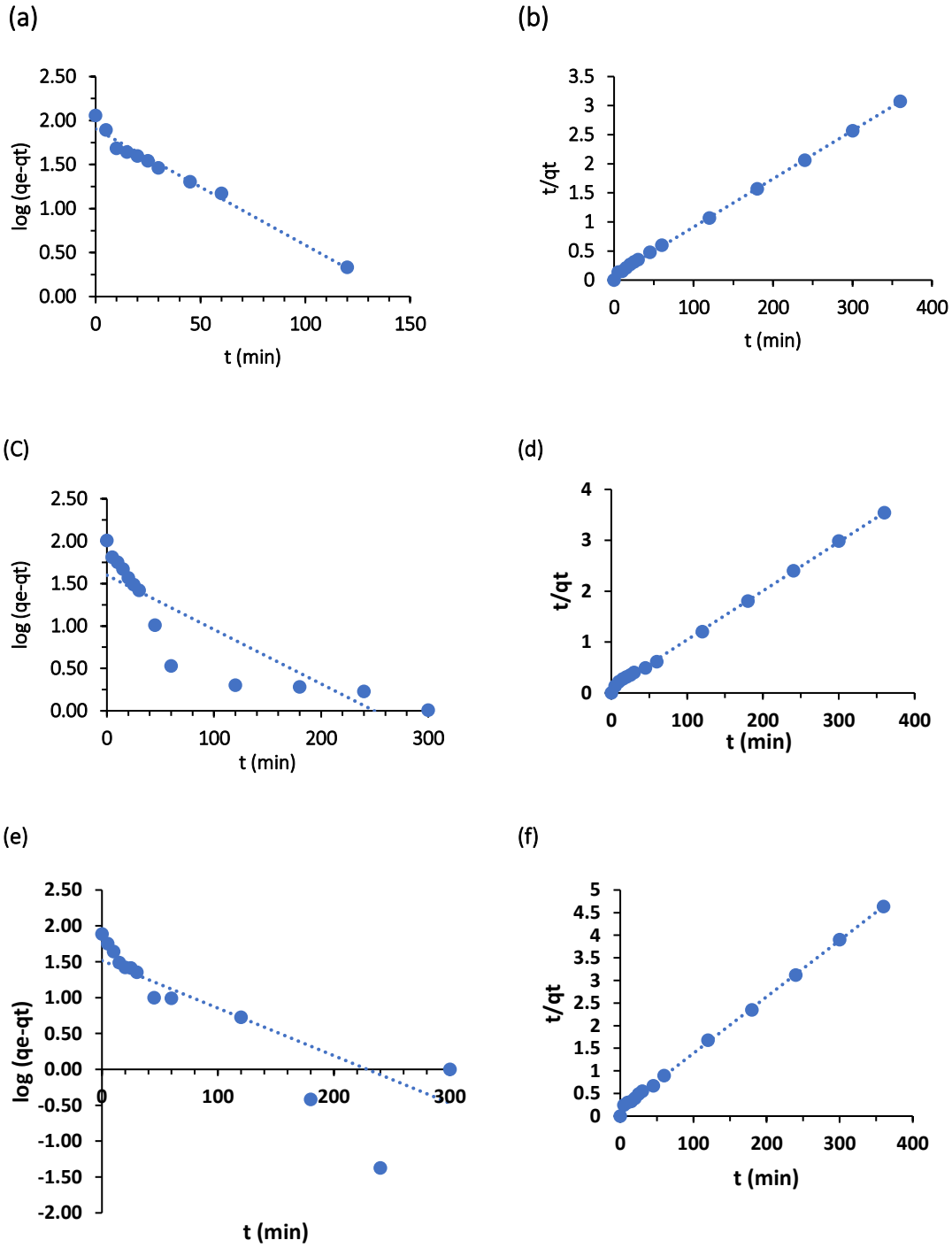

Fig. 40 Kinetic models of MB adsorption by using MCM-41-MW: (a) Pseudo first order (b) Pseudo second order model, using CM1: (c) Pseudo first order (d) Pseudo second order model and using SC-H1: (e) Pseudo first order (f) Pseudo second order model

Table 9 Kinetic parameters of methylene blue dye adsorption on MCM-41-MW, CM1 and SC-H1 materials

Adsorbent	Pseudo first order			Pseudo second order		
	$q_{e,\ cal}$ (mg g^{-1})	k_1 (min^{-1})	R^2	$q_{e,\ cal}$ (mg g^{-1})	k_2 (g mg^{-1} min^{-1})	R^2
MCM-41-MW	80.35	0.030	0.9766	120.48	0.008	0.9993
CM-1	39.72	0.015	0.7853	104.17	0.0011	0.9990
SC-H1	32.79	0.015	0.7018	80.00	0.0011	0.9990

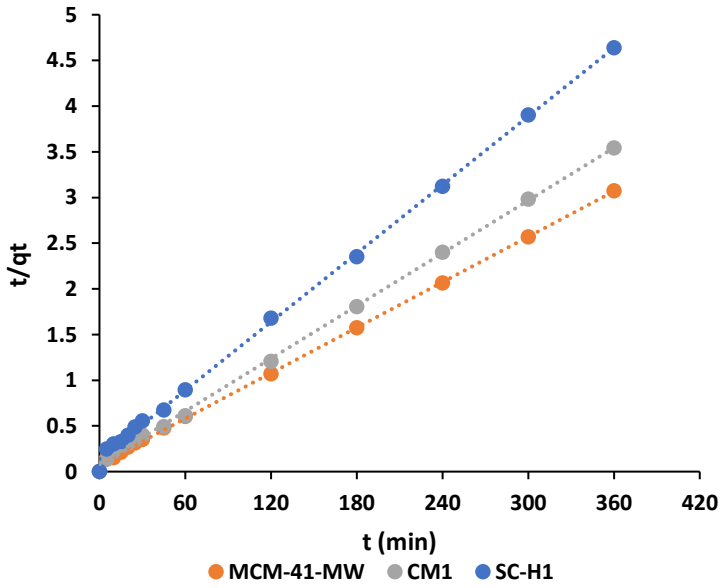

Fig. 41 Pseudo second order model of methylene blue dye solution by MCM-41-MW, SC-H1 and CM1 materials

2.6.3 Isotherm study

Adsorption isotherms describe the amount of adsorbate adsorbed and remained at a fixed temperature in the equilibrium solution. The investigation of adsorption isotherm is necessary to the design of adsorption conditions and the homogeneity and heterogeneity of the surface of adsorbent were also indicated by this study. Adsorption isotherms can be classified into a variety of types, but in this work Langmuir model and Freundlich model were studied. This is because the investigation of adsorption isotherm for porous materials mostly fitted with these isotherms.[60,65,69,93]

Langmuir isotherm and Freundlich isotherm of methylene blue dye adsorption on by MCM-41-MW, CM1 and SC-H1 materials were shown in **Fig. 42**. A comparison of Langmuir and Freundlich isotherm models based on R^2 (**Table 10**), suggested that the Langmuir isotherm is considered the more favorable model for depicting the methylene blue dye adsorption processes for MCM-41 (MCM-41-MW), its composite (CM1) and silica derived from rice husk (SC-H1) due to the high correlation coefficient (R^2> 0.99) which were found that R^2 = 0.9990, 0.9909 and 0.9934 for MCM-41-MW, CM1 and SC-H1, respectively.

This Langmuir isotherm, assumes that the monolayer adsorption process occurs on the homogeneous surface of the adsorbent without considering the interaction between adsorbate molecules.[278,282,285] Whereas, the Freundlich model describes a multilayer adsorption process on the heterogeneous surface of the adsorbent.[93] The results show that all materials have the relatively low value of R^2 for Freundlich isotherm which including, 0.8646 for MCM-41-MW, 0.7131 for CM1 and 0.3700 for SC-H1, respectively.

Moreover, the Langmuir separation factor (R_L) used to predict isothermal type and R_L values (0-1), indicating that the adsorption process is favorable. Thus, R_L used to predict isothermal type in this study and it was found to be 0.014-0.062, 0.021-0.088, and 0.015-0.067 for MCM-41-MW, CM1 and SC-H1, respectively, implying the favorable value.

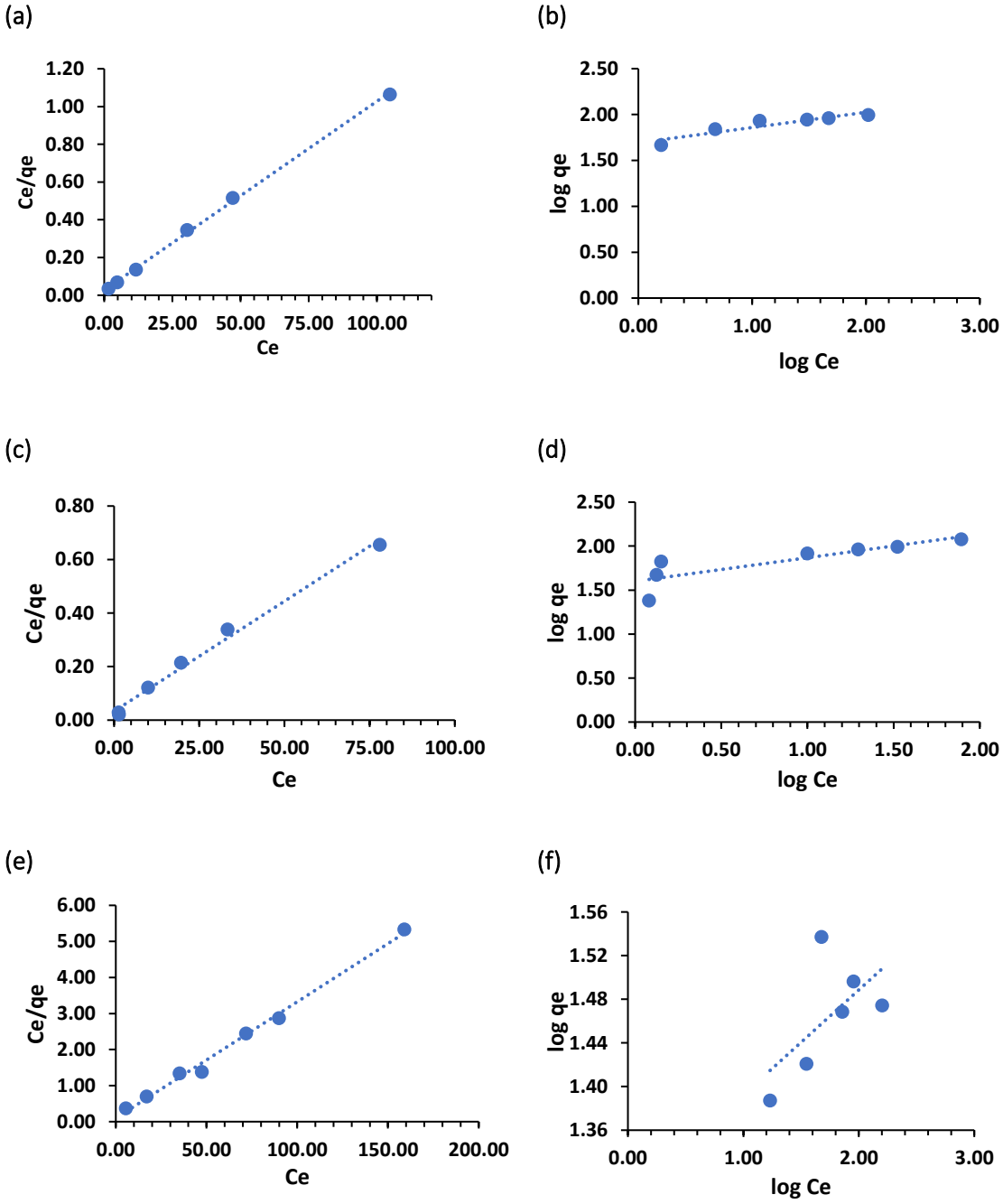

Fig. 42 Isotherm models of MB adsorption on MCM-41-MW: (a) Langmuir isotherm (b) Freundlich isotherm, on CM1 composite material: (c) Langmuir isotherm (d) Freundlich isotherm and on SC-H1: (e) Langmuir isotherm (f) Freundlich isotherm

A comparison of linear forms of Langmuir isotherm model of methylene blue dye adsorption onto MCM-41-MW, CM1 and SC-H1 also shown in **Fig. 43**. The isotherm parameters of adsorption experiments in this study reveal that the maximum adsorption capacities were 100.00 mg g^{-1} for MCM-41-MW, 121.95 mg g^{-1} for CM1 and 30.96 mg g^{-1} for SC-H1, respectively. This might because mesoporous structure of composites could be well dispersed in solution-resulting in greater value of maximum adsorption capacity of CM1 than MCM-41-MW. It should be noted that both MCM-41-MW and its composite (CM1) have high maximum adsorption capacities and suitable for using as adsorbent for MB dye adsorption.

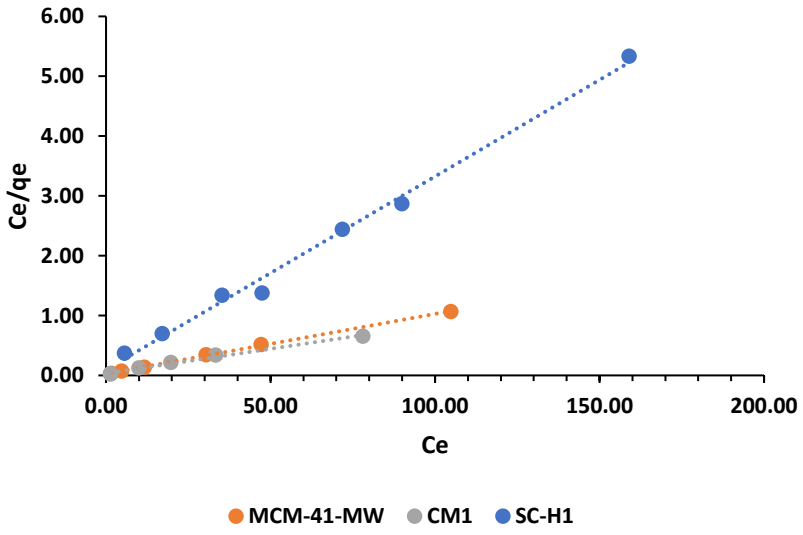

Fig. 43 Langmuir isotherm of methylene blue dye adsorption on by MCM-41-MW, CM1 and SC-H1 materials

Table 10 Isotherm parameters of methylene blue dye adsorption onto by MCM-41-MW, SC-H1 and CM1 materials

Adsorbent	Langmuir				Freundlich		
	q_m (mg g^{-1})	k (L mg^{-1})	R_L	R^2	1/n	k_f	R^2
MCM-41-MW	100.00	0.3750	0.014-0.062	0.9990	0.166	49.26	0.8646
CM1	121.95	0.2477	0.021-0.088	0.9909	0.268	39.80	0.7131
SC-H1	30.96	0.3372	0.015-0.067	0.9934	0.096	19.79	0.3700

2.6.4 Thermodynamic study

To study the effect of temperature on the adsorption process of MB dye on adsorbent and investigate the nature of process, the thermodynamic properties were studied in this part.

Isotherm parameters of methylene blue dye adsorption process onto MCM-41-MW at 298 K, 318 K and 338 K shown in Table 11. From these results, the correlation coefficient (R^2) of all temperatures is relatively high value (>0.99) which were fitted with Langmuir model. The calculated maximum adsorption capacity of MCM-41-MW at 298 K, 318 K and 338 K were found to be 100.00 mg g^{-1}, 116.28 mg g^{-1} and 138.89 mg g^{-1}, respectively. This result illustrates that the higher value of maximum adsorption capacity at higher temperature, which implies that this adsorption process is endothermic in the nature.[62,279,286] The increase in temperature could increase the mobility of the large MB

molecules and enables their penetration within the adsorbent.[287] The Langmuir isotherms of methylene blue dye adsorption on MCM-41-MW at 298 K, 318 K and 338 K were also shown in **Fig. 44**.

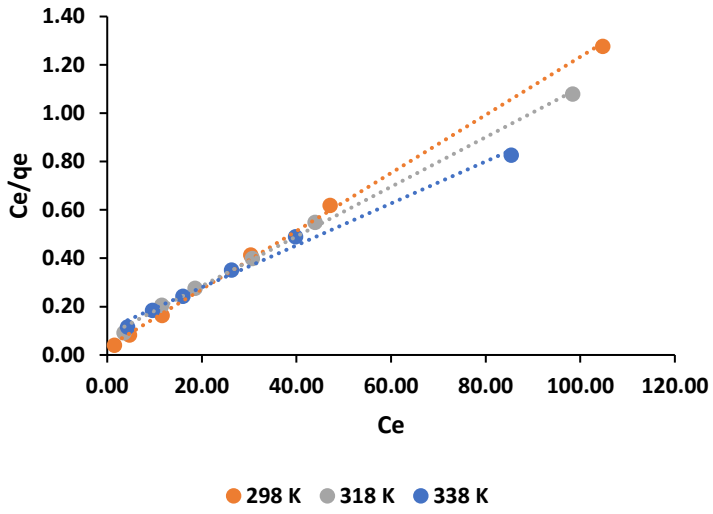

Fig. 44 Langmuir isotherms of methylene blue dye adsorption on MCM-41-MW

Table 11 Isotherm parameters of methylene blue dye adsorption on MCM-41-MW

Temperature (K)	q_m (mg g^{-1})	k_L or b (L mg^{-1})	R_L	R^2
298	100.00	0.375	0.014-0.062	0.9990
318	116.28	0.1293	0.039-0.153	0.9982
338	138.89	0.0814	0.061-0.229	0.9914

The calculated thermodynamic parameters for adsorption of MB onto MCM-41-MW are summarized in **Table 12**. The values of Gibbs free energy change (ΔG) are negative values which indicates that the adsorption of MB dye onto MCM-41-MW is spontaneous in nature.[286] The increasing of temperature resulted in the decreasing of ΔG (more negative

value) which indicate that the adsorption process become more spontaneous which favours in adsorption process.

In addition, the positive values of enthalpy (ΔH) can confirm that this adsorption process is endothermic adsorption. The positive value of entropy (ΔS) confirms the increased randomness at the solid–solution interface during adsorption.[280] This could be that MB has water molecules associated with it (as does the surface), and that these become liberated on adsorption, therefore increasing randomness. The Van't Hoff plot is represented in Fig. 45.

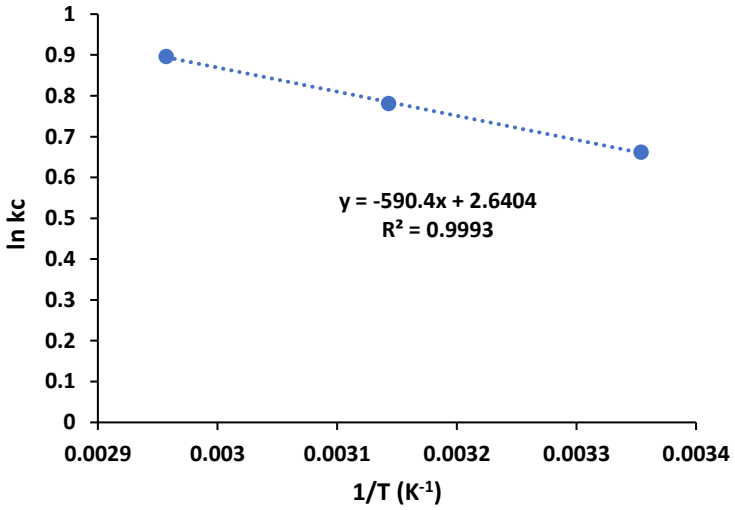

Fig. 45 Plot of ln k versus 1/T for calculation of the adsorption thermodynamic parameters of MCM-41-MW

Table 12 Thermodynamic parameters of MCM-41-MW at different temperature

Temperature (K)	k_c	ΔG (kJ mol^{-1})	ΔH (kJ mol^{-1})	ΔS (J $mol^{-1}K^{-1}$)
298	1.93	-1.64	4.91	21.95
318	2.18	-2.07		
338	2.45	-2.52		

Isotherm parameters of methylene blue dye adsorption process onto CM1 at 298 K, 318 K and 338 K shown in Table 13. From these results, the correlation coefficient (R^2) of all temperatures is relatively high value (>0.99) which were fitted with Langmuir model as also shown in Fig. 46. The calculated maximum adsorption capacity at 298 K, 318 K and 338 K were found to be 121.95 mg g^{-1}, 153.85mg g^{-1} and 169.49 mg g^{-1}, respectively.

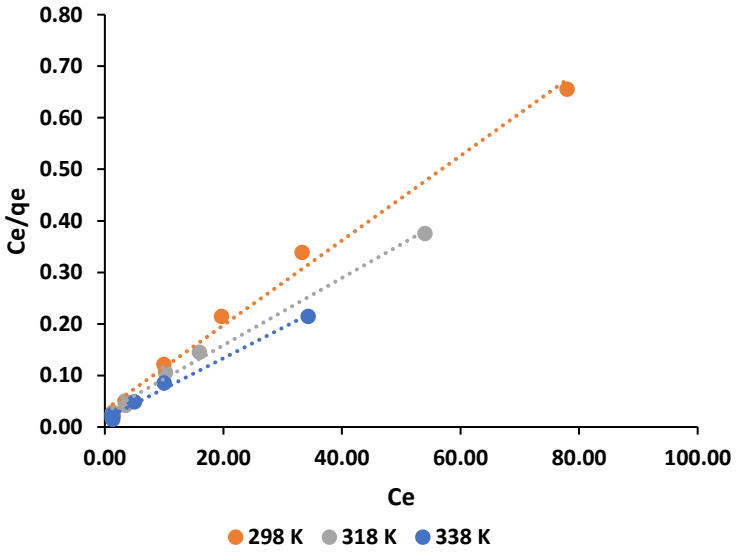

Fig. 46 Langmuir isotherm of methylene blue dye adsorption on CM1 composite material

The increasing of temperature resulted in the increase of the maximum adsorption capacity (q_m) which is in good agreement with an endothermic adsorption process. The Langmuir isotherms of methylene blue dye adsorption on CM1 at different temperature of 298 K, 318 K and 338 K are represented in **Fig. 47**.

Table 13 Isotherm parameters of methylene blue dye adsorption on CM1 composite material

Temperature (K)	q_m (mg g^{-1})	k_L or b (L mg^{-1})	R_L	R^2
298	121.95	0.2477	0.021-0.088	0.9909
318	153.85	0.2320	0.022-0.093	0.9945
338	169.49	0.3831	0.014-0.059	0.9916

The negative values of Gibbs free energy change (ΔG) at different temperature which indicate that the adsorption of MB dye onto CM1 is spontaneous in nature.[286] The thermodynamic parameters for adsorption of MB onto CM1 are summarized in **Table 14**. It was found that the increasing of temperature resulted in more negative values of ΔG, which implies that the adsorption process become more spontaneous, which favours the adsorption process. The Van't Hoff plot of CM1 is also represented in **Fig 48**.

The positive value of enthalpy (ΔH) was calculated to be 28.97 kJ mol^{-1} for CM1 which confirms that this adsorption process is endothermic. Furthermore, the positive value of entropy (ΔS) confirms the increased randomness at the solid–solution interface during adsorption.[280]

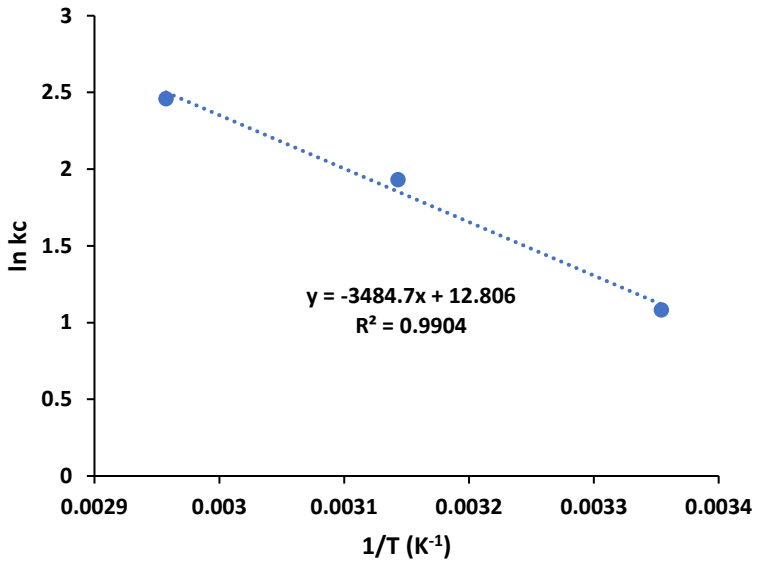

Fig. 47 Plot of ln k versus 1/T for calculation of the adsorption thermodynamic parameters of CM1 composite material

Table 14 Thermodynamic parameters of CM1 at different temperature

Temperature (K)	k_c	ΔG (kJ mol^{-1})	ΔH (kJ mol^{-1})	ΔS (J $mol^{-1}K^{-1}$)
298	2.95	-2.68	28.97	106.47
318	6.90	-5.11		
338	11.70	-6.91		

Isotherm parameters of methylene blue dye adsorption on SC-H1 at 298 K, 318 K and 338 K and were summarized in Table 15. The correlation coefficient (R^2) of Langmuir isotherms were found to be 0.9934, 0.9956 and 0.9939 at 298 K, 318 K and 338 K for CM1. This is relatively high value (>0.99) for all conditions which were fitted with Langmuir model. The Langmuir isotherms of methylene blue dye adsorption on SC-H1 at 298 K, 318 K and 338

K was also shown in **Fig. 48**. The maximum adsorption capacity of CM1 at 298 K, 318 K and 338 K were calculated to be 30.96 mg g^{-1}, 37.45 mg g^{-1} and 42.37 mg g^{-1}, respectively. It should be noted that that this adsorption process is endothermic due to the increasing value of maximum adsorption capacity resulted in the increasing of temperature.[279,286,287]

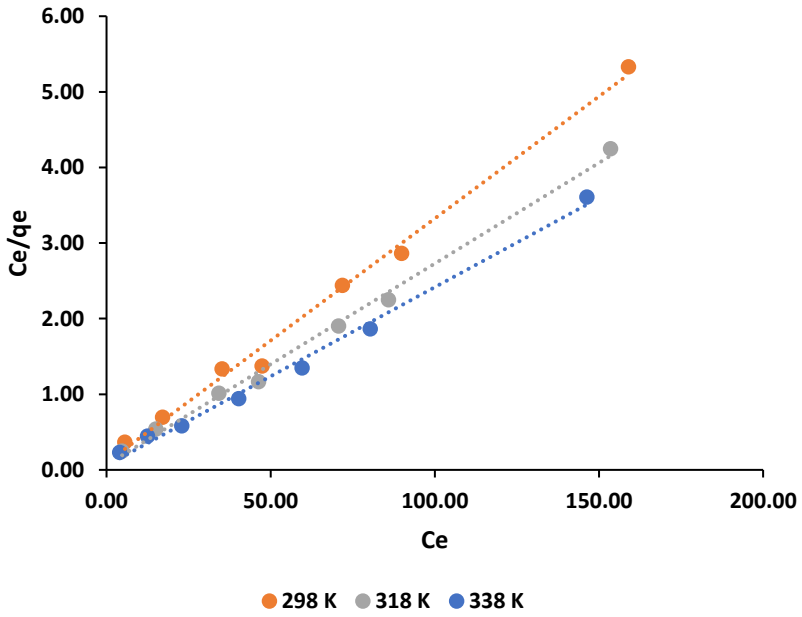

Fig. 48 Langmuir isotherm of methylene blue dye adsorption on SC-H1

Table 15 Isotherm parameters of methylene blue dye adsorption on SC-H1

Temperature (K)	q_m (mg g^{-1})	k_L or b (L mg^{-1})	R_L	R^2
298	30.96	0.3372	0.015-0.067	0.9934
318	37.45	0.4684	0.011-0.048	0.9956
338	42.37	0.4034	0.013-0.058	0.9939

The negative values of Gibbs free energy change (ΔG) at different temperature which indicate that the adsorption of MB dye onto SC-H1 is spontaneous in nature.[286] The thermodynamic parameters for adsorption of MB onto CM1 are shown in **Table 16** and the Van't Hoff plot of SC-H1 is also illustrated in **Fig. 49**. It was found that the increasing of temperature resulted in more negative value of ΔG, which implies that the adsorption process become more spontaneous, which favours the adsorption process.

The positive value of enthalpy (ΔH) of SC-H1 was calculated to be 9.40 kJ mol^{-1} which could be confirm that this adsorption process is endothermic adsorption. In addition, the positive value of entropy (ΔS) is found to be 34.54 J $mol^{-1}K^{-1}$ which could be described that the increased randomness at the solid–solution interface during adsorption.[280]

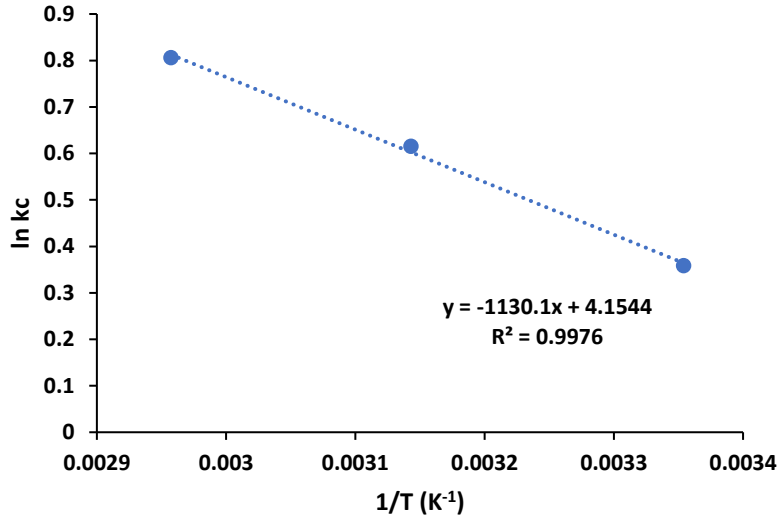

Fig. 49 Plot of ln k versus 1/T for calculation of the adsorption thermodynamic parameters of SC-H1

Table 16 Thermodynamic parameters of SC-H1 at different temperature

Temperature (K)	k_c	ΔG (kJ mol^{-1})	ΔH (kJ mol^{-1})	ΔS (J $mol^{-1}K^{-1}$)
298	1.43	-0.89	9.40	34.54
318	1.85	-1.63		
338	2.24	-2.27		

2.7 Conclusion

In this work, the developed method aimed to valorise abundant agricultural waste biomass in Thailand like rice husk into value-added products though the mild conditions and avoid to use the harsh and toxic chemicals. Furthermore, attempts were made to use this waste as starting materials to synthesis of bio-derived mesoporous materials. These were successfully prepared via the microwave-assisted method as well as using these as-obtained products as adsorbents for the application for MB dye adsorption in aqueous solution.

It was found that the as-prepared bio-based mesoporous magnetite composite product (CM1) exhibits an excellent adsorption property which can be one of the promising materials as adsorbent for water treatment. It is no significant benefit in terms of adsorption but it can be easily separated from wastewater by external magnet resulting in an easier process for waste management after treatment procedure. For example, this material could be reused in the waste water treatment cycle after proper processing. It should be noted that this could be the interesting issue for further investigation.

Chapter 3

Production of cellulose microfibrils/nanofibrils from water hyacinth for bio-composite films preparation

3.1 Production of defibrillated celluloses from water hyacinth

Cellulose is the main structural component in plants, mostly located in the secondary cell wall of plants which is composed of bundles of fibrils of a few microns thickness. Nanocellulose is commonly described as nanoscale of cellulose fibrils which are derived from plant cell walls or bacteria.[157,288-290] Lignocellulosic biomass is composed of cellulose, hemicellulose and lignin so it requires pretreatment to remove noncellulosic components in order to increase the cellulose accessibility and to disrupting cellulose crystallinity.[218] Various pretreatment methods, for example, mechanical treatment, chemical treatments (using alkaline, acid, organosolv, ionic liquid, and so on) have been developed for biomass pretreatment procedures.[10,219,291,292] This part investigated the pretreatment method for production of defibrillated celluloses from water hyacinth and the effect of different pretreatments on the as-obtained products as well reporting on the application for preparation of bio-composite films from as-obtained defibrillated celluloses.[120,148,157,293,294]

3.1.1 Microwave-assisted hydrothermal pretreatment method

Generally, the pretreatment method is one of the important processes to alter lignocellulosic biomass to value-added products.[110] Chemical treatment, physical pretreatment and combination methods have been used for pretreatment such as acid pretreatment, alkaline pretreatment, ionic liquid treatment, ultrasound, steam explosion, etc.[218,236,295] This part describes a mild condition for pretreatment by microwave-assisted hydrothermal pretreatment method without using any chemicals to obtain defibrillated celluloses.[288,296] Microwave-assisted hydrothermal pretreatment method for defibrillated celluloses production shown in Fig. 50.

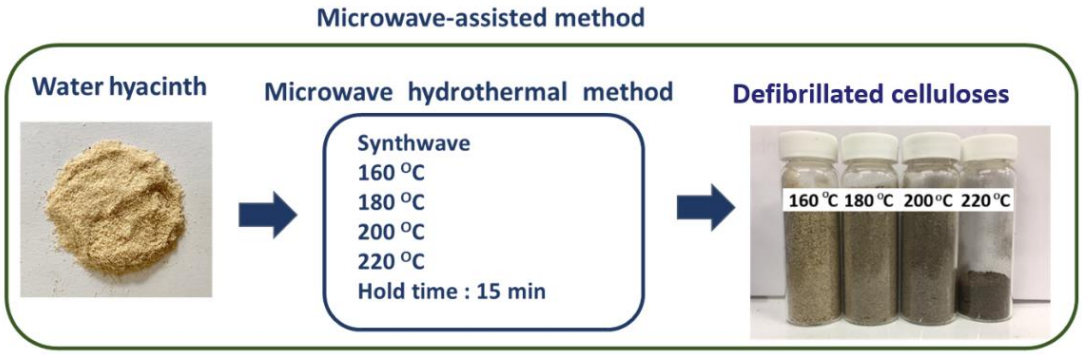

Fig. 50 Diagram of microwave-assisted method for defibrillated celluloses production

Raw fibers (denoted as WH Raw) displayed a light brownish color because of the existence of non-cellulosic substances. In this study microwave-assisted method was selected for pretreatment instead of conventional heating. Microwave hydrolysis is undertaken in an aqueous medium at a lower temperature (100–250 ^{O}C). An increase of brownish color was noted with the increasing of temperature, this may be caused from the degradation and caramelization of carbohydrates.[9,296] Typically, during the acidic hydrolysis process, the hydronium ions penetrated the cellulose chains in these susceptible amorphous regions and accelerated the hydrolytic cleavage of the glycoside bonds, and thus released eventually the individual crystallites.[34]

The as-obtained defibrillated celluloses obtained after microwave treatment at 160 ^{O}C, 180 ^{O}C, 200 ^{O}C and 220 ^{O}C were denoted as WH 160, WH 180, WH 200 and WH 220, respectively.

The crystal structure and degree of crystallinity of the cellulose fibers were determined by an XRD technique, using an X-ray diffractometer. XRD patterns (Fig. 51) exhibited the characteristic diffraction peaks at 15.1° and 22.7° corresponding with (110) and (200) planes, which confirmed the characteristic of cellulose crystal structure.[114] This phenomenon was caused by the interaction between the hydroxyl group bonds in the cellulose forming a crystalline structure. The intensity of 200 plane gradually increased implying that the crystallinity of material increased accordingly.

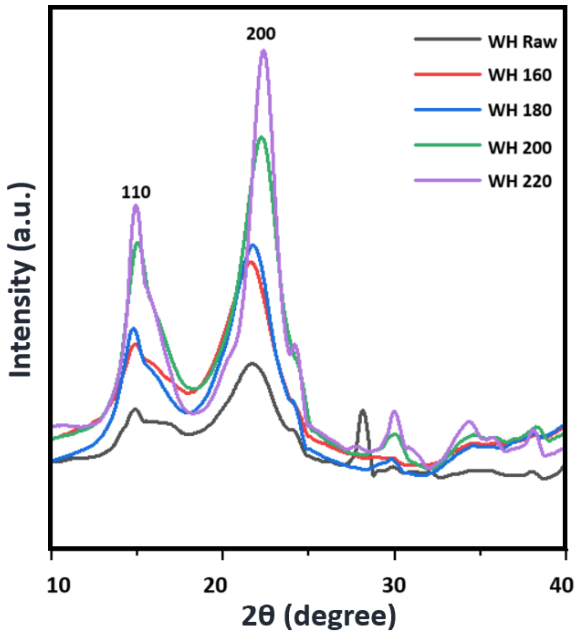

Fig. 51 XRD pattern of the as-obtained celluloses from water hyacinth using microwave-assisted method

Table 17 Crystallinity index and mass recovery (%) of defibrillated cellulose and raw fiber of water hyacinth via microwave assisted method

Samples	CI (%)	Mass recovery (%)
WH Raw	37.9	-
WH 160	45.0	51.4
WH 180	54.9	47.9
WH 200	61.3	37.1
WH 220	72.9	29.2

Mass recovery (%), crystalline structure, and CI analysis were shown in **Table 17** and **Fig. 52**, the CI of defibrillated celluloses from water hyacinth was calculated using the Segal's equation.

CI of raw fibers was found to be 37.9%- a relatively low value compared to the defibrillated celluloses. After treatments via microwave-assisted method, the as-obtained defibrillated celluloses were found to have relative higher CI ranging from 45.0% to 72.9% with the increasing of temperature (for WH 160, WH 180, WH 200 and WH 220). A significant increase in CI was considerably attributed to an efficient elimination of the large amounts of amorphous domains typically consisting of hemicellulose and lignin compounds.[121]

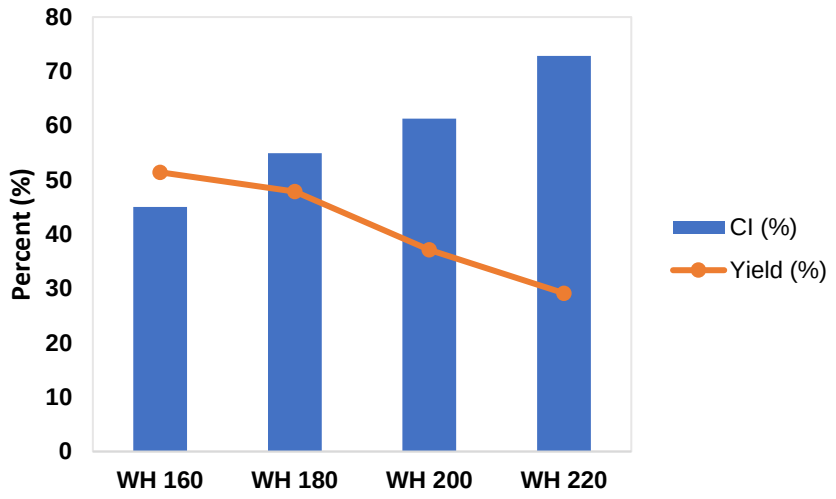

Fig. 52 Yield and crystalline index of the as-obtained defibrillated celluloses at 160 ^{O}C, 180 ^{O}C, 200 ^{O}C and 220 ^{O}C

As can be seen in **Fig. 53**, all spectra exhibited the broad peak around 3300-3400 $cm^{-1}$and 890 cm^{-1} attributable to O–H stretching vibrations and hydrogen bonding in phenolic and aliphatic structures and C-H deformation of anhydroglucose unit in cellulose and hemicellulose of lignocellulosic biomass materials, respectively.[117] Both peaks around 2930 cm^{-1} and 2845 cm^{-1} were assigned to and C-H stretching in aromatic methoxyl groups and in methyl and methylene groups of side chains. All samples also exhibit peak

at 1640 cm^{-1} was attributed to O-H bending vibration in water and at 1,060 cm^{-1}, attributable to C–O stretching of the cellulose structure.[9]

WH Raw, WH 160 and WH 180 also show a shoulder peak at 1730 cm^{-1}, denoting a C=O stretching vibration in carbonyl derivatives in ferulic and p-coumeric acids of lignin.[9,297] Moreover, the peaks at 1510 cm^{-1} and 1260 cm^{-1} were associated with C=C stretching of aromatic skeleton in lignin and C-O vibration of guaiacyl ring in lignin molecules.[117] These peaks could also be found in raw fibers, WH 160 and WH 180 samples but were significantly decreased in WH 200 and WH 220. This could imply that major fraction of lignin was mostly removed at 200 ^{O}C by using microwave-assisted method. Decomposition of lignocellulosic components under pressurized compressed hot water under the microwave irradiation has been reported to occur at different temperatures.[36,298] Hydrolysis of hemicellulose starts at 160 °C, while lignin start melting at 170–180 °C and partially reprecipitated on the biomass surface after the pretreatment.[298] The purer cellulose was found at 200 °C thus the optimum condition for defibrillated cellulose production could be at 200 ^{O}C. Assignment of FTIR spectra of Raw fiber, WH 160, WH 180, WH 200 and WH 220 is given in Table 18.

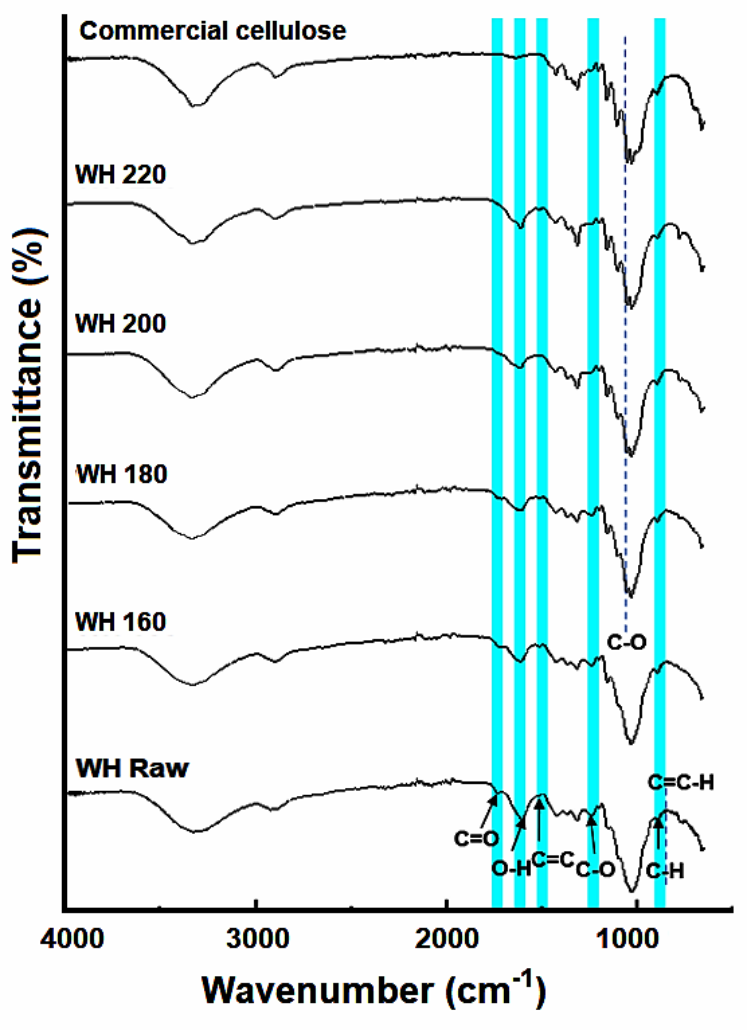

Fig. 53 FTIR spectra of WH Raw, WH 160, W 180, WH 20, WH 220 and commercial cellulose

Table 18 Assignment of FTIR spectra of Raw fiber, WH 160, WH 180, WH 200 and WH 220

Wavenumber (cm^{-1})	Assignment
3300-3400	O–H stretching vibrations and hydrogen bonding in phenolic and aliphatic structures
2930 and 2845	C-H stretching in aromatic methoxyl groups and in methyl and methylene groups of side chains
1730	C=O stretching vibration in acetyl groups of hemicellulose or ester linkage in carboxylate derivatives in ferulic and p-coumeric acids of lignin
1510	C=C stretching of aromatic skeleton in lignin molecules
1260	C-O vibration of guaiacyl ring in lignin molecules
1060	C–O stretching in cellulose
1030	C–C stretching vibration in cellulose
890	C-H deformation of anhydroglucose unit in cellulose and hemicellulose of lignocellulosic biomass materials

The thermal properties of WH Raw, WH160, W180, WH200 and WH220 were investigated by differential thermogravimetric analysis (DTG) which is shown in Fig. 54. The first transition occurred over a temperature range between 75 and 125 °C, corresponding to the dehydration of adsorbed water molecules in fibers.[131] The second transition temperature begins from 220 ^{O}C to 315 ^{O}C, attributed to the decomposition of the

hemicellulose found in the water hyacinth fibers. Cellulose subsequently decomposed from 315 ^{O}C to 400 ^{O}C due to the decomposition of glycosidic linkages.[9] It is believed that the main degradation for water hyacinth raw fiber and defibrillated celluloses which occurred between 250 °C and 358 °C was due to the depolymerisation, dehydration and decomposition of glycosyl units. In this part, the highest peak degradation was found to be 358 °C which implied that WH 200 can maintain its thermal stability better than WH 220.[131] As a consequence, WH 200 was selected for used as reinforcement in bio-composite films preparation in the latter part. The lower decomposition temperature of WH Raw than WH160, W180, WH200 and WH220 due to it containing lignin and hemicelluloses.

Lignin decomposition occurred over a wider range of temperature (between 200 ^{O}C and 600 ^{O}C) than hemicellulose and cellulose owing to its structure composed of various functional oxygen groups with different thermal stabilities. Thermal decomposition of lignin can be divided into two major stages.[164,299] A small component of lignin was degraded at the initial decomposition of lignin which found between 120 ^{O}C and 300 ^{O}C, resulted in the fragmentation in the phenyl propane side chains at the end positions.[300] The main thermal decomposition occurs between 300 and 480 °C, resulting in the fragmentation and cleavage of the major chain linkages between monomeric phenol units in the lignin structure yield carbon dioxide, carbon monoxide, methanol, water, methane, and two phenolic compounds (guaiacol and a 2-methoxy-4-alkyl-substituted phenol).[299,301] In contrast, cellulose is more stable at high temperature due to it having a highly ordered arrangement of linear polysaccharide polymer with higher molecular weight than hemicellulose.

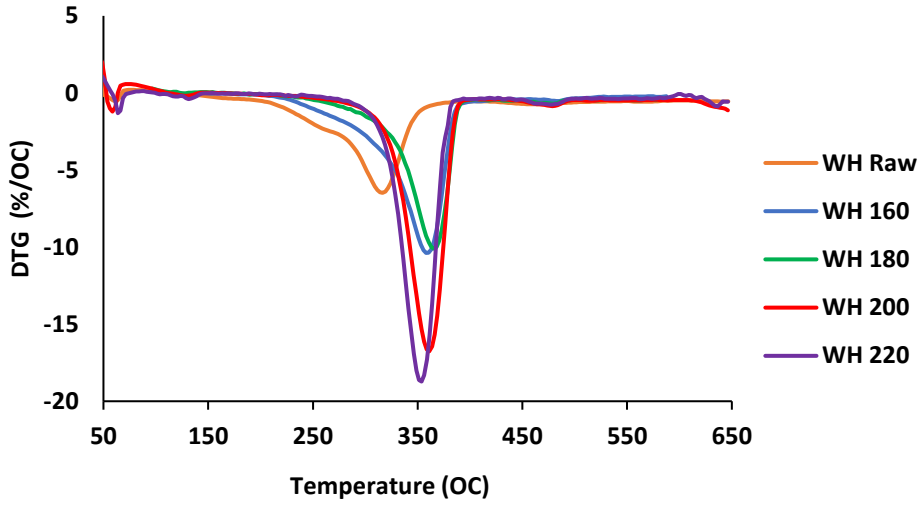

Fig. 54 Differential thermogravimetric analysis (DTG) of WH Raw, WH160, W180, WH200 and WH220

This part demonstrated that defibrillated celluloses from water hyacinth were successfully prepared using a microwave-assisted method. FTIR analysis strongly confirmed that the successful removal of hemicellulose and lignin after HCW pretreatment under microwave irradiation at 200 ^{O}C.[116] Microwave heating has a potential to increase the temperature and the cellulosic structure with the expansion of water molecules resulting in the increasing efficiency of hydrolysis step.

The structural properties of WH Raw and the as-prepared WH 200 were characterized by SEM spectroscopy presented in Fig. 55. The ground WH Raw shows the rigid and smooth surface being still intact. After pretreatment by microwave-assisted method the raw fibrous structure has been disorganized and the surface of each bundle has loosened and swelled after pretreatment.[302] However, there are still some irregular shapes which might be a proportion of lignin or other impurities, which were observed in Fig. 55 (c).

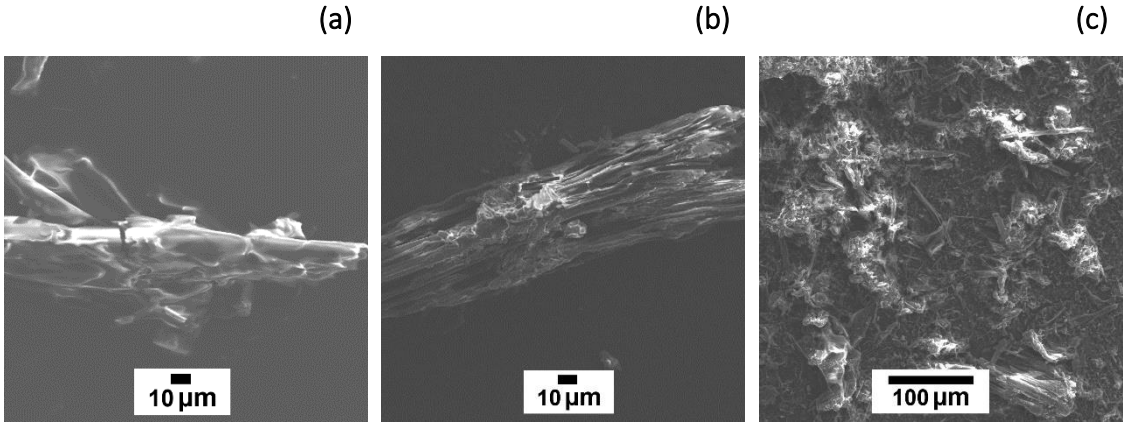

Fig. 55 SEM images of (a) WH Raw (b-c) WH 200 at different magnification

3.1.2 Chemical treatment

Over the past few decades, various pretreatment methods, such as mechanical and chemical treatments using alkali, acid, organosolv and ionic liquids have been developed for pretreatment methods.[24,218,239,303] This part represented the alkaline-treated fibers (denoted as WH-A), bleached fiber with using $NaClO_2$ (denoted as WH-B1) and bleached fiber with chlorine free method (denoted as WH-B2). Chemical pretreatment of water hyacinth is shown in Fig. 56.

Fig. 56 Diagram of chemical pretreatment of water hyacinth

3.1.2.1 Alkaline pretreatment

Alkaline pretreatment using sodium hydroxide is one of the most common steps used to study the conversion of lignocellulosic biomass. It is an effective way to increase the digestibility of biomass like water hyacinth with low lignin content.[9,180] Thus, cellulose obtained via alkaline treatment has been the primary focus of many researchers due to its advantages, including the employment of relatively low temperatures and pressures than other pretreatment technologies, alkaline processes also cause less sugar degradation than acid processes.[218,304]

3.1.2.2 Bleaching step (Chlorine and chlorine-free bleaching method)

After alkaline treatment subsequently by bleaching step, the as-obtained fibers became colorless and white fibers could be prepared from this step due to the elimination of lignin by the reactions of the chlorine and chlorite ions from $NaClO_2$.[9]

3.1.2.3 Comparison of chemical properties of cellulose fibers after alkaline pretreatment and bleaching step

The crystallinity and CI of WH-Raw, WH-A, WH-B1 and WH-B2 was determined using X-ray diffraction (XRD) as can be seen in **Fig. 57**. Due to the degree of crystallinity of natural fibers is improved by removing the non-crystalline constituents from the fibers through pretreatment method.[121] The dissolution of amorphous cellulose has been observed when cellulose was alkaline-treated-resulting in an increase in crystallinity of the cellulose sample.[305] Therefore, the amorphous cellulose could be removed in alkaline treatment and further removed in bleaching step.[121]

XRD patterns of WH-Raw, WH-A, WH-B1 and WH-B2 before and after pretreatment represents the characteristic peaks of cellulose at 15.6^{O} and 22.5^{O} which corresponding to the 110 and 200 crystal planes of the cellulose. After alkaline treatment, the intensity of XRD peak increased at 22.5^{O} – caused by the removal of the amorphous phase of cellulose. This resulted in the higher percentage of the crystallinity of fibers which was

found that WH-A has relatively high CI value of 76.03%.[131] The same trend with the WH-B1 and WH-B2 after bleaching step, the intensity of XRD peak increased due to the further remove of amorphous phase of cellulose, hemicellulose and lignin, resulting in the higher CI values of WH-B1 (77.55%) and WH-B2 (78.90%) are demonstrated in **Table 19**.

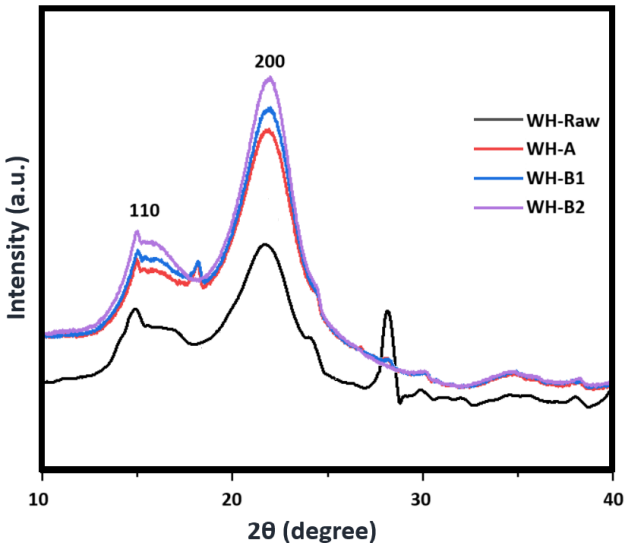

Fig. 57 XRD pattern of the as-obtained WH-Raw, WH-A, WH-B1 and WH-B2

Table 19 Crystallinity index of WH-Raw, and the as-obtained WH-A, WH-B1 and WH-B2 after chemical pretreatment

Samples	CI (%)
WH-Raw	37.89
WH-A	76.03
WH-B1	77.55
WH-B2	78.90

The resulting CI values of WH-A, WH-B1 and WH-B2 are in good agreement with CI values reported by Tanpichai *et al*.[9] Due to an efficient elimination of the large amounts of amorphous domains which consisted of hemicellulose and lignin compounds, significant increases in CI values of WH-A, WH-B1 and WH-B2 are seen.[9]

Fig. 58 represents FTIR spectra of raw fibers, alkaline-treated fibers, and fibers after bleaching process compared to standard cellulose. The peak at 1640 cm^{-1} was assigned to be O-H group from water absorption. The peak at 1260 cm^{-1} were associated with C-O vibration of guaiacyl ring in lignin molecules.[117] It was found that after alkaline treatment, the intensity of peak at around 3400 cm^{-1} was increased due to the deposition of lignin and hemicellulose on the surface and within the fibers was eliminated - in good accordance with the disappearance of the shoulder at around 1,730 cm^{-1} which was ascribed to either acetyl and uronic ester groups of hemicellulose or ester linkages of carboxylic groups of the ferulic and p-coumaric acids of lignin and/or hemicellulose.

The peaks at 1,510 cm^{-1} and 1,260 cm^{-1} were attributed to C = C stretching in the aromatic rings of the lignin structure and assigned to ester, ether or phenol compounds were absent – in good agreement with the stronger intensity of peak at 1061 cm^{-1} presenting the higher content of cellulose.[113] The characteristic peak of lignin's aromatic ring vibration presents at wavenumber 1200–1300 cm^{-1}. This peak was found in raw fibers but were disappeared in alkaline-treated fibers. This should be noted that major fraction of lignin was removed after alkaline-pretreatment method. This is because the alkaline hydrolysis is essentially a delignification process that also results in the solubilization of a considerable percentage of hemicellulose.[304]

Moreover, the pattern of FTIR spectra of WH-B1 and WH-B2 were found the similar pattern in commercial cellulose.[117] This could be confirmed that after bleaching step can be obtained purer celluloses and further lignin and hemicellulose could be eliminated.[240]

Assignment of FTIR spectra of WH-Raw, WH-A, WH-B1 and WH-B2 was summarized in Table 20. These results suggested that after alkaline treatment, the extracted water hyacinth fibers still contained hemicellulose and lignin phases however, the final product after bleaching step can provide the purer cellulose. [9]

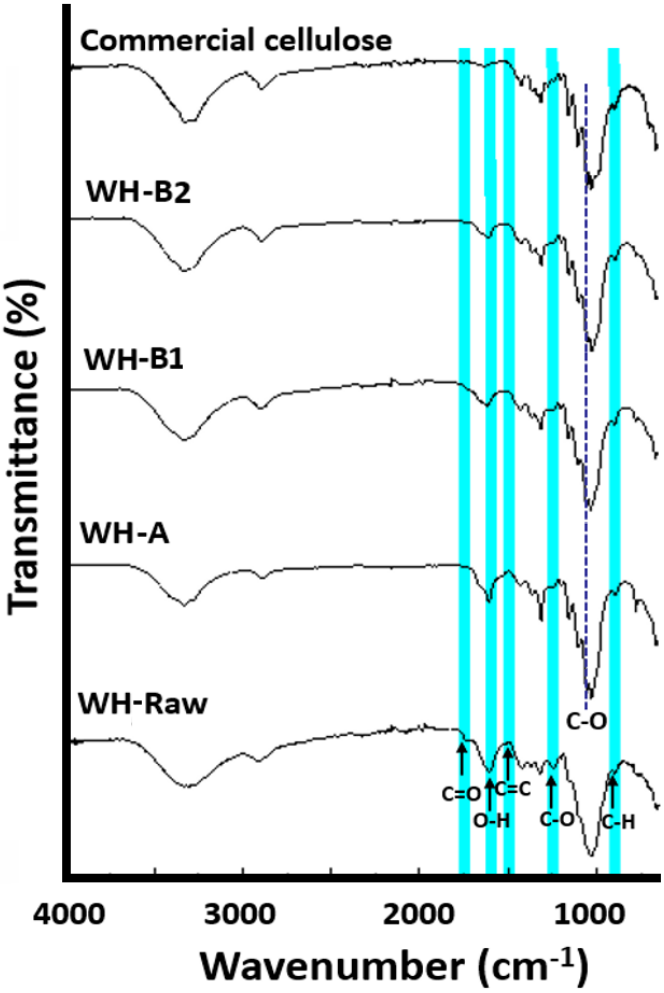

Fig. 58 FTIR spectra of commercial cellulose, alkaline-treated fibers denoted as WH-A, bleached fiber denoted as WH-B and raw fibers denoted as WH-Raw

Table 20 Assignment of FTIR spectra of WH-Raw, WH-A, WH-B1 and WH-B2

Wavenumber (cm^{-1})	Assignment
3300-3400	O–H stretching vibrations and hydrogen bonding in phenolic and aliphatic structures
2930 and 2845	C-H stretching in aromatic methoxyl groups and in methyl and methylene groups of side chains/ polysaccharides
1730	C=O stretching vibration in acetyl groups of hemicellulose or ester linkage in carboxylate derivatives in ferulic and p-coumeric acids of lignin and/or hemicellulose
1510	C=C stretching of aromatic skeleton in lignin molecules
1260	C-O vibration of guaiacyl ring in lignin molecules
1030	C–C stretching vibration in cellulose

Thermogravimetric analysis was carried out in order to study the thermal stability of water hyacinth after alkaline pretreatment and after bleaching step. The thermal stability of fibers after pretreatment by alkaline pretreatment and bleaching step was investigated by DTG curves are shown in Fig. 59. Stage I occurred in the range of 50-125 ^{O}C due to the evaporation of moisture and light volatile component.[11,306] Stage I of WH-Raw started at 50 ^{O}C and finished at 125 ^{O}C which corresponded to the release of moisture and light volatile compounds.[307] This evaporative stage was clearly endothermic. While stage II occurred in the range of 290-390 ^{O}C which correspond to a significant degradation of cellulose, accounting for 30-50% of mass loss. DTG curve shows that WH-A reached the peak of degradation at 350^{O}C.[121] The main degradation of fibers occurred between 250 ^{O}C and 378 ^{O}C due to the depolymerization, dehydration and decomposition of glycosyl

units. Meanwhile, DTG curve of alkaline-treated fiber shows a shoulder at 249 ^{o}C and peak maximum at 350 ^{o}C, indicating the degradation of hemicellulose and cellulose, respectively.[306] The third transition occurred in the range of temperature from 315 °C to 390 °C, corresponding to the decomposition of the cellulose phase. Finally, the weight percent of all samples remained the same and reached the plateau.[308]

Cellulose is extracted by exposing ground fibers to sodium hydroxide, which favorably and efficiently increases the accessibility of the cellulose. The modification of fibers was done by alkaline treatment is the disruption of OH bonding in the fiber network structure by ionizing the hydroxyl groups of the various materials in the fibers to become alkoxide as shown in the following Eq.

$$\text{Fiber-OH} + \text{NaOH} \rightarrow \text{Fiber-O}^{-}\text{Na}^{+} + \text{H}_2\text{O}$$

This leads to the separation of the interfibrillar regions from the cellulose fibers. Even so, the detached cementing materials would be subjected to the alkali dissolution resulting in the bundles of cellulose fibrils that can be separated with a reduction in cellulose fibers dimension.[222] The dissolution of non-cellulosic constituents in alkali creates voids in the fiber structure which leads to the significant swelling and changes in the physical structure, dimensions, morphology and mechanical properties.[108,222,309]

The alkali treatment could be categorized into two types of methodologies, including alkali solution heating and alkali cooking by autoclave or digester. Alkali solution heating is carried out using a combination of relatively low temperature (70–90 °C) and mechanical stirring.[121] Moreover, DTG curves of bleached fibers (WH-B1 and WH-B2) show a shoulder at 250 ^{o}C and maximum peak at 348 ^{o}C, corresponding to the degradation of hemicellulose and cellulose, respectively.[306] Compared to WH-Raw, the thermal stability of WH-A, WH-B1 and WH-B2 increased due to chemical treatment could remove of hemicellulose and lignin.[164,218]

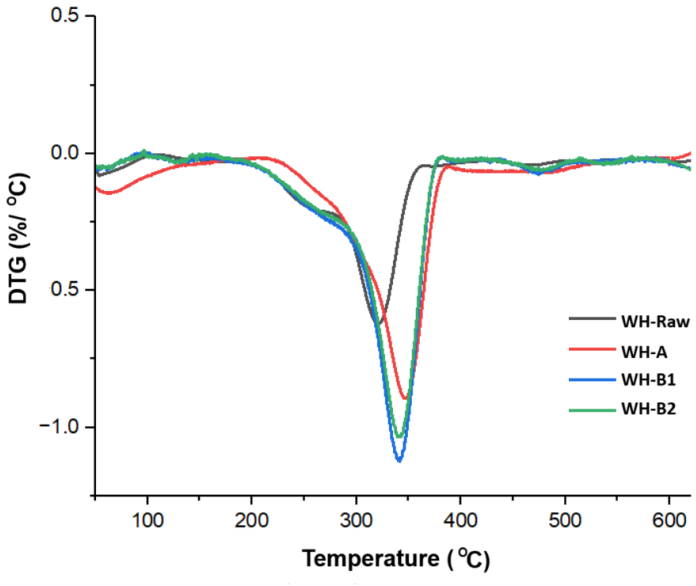

Fig. 59 DTG curve of WH-Raw, WH-A, WH-B1 and WH-B2

The surface morphology of as-obtained WH-A, (b) WH-B1 and (c) WH-B2 samples were investigated by SEM. These images represent the smooth surface of bundle of microfibers. After alkaline pretreatment, the bundles of fibers became loosened and were separated as can be seen in Fig. 60. This is due to a breakage of hemicellulose and lignin, which occurred in alkalization process. After alkaline treatment, bleaching step was carried out (chlorine and chlorine free method). The bleaching step was used to remove further hemicellulose and lignin. In the chlorine free method, hydrogen peroxide was used- this resulted in the degradation of non-cellulosic contents due to it being oxidized by peroxide-in good agreement with FTIR spectrum.[310] It was found that the as-obtained WH-B1 and WH-B2 illustrate the similar results of clean surface microfibrils with desired diameters in the range of 5-10 µm but the chlorine free method to provide WH-B2 is beneficial in that it uses less toxic chemical than using of the chlorite method. As well as toxicity, chloride is corrosive towards steel and water hyacinth is a freshwater plant, so processing and generating a waste water with significant chloride would be ecologically damaging. Thus, chlorine free method could be an effective way to prepare fibrillated

cellulose derived from water hyacinth, in accordance with the surface morphology reported by Tanpichai *et al*.[9]

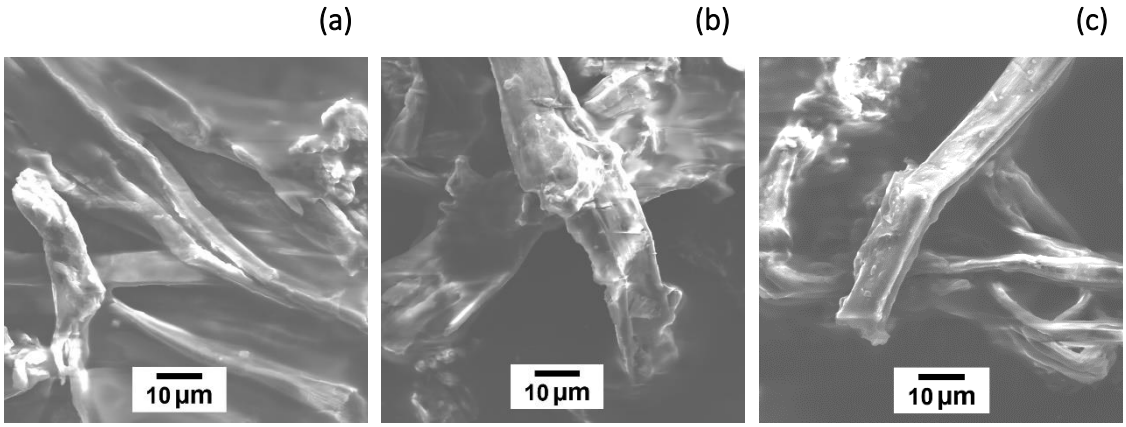

Fig. 60 SEM images of (a) WH-A, (b) WH-B1 (chlorine method) and (c) WH-B2 (chlorine-free method)

3.1.2.4 Acid hydrolysis

In order to prepare cellulose nanofiber (CNF), which is also sometimes called cellulose nanofibers or/and cellulose nanocrystal (CNC), acid hydrolysis was subsequently used after alkaline treatment and bleaching step.[102] Acid hydrolysis is commonly used to extract CNC from biomass.[10] Typically, production of nanocellulose from lignocellulosic biomass is a two-step process involving chemical methods, which includes the purification of cellulose material by the removal of lignin, hemicellulose and extractives i.e. wax and pectin, then the isolation of nanocellulose can be carried out by acid hydrolysis step.[107] The most common use of acid is sulfuric acid for this step. As a result, WH-B2 was subsequently hydrolysed by using diluted H_2SO_4 solution (50% v/v) in this part.[10] The as-obtained sample (referred to as WH-C).

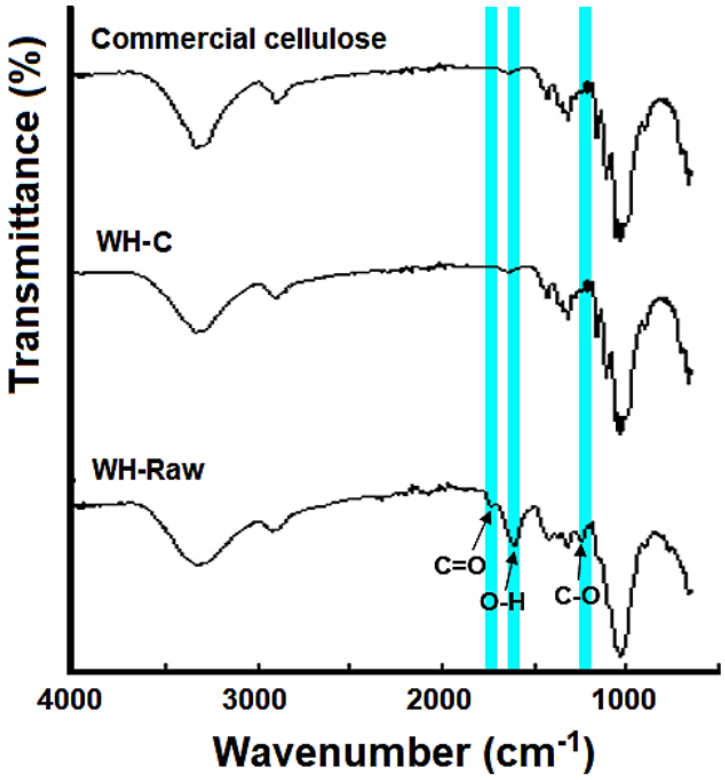

Fig. 61 FTIR spectra of WH-Raw, WH-C and commercial cellulose

Functional groups on the surface of the WH-Raw, WH-C and commercial cellulose were monitored using a Fourier transform infrared spectrometer in an ATR mode. The cellulose fibers were dried at 100 °C for 12 h. The spectra were scanned over the wavenumber ranging from 650 and 4000 cm^{-1}.

FTIR spectra WH-Raw, WH-C and commercial cellulose shown in Fig. 61. Both WH-C and commercial cellulose illustrates the similar patterns. Assignment of FTIR spectra of WH-Raw, WH-C and commercial cellulose also shown in Table 21. The broad band located in the range of 3400-3300 cm^{-1} region corresponding to the-OH stretching vibrations for inter- and intra- molecular hydrogen bonding in all cellulose materials. The peak at 2,918 cm^{-1} was assigned to the aliphatic saturated C-H stretching of cellulose molecules.[311] Bands at 1061 cm^{-1}, 1,030 cm^{-1} and 829 cm^{-1} were attributed to the C-O-C stretching of the β-1,4-glycosidic linkages of cellulose chains, C–C stretching vibration in cellulose and

C-H rocking vibrations of cellulose molecules, respectively which can be seen in all cellulose samples. These peaks were stronger in WH-C and commercial cellulose which consistent with the higher content of cellulose.[113,247] However, water hyacinth after acid hydrolysis treatment, the results revealed the FTIR absorption peak at 1260 cm^{-1} was attributed to C–O (stretching) bonds in lignin which had disappeared. This implied that the syringyl lignin was removed after the acid hydrolysis.[308]

Table 21 Assignment of FTIR spectra of WH-Raw, WH-C and commercial cellulose

Wavenumber (cm^{-1})	Assignment
3300-3400	O–H stretching vibrations and hydrogen bonding in phenolic and aliphatic structures
2981	C-H stretching of cellulose molecules
2930 and 2845	C-H stretching in aromatic methoxyl groups and in methyl and methylene groups of side chains
1730	C=O stretching vibration in acetyl groups of hemicellulose or ester linkage in carboxylate derivatives in ferulic and p-coumeric acids of lignin and/or hemicellulose
1510	C=C stretching of aromatic skeleton in lignin molecules
1260	C-O vibration of guaiacyl ring in lignin molecules
890	C-H deformation of anhydroglucose unit in cellulose and hemicellulose of lignocellulosic biomass materials

The morphology and size of water hyacinth fibers after acid hydrolysis step was characterized by SEM and TEM (Fig. 62). Prior to SEM and TEM characterization, the aqueous suspension of the as-obtained WH nanocrystal was diluted (0.5 wt%) with DI

water. After acid hydrolysis process, water hyacinth yielded nanostructure including nanorods or nano whiskers with the average range of 100-500 nm and average diameter of 5-10 nm and spherical-shaped of CNCs, with the average diameter size in a range of 50-80 nm.

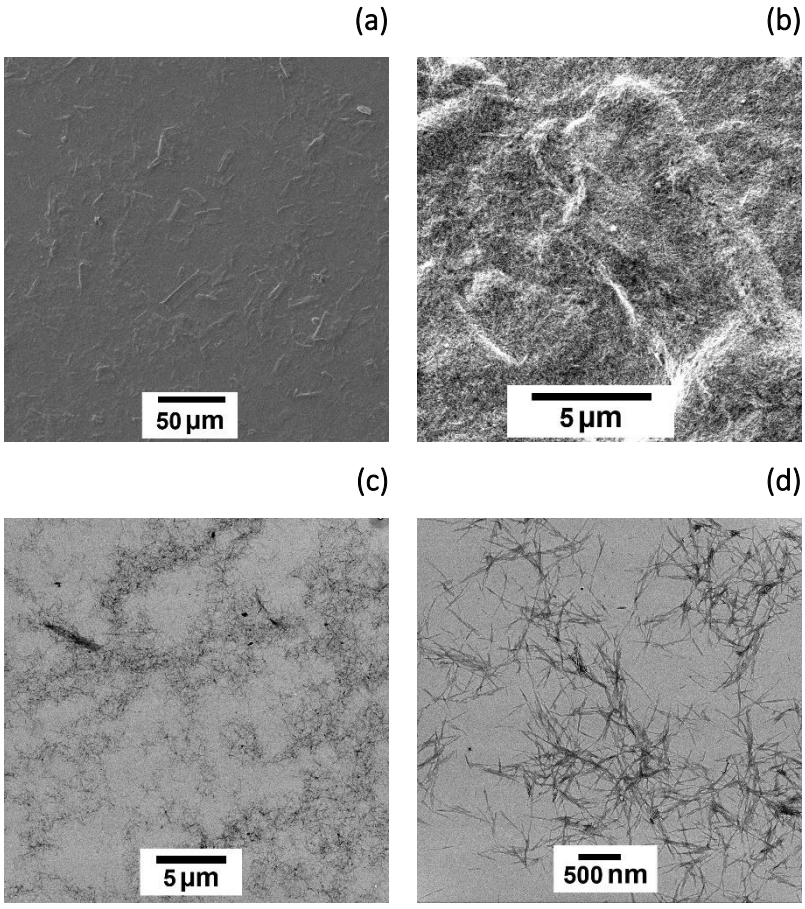

Fig. 62 SEM (a,b) and TEM (c,d) images of the as-obtained WH-C

Due to the suspension of CNCs forming gel-like which was found the agglomeration of homogenous phase of CNC particles as can be seen in SEM images and it could be seen much clearer of nano whiskers dispersion in TEM image. WH-C is the most homogenous of all samples with the smallest diameter in the range of nanometer. The as-obtained WH-C from this part was used in bio-composite film as reinforcement in the matrix of film preparation which discussed later.

3.1.3 Mechanical treatment

The mechanical treatment of homogenisation is known to modify the original cellulose fibers by defibrillation resulting in releasing microfibrils and microfibril bundles in the water suspension.[312] This part investigated the morphology of the resulting cellulose suspension after homogenisation, with a view to preparation of bio-composite films in next part. Two different methods were studied which including MW-assisted pretreatment to produce defibrillated celluloses, subsequently homogenisation (referred to as method MW-M) and WH-B2 obtained by chemical treatment after bleaching step with using chlorine free method was subsequently fibrillated through homogenisation (denoted as method C-M).

3.1.3.1 Method MW-M

From the previous section, the-as prepared WH 200 were characterized by SEM which shows that some irregular shapes and micro fibers were obtained. After MW-assisted pretreatment to produce defibrillated celluloses, subsequent homogenisation to produce microfibrils and more homogenous phase of as-prepared product was described. The next part was to study the application for bio-composite film preparation; however it was found that WH 200 could not mix with solution and the agglomeration of defibrillated celluloses was observed. This meant that a film could not prepared from WH 200 sample, thus the mechanical pretreatment such as homogenisation was subsequently used for producing of micro/nano fibers.

From results described previously, WH 200 obtained from microwave-assisted pretreatment method was found to be in the state of a heterogeneous mixture with both distinctly large and small fibers. After homogenisation for 1 h, the as-obtained WH-MW-H provided more homogeneous mixture with smaller fiber diameters in the range of 0.5-12 µm as shown in **Fig. 63**.

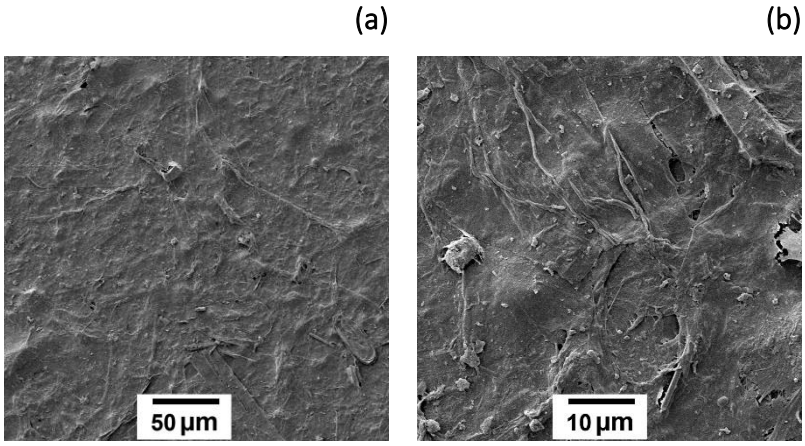

Fig. 63 SEM images of WH 200 after homogenized for 1 h (referred to as WH-MW-H)

TEM images (Fig. 64) also display the same trend of more homogeneous phase of smaller fiber diameters in the micron range. A few fibers in nanoscale (10-50 nm in diameter) can be found in the as-obtained sample. This suggested that micro/nano fibers could be produced from microwave-assisted pretreatment method subsequently by homogenisation.

Although, some heterogenous phase can be found in this sample but this obtained WH-MW-H could be mixed with mixture solution for film preparation which discussed in the latter part.

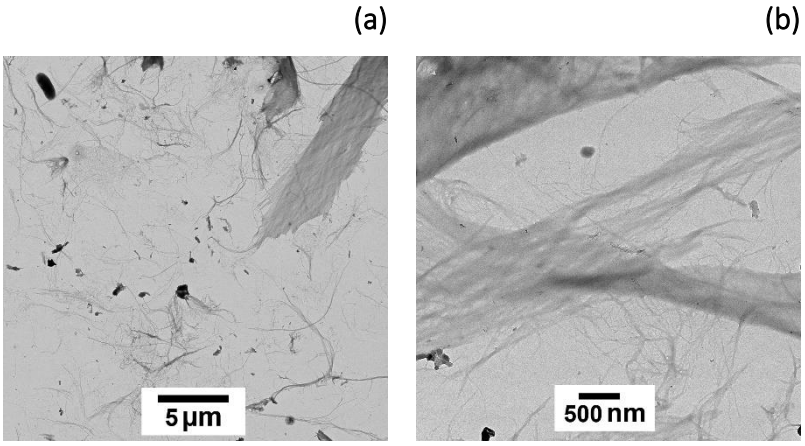

Fig. 64 TEM images of WH 200 after homogenized for 1 h

3.1.3.2 Method C-M

Cellulose fibrils derived from water hyacinth obtained by chemical pretreatment were fibrillated into cellulose micro/nanofibers through a subsequent homogenisation for 15 min, the as-obtained product denoted as WH-B2-H1. The morphology was investigated by SEM and TEM which illustrate that after homogenisation for 15 min a smaller size of microfibers and provided uniform of microfibers/nanofibers from this step. SEM images reveal that fibrillated celluloses obtained with diameters in a range of 1-8 µm which is smaller than the as-obtained WH-B2 (before homogenisation).[313]

After homogenisation for 1 h, the as-obtained product, denoted as WH-B2-H2, was found to be in a gel-like was form as can be seen in SEM images (**Fig. 65**) which is in good accordance with the gel-like form behavior reported by Hubbe *et al*.[102] The fibrillated celluloses obtained with smaller diameters were investigated (0.5-5 µm). The morphology was also investigated in more details by TEM characterization.

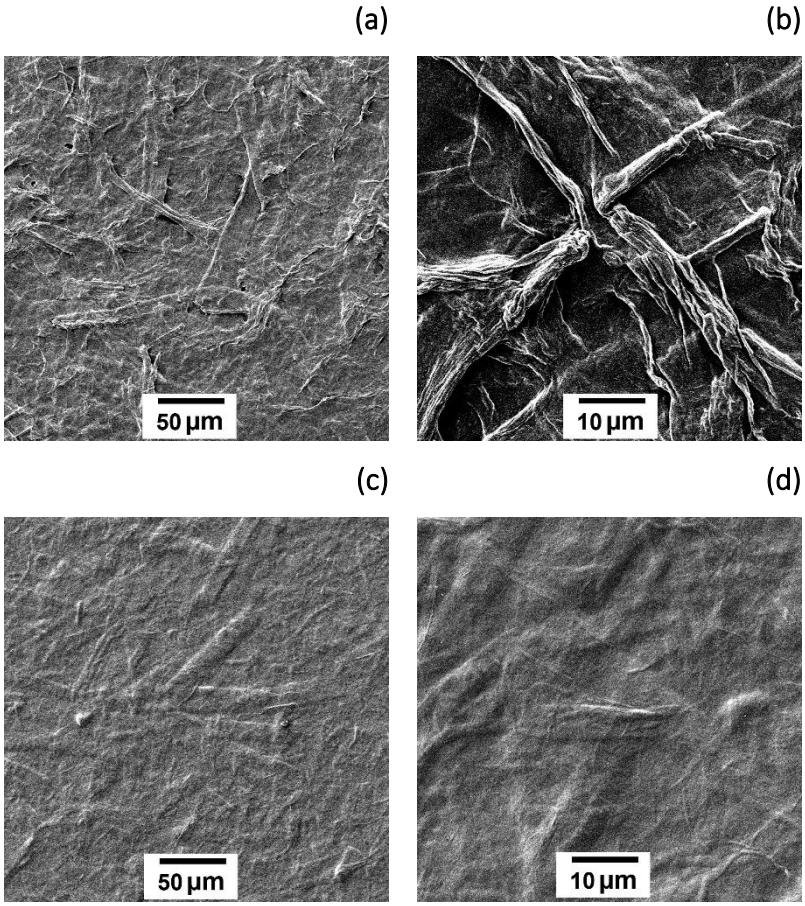

Fig. 65 SEM images of WH-B2-H1 after homogenisation for 15 min (a,b) and WH-B2-H2 after homogenisation for 1 h (c,d), respectively

TEM images represent microfibers and nanofibers obtained after homogenisation with desired diameters in the range of 10-20 nm and the length in the range 120-200 nm. There were some cellulose microfibers mixed with cellulose nanofibers in the obtained suspension after homogenisation. Prolonging time for homogenisation (1 h) could cause the gel-like formation of sample (**Fig. 66**), microfibers/nanofibers were obtained from this condition and also provided more homogenous phase of nanofibers than using homogenisation for 15 min. This could suggest that cellulose nanofibrils can be prepared from chemical pretreatment followed by homogenisation.

Most of fibers can be seen to exist on the nanometer scale based on TEM image. However, even-a prolonged time for homogenisation (1 h), yielded mixed phases of microfibers and

nanofiber obtained from this condition which could cause the limitation of up-scalable production.

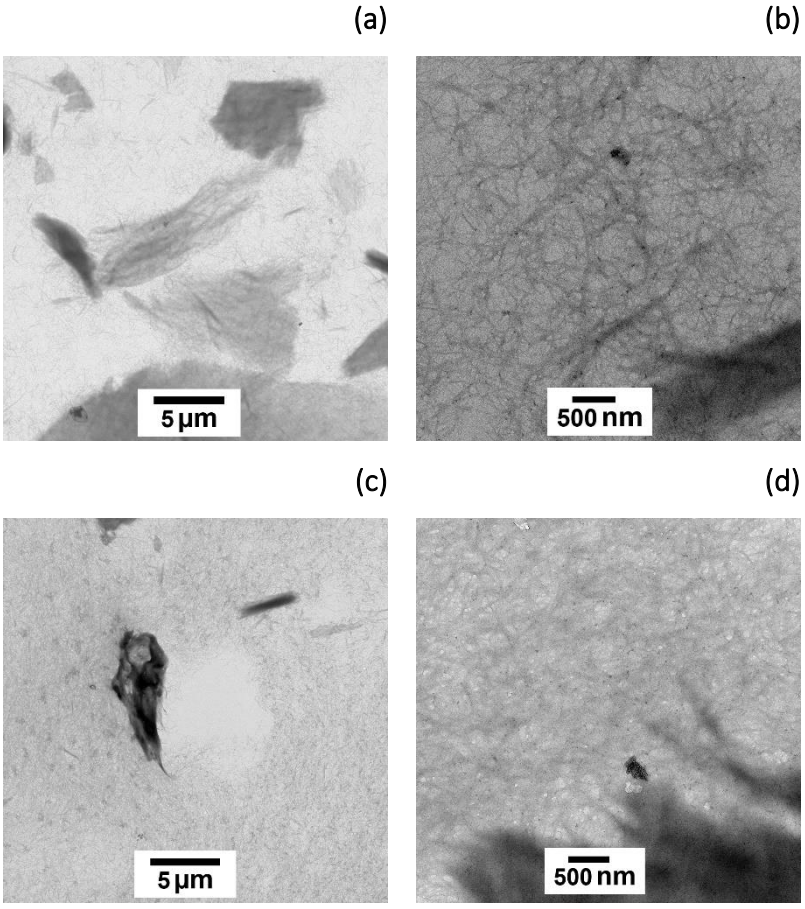

Fig. 66 TEM images of WH-B2-H1 (Chorine-free method) after homogenisation for 15 min (a,b) and WH-B2-H2 (Chorine-free method) after homogenisation for 1 h (c,d)

Optical properties like transparency are amongst one of the most important parameters for food packaging because it is necessary for customer acceptability to view the quality of products. This part aimed to prepare the transparent bio-composite film with good quality of mechanical property so the as-obtained cellulose microfibrils (CMFs)/ cellulose nanofibrils (CNFs) materials after homogenisation for 15 min was used for film preparation.

3.2 Application for film preparation

Plastic film is one of the most commonly used materials, and is produced from polypropylene (PP), polyethylene (PE), polyvinyl chloride (PVC), etc. Such materials bring convenience to the development of food production and distribution because its transparency, high mechanical properties and good barrier properties. However, a large amount of waste is generated each year and such waste requires more than a few decades for degradation.

Packaging plays an important role in protecting food against physicochemical damage and microbial activity. Currently, biodegradable polymers have been widely used as alternative food packaging because of their eco-friendly compositions. The use of natural polymers has benefits such as biocompatibility and biodegradability. Moreover, sustainable development for environment preservation have been great attention, thus this part focused on potential replacements for conventional plastic materials and attempt to enhance their mechanical properties, thermal and barrier properties.[144,293]

Polyvinyl alcohol (PVA) polymer is widely used in various industrials application such as films, hydrogels, adhesives and paper coating agents due to its unique characteristics such as biodegradability, good mechanical strength, thermal stability, water solubility, nontoxicity, high hydrophilic properties and improved barrier properties.[250,293,314] PVA is also cost-effective and forms good quality films easily. Thus, PVA was used for film preparation in series A1.[315]

Moreover, plasticizers are important factors to improve the thermoplastic processing of PVA. Plasticizers such as urea, formamide, glycerol have been to make films flexible, and can be legally used for industrial purposes and easy processing.[250] Polymer blending is one of the most effective processes to create new materials with desired properties. Compared to film prepared from an individual component, films prepared from blending of polymers usually explore modified properties.[144] Micro/nanocellulose is expected to

be used as a substitute and filler in many plastics. The optimization conditions for bio-films preparation as well as nanocomposites with using nanofillers to provide new materials with specific properties such as mechanical properties described in this part.

This part investigated various conditions for bio-composite film preparation which include optimization condition for film preparation of PVA films blended with glycerol (referred to as series A1), bio-composite film preparation from WH-MW-H (referred to as series A2), bio-composite film preparation from WH-B2 after homogenisation for 15 min (referred to as series A3) and bio-composite film preparation from WH-C (referred to as series A4) and their properties were discussed in the following chapter.

3.2.1 Optimisation conditions for film preparation

In this section, the optimum conditions were studied for film preparation. PVA was dissolved in deionised water by heating to 80 °C under vigorous stirring to create well-defined solutions at 2–20 wt % concentration.[316] The influence of water content on the preparation of film and the optimum percentage of PVA was also studied. Compared to the previous reports PVA film prepared by 5% (w/v) of PVA solution studied by Fong *et al*.[316], PVA film of 10% (w/v) prepared by Rahmadiawan *et al.*[258], film preparation of 4% (w/v) PVA solution prepared by Suganthi *et al.*[259] and 5% (w/v) of PVA solution for film preparation prepared by Bahrami *et al*.[293], it was found that the preparation of film with the optimum concentration of 5% w/v for PVA solution provide the best physical properties such as smooth and clean surface of the as-obtained film.

In contrast, the concentration of 10%-20% (w/v) of PVA provided thicker, less flexible and harder films than the 5% w/v for PVA film due to increased levels of PVA increasing the film thickness.[294] This suggested that 5% (w/v) of PVA solution was the optimum concentration for film preparation.[293]

3.2.1.1 Film preparation series A1

This part, the optimum condition for film preparation was investigated. Due to PVA alone can provide the brittle film. Even though the pure PVA film has good mechanical strength and thermal stability, a plasticizer like glycerol blended with PVA film can improve its flexibility. This is due to its plasticizing effect, as the glycerol interacts through hydrogen bonding with PVA, which leads to the increased spacing between PVA chains.[317]

However, increasing concentration of glycerol added in PVA film can cause a decrease of the toughness.[294] Previous reports by researchers reported the desired glycerol concentration (2.5%-5% w/w) was added into mixed solution reported by Cazón *et al*.[294], this could suggest that the optimum concentration of glycerol could be between 0.5% and 3% (v/v). As a consequence, the preparation of bio-films for this work used the range of this concentration for film blending.[293,317,318] In addition, adding glycerol for film preparation can cause the decrease of brittleness and an increase in the flexibility of the as-prepared film. Glycerol also provided a UV protective affect for as-prepared bio-films as well as the effect for food packaging to prevent lipid oxidative deterioration.[294] In contrast, it can cause the negative effect for increasing the film permeability.[294]

UV and Visible Light Transparency was determined to investigate the optical properties and UV-shielding. Fig. 67 represents the film surface which are highly transparent. After adding glycerol, the transparency was decreased. The UV spectrum can be divided into three regions including UV-A (320-400 nm), UV-B (280-320nm) and UV-C (220-250 nm).

The optical transmittance might be influenced by various factors, including the dispersibility, film thickness, refractive index of the material, and crystallization inside the PVA film.[256,319] The transparency curve is shown in the range of the 200–800 nm (Fig. 67). Pure PVA film is the most transparent of all films.[258] The as-prepared A1 films by adding 0%, 1%, 2%, 3% and 5% v/v of glycerol were denoted as A1-0, A1-1, A1-2, A1-3 and A1-4 samples, respectively.

Light transmittance of as-prepared films was investigated in visible region. It was found that highest transparent film was A1-0 with 99.7% of light transmittance at 500 nm.[247] Whereas, the increasing of percentage of glycerol blending in mixture -causing the decreasing of light transmittance. The light transmittance rate decreased from 98.7%, 97.2%, 95.0% and 93.9% for as-prepared films containing 1%, 2%, 3% and 5% respectively. However, the neat PVA film showed a poor UV-shielding property as it could not absorb UV radiation (wavelength of 260–400 nm), having high UV transmittance of 80%.[320,321]

From these results, the optimum concentration of glycerol for PVA film preparation was found in the range of 1-3% v/v- in good agreement with film prepared by Cazón *et al*.[294]

In contrast, adding higher amount of glycerol (4-5% v/v) into the mixture-led to a greasy film being obtained due to the excess amount of glycerol released from the as-obtained films.[294] It should be noted that pure PVA film has the highest transmittance value (99.7%). However, the pure PVA film was brittle so optimum amount of glycerol blending in film preparation can improve this property to make it more flexible and less brittleness but it can cause the decreasing of light transmittance.

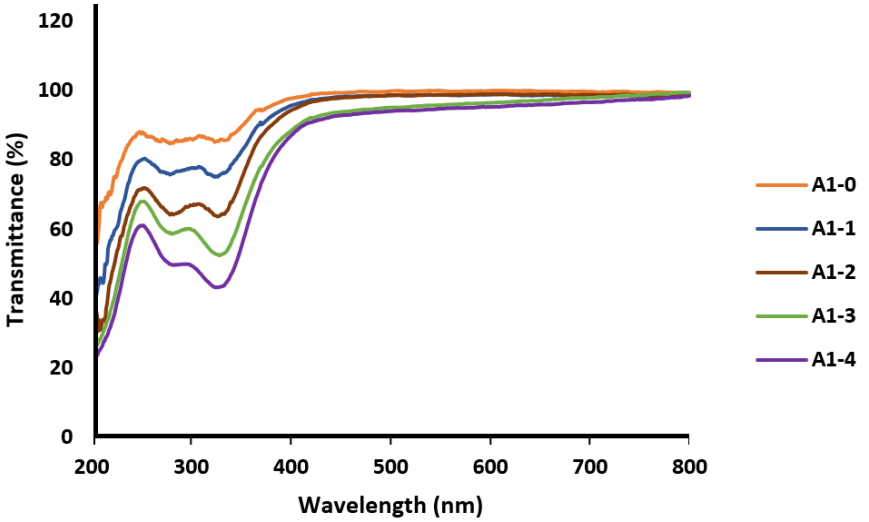

Fig. 67 Optical properties of as-prepared films in UV and visible light wavelength range

The mechanical properties of the as-prepared films were performed by the tensile testing as shown in Fig. 68. Tensile strength and elongation at break of the as-prepared films were investigated. Elongation at break, also known as fracture strain, is the ratio between changed length and initial length after breakage of the test specimen at a controlled temperature.[249,322]

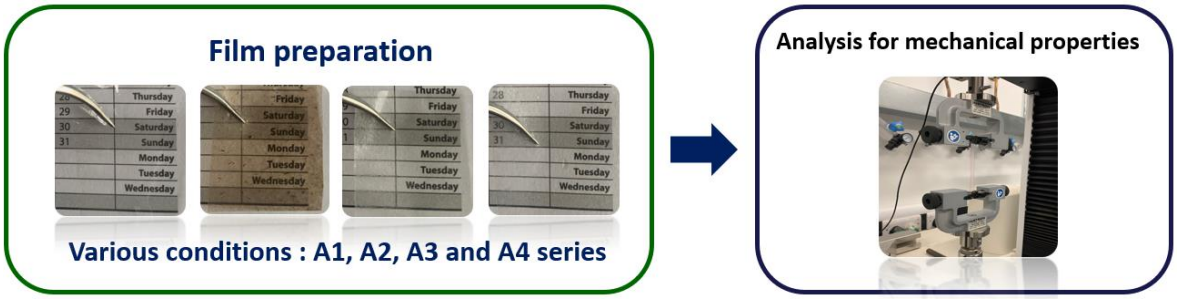

Fig. 68 Mechanical properties analysis for as-prepared bio-composite films

Tensile properties of as-prepared films series A1, represent that adding optimum content of glycerol can cause the positive effect for as-prepared films due to the tensile strength increasing from 29.41 MPa of pure PVA film to 31.49 MPa of A1-1 and 30.43 MPa of A1-2, respectively. The as-prepared films with different contents of glycerol led to the increasing of elongation at break from 157.78 % of A1-0 film (pure PVA film) to the range of 234.95%-609.54% as can be seen in Table 22.

Table 22 Tensile properties of as-prepared A1 film series

Film series A1	Tensile strength (MPa)	Elongation at break (%)
A1-0	29.41 ± 0.26	157.78 ± 2.28
A1-1	31.49 ± 0.29	609.54 ± 7.98
A1-2	30.43 ± 0.44	335.26 ± 8.23
A1-3	21.80 ± 0.54	455.5 ± 9.11
A1-4	17.93 ± 0.59	234.96 ± 12.99

However, both tensile strength and elongation at break are important for food packaging, the optimum condition led to good mechanical properties and flexible. Fig. 69 represents tensile strength and elongation at break of A1 series which suggests that the optimum glycerol content of 1-3% v/v results in both relatively high tensile strength and elongation at break, compared to the A1-0 with no additive, which is in good accordance with results reported by Cazón *et al*.[294] In this part 1%-2% (v/v) of glycerol were used for bio-composite film preparation in the next part because the results exhibit the higher value of tensile strength than the pure one and relatively high value of elongation at break.[323]

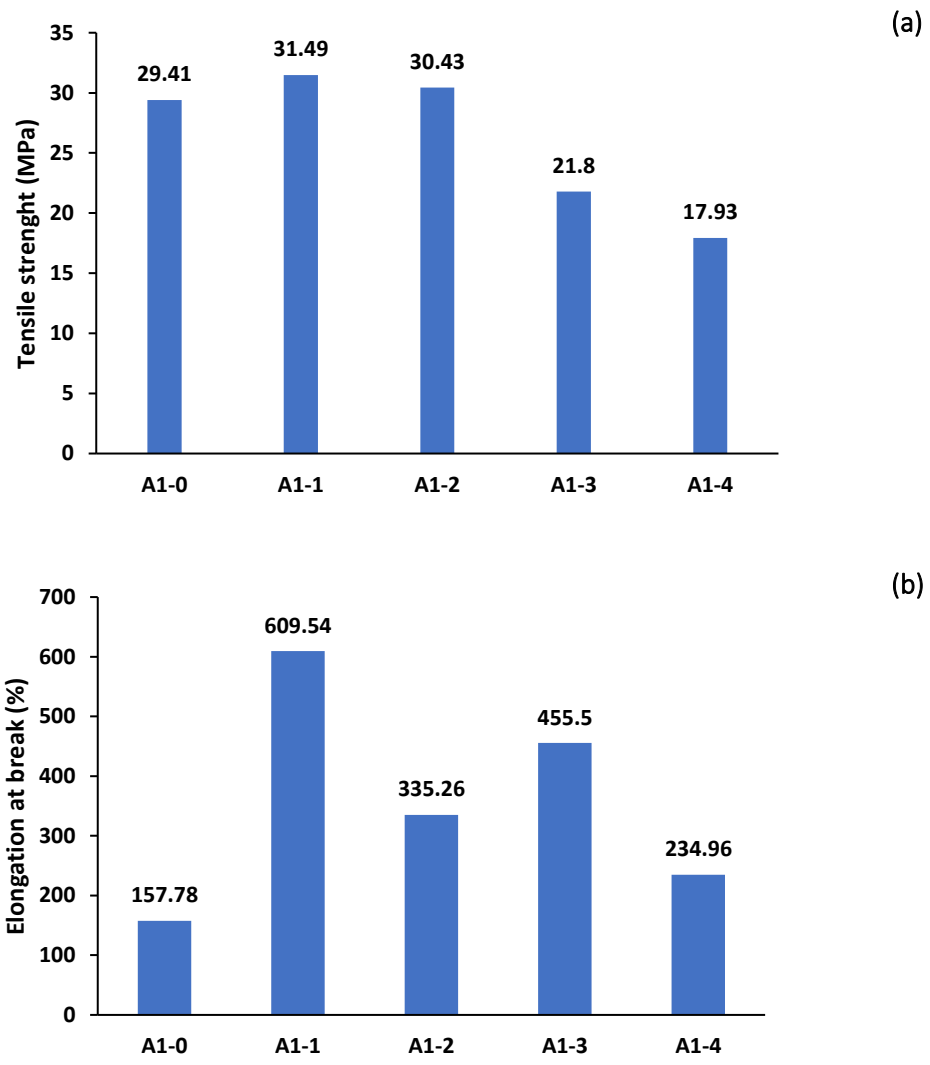

Fig. 69 Tensile strength (a) and elongation at break (b) of as-prepared A1 film series

3.2.2 Bio-composite film preparation

The previous part reported the optimum ratio of PVA and glycerol for film preparation, the development of bio-composite film preparation by adding defibrillated celluloses as reinforcing agent was studied. The aim of this part was to prepare bio-composite films obtained from the optimum mixture of cellulose obtained from WH, glycerol and PVA.

As mentioned before, PVA was used for mixing solution with glycerol and cellulose because it is biodegradable, soluble in water and non-toxic. [324] However, good mechanical properties are very important for food packaging during transportation, handling and storage of packaged foods. Thus, the optimum condition for bio-composite film preparation with good barrier properties can improve the shelf life of packaged foods by decreasing the rate of oxidation process of lipids.[325]

3.2.2.1 Film preparation series A2

This part describes the film preparation from WH 200 obtained from MW-assisted pretreatment for food packaging. From the results, it was found that the as-prepared WH 200 could not mix well with PVA mixing solution for film preparation. As discussed before, some irregularly shaped impurities (which could be from some residues such as lignin and hemicellulose which are amorphous) and some of caramelised sugar, formed at high temperature can cause problems in mixing at low temperature. To develop a technique which provides the homogeneous phase of mixing solution for film preparation, homogenisation was used for producing a well-mixed homogenous phase of cellulose in solution.[129] As a result, homogenisation was used for defibrillation of WH 200 to obtain WH-MW-H in order to prepare a mixture for film preparation. In this step, glycerol was added in mixing solution also in order to reduce the brittleness of the as-prepared film.[294]

The brownish color of films could derive from the proportional of lignin, which contains chromophore groups such as phenolic units and ketones that can absorb light. The lower light transmittance of these samples could therefore be caused by the lignin content and caramelized sugar remaining in the fibers.[106,310]

The as-obtained defibrillated cellulose from microwave-assisted method by using deionized water as liquid media and WH 200 was used for film preparation. The result shows that the as-prepared fibers were brownish, resulting in the dark brown color of film was obtained.

UV-visible transmittance of the PVA film, containing the different content of microfibril celluloses from water hyacinth is represented in Fig. 70. Bio-derived films contained different amounts of WH-MW-H after homogenisation for 1 h in order to mix with mixture of PVA and glycerol. The A2-0, A2-1, A2-2, A2-3 and A2-4 referred to as the as-obtained films containing 0%, 1%, 2%, 3% and 5% (w/v) of WH-MW-H, respectively. The optimum content of glycerol was found to be 2%v/v, and this was used for film preparation as the films displayed a good degree of flexibility. Films obtained with lower amounts of glycerol (1% v/v) were less flexible and displayed brittleness for packaging. The result reveals that A2-0 film was transparent with from 97.2% light transmittance at wavelength of 500 nm. With increasing addition of WH-MW-H in the film preparation, the transmittance declined significantly. Specifically, the as-prepared bio-composite films showed that the light transmittance decreased from 92.5%, 87.2%, 83.5% and 76.5% for A2-1, A2-2, A2-3 and A2-4 bio-composite films, respectively. Moreover, with increasing addition of WH-MW-H in the film preparation, the UV-shielding increased gradually especially for A2-4 film (approximately 40% of transmittance in UV region). However, it was found that 5% (w/v) was the maximum amount of WH-MW-H for film bio-composite preparation because higher content of WH-MW-H led to the precipitation of the excess amount of WH-MW-H during film preparation and can cause some left over defibrillated celluloses on the Petri dish was observed.[9]

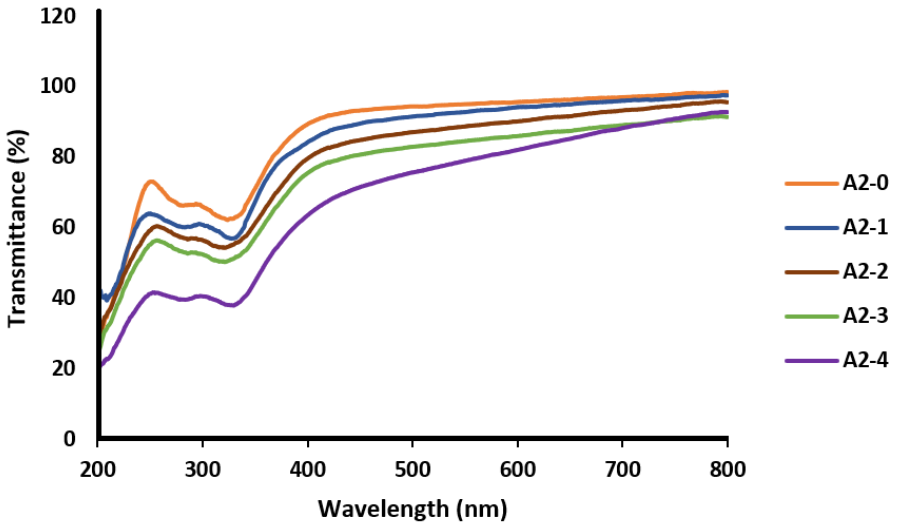

Fig. 70 Optical properties of bio-composite films in UV and visible light wavelength range prepared from WH-MW-H

The tensile properties of A2-0, A2-1, A2-2, A2-3 and A2-4 were shown in Table 23. The optimum content of glycerol (2%v/v) was used for film preparation for the reasons described above. A2-0 of PVA blended with 2%v/v of glycerol had low performance in tensile strength. After blending with glycerol and WH-MW-H, tensile strength increased slightly but elongation at break decreased significantly as can be seen in Fig. 71.

The increasing of WH-MW-H fibers contents added in film preparation resulted in slight increase of tensile strength of A2-1, A2-2 and A2-3, respectively. The excessive amounts of WH-MW-H fibers at 5% could affect the incorporation of WH-MW-H fibers, and resulted in a decline in the tensile strength of bio-composite films from 34.77 MPa (A2-3) to 32.57 MPa of A2-4. This might be caused by the presence of the non-nanoscale cellulose in WH-MW-H fibers, which hinders its homogeneous dispersion in PVA and weakens the hydrogen bond interaction between WH-MW-H fibers and PVA matrix hence the polymer molecular chains cannot be compactly stacked, and the defects are easily formed.[326]

Table 23 Tensile properties of as-prepared A2 film series

Film series A2	Tensile strength (MPa)	Elongation at break (%)
A2-0	30.43 ± 0.44	335.26 ± 8.23
A2-1	31.85 ± 1.40	65.56 ± 10.22
A2-2	32.24 ± 1.78	127.80 ± 10.84
A2-3	34.77 ± 1.12	113.42 ± 9.11
A2-4	32.57 ± 2.30	47.66 ± 8.38

On the other hand, these results represent that a significantly decrease of elongation at break were investigated with the increasing in addition of WH-MW-H in bio-composite film preparation. It was found that the elongation at break dropped from 335.26% of A2-0 to 47.66-127.80% of 1-5% addition of WH-MW-H in this series. A dramatic drop of elongation at break for only A2-1 and A2-4, this might be caused by the proportion of heterogenous phase of A2-1 was formed during film preparation due to a small amount of defibrillated celluloses dispersed in matrix less than the optimum concentration resulted in agglomeration of fibers.[294] Moreover, A2-4 also reveals the least value of elongation at break just only 47.66%- influenced by the precipitation of the excess amount of WH-MW-H during film preparation and the fibers agglomerated in film which attributed to less formation of hydrogen bonding between fibrils.[9]

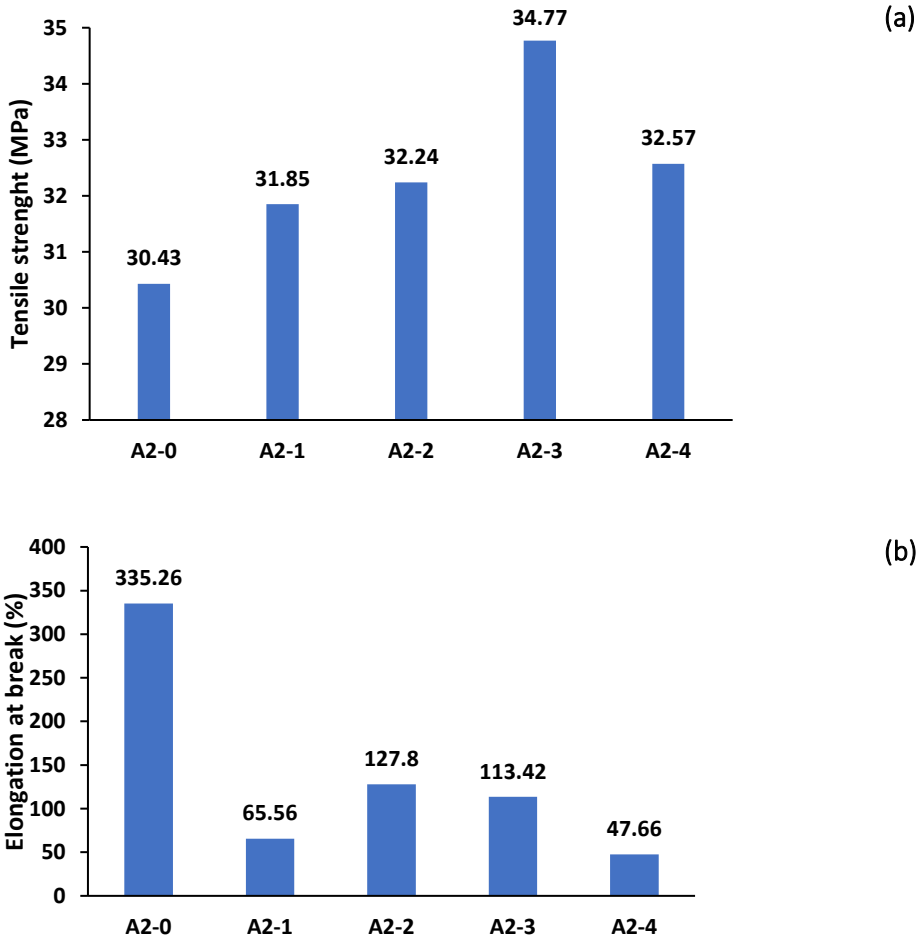

Fig. 71 Tensile strength (a) and elongation at break (b) of as-prepared A2 film series

3.2.2.2 Film preparation Series A3

This part investigated various conditions for bio-composite film preparation from WH-B2 after homogenisation for 15 min (series A3) and WH-C (series A4). Bio-composite films preparation from defibrillated cellulose derived from water hyacinth as can be seen **Fig. 72**. Its optical and mechanical properties were also investigated which will be discussed in latter part.

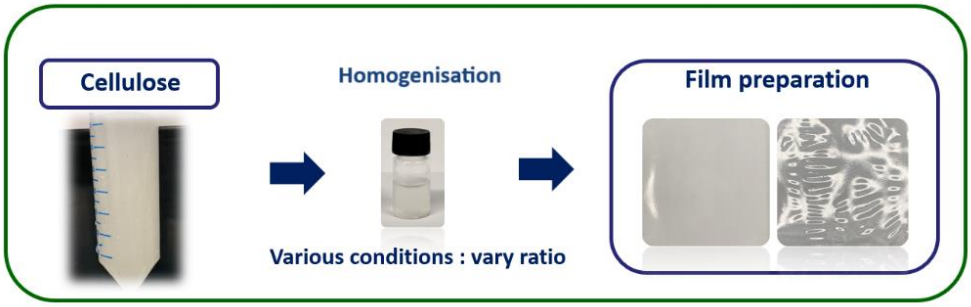

Fig. 72 Schematic of bio-composite films preparation (series A2-A4)

The total light transmittances of the films in the wavelength range 200–800 nm are presented in Fig. 73. Optical property of bio-composite films obtained from WH-B2 after homogenisation for 15 min with containing 0%, 1%, 2%, 3% and 5% (v/v) for film preparation denoted as A3-0, A3-1, A3-2, A3-3 and A3-4, respectively. The optimum content of glycerol was 1% (v/v) represents the highest light transmittance of 98.7% at wavelength of 500 nm, due to higher content of glycerol can cause negative effect for increasing the film permeability.[294]

The results for A3 film series show that the light transmittance was decreased from 98.0%, 96.4%, 93.3% and 88.3% for A3-1, A3-2, A3-3 and A3-4 bio-composite films, respectively. A gradual decrease of transmittance occurred in A3 series with the increasing of addition of WH-B2-H1 in film preparation. These film series exhibit high value of light transmittance with suitable levels of transparency for food packaging applications.[327] For UV-shielding, %transmittance was decreased from 80% (A3-0) to 40% (A3-4) in UV region which suggests that a poor UV-shielding property was observed in A3 series.

However, it was found that 5% (v/v) was the excess amount of glycerol resulted in the negative effect for increasing the film permeability and greasy film obtained from this condition.

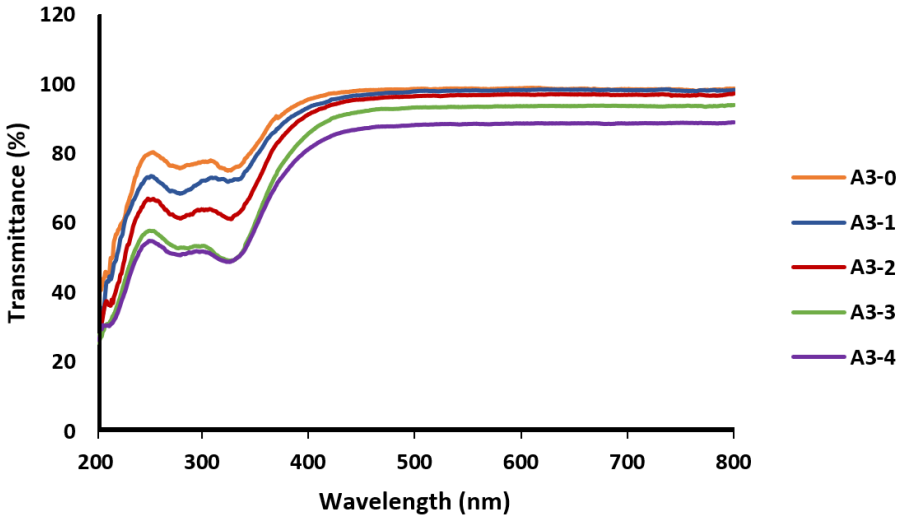

Fig. 73 Optical properties of bio-composite films in UV and visible light wavelength range prepared from WH-B2-H1

Mechanical testing was performed to analyse the mechanical properties of the as-prepared bio-composite films blended with WH-B2-H1. Tensile strength and strain at break of as-prepared films shown in Table 24. An increase of tensile strength was observed with the increasing of the percentage of WH-B2-H1 blending with film preparation from 38.56 MPa of A3-1 to 45.25 MPa of 45.25 MPa. A significant increase of tensile strength for 43.7% of 5% WH-B2-H1 addition, compared to A3-0.

In addition, the increasing the WH-B2-H1 content for as-prepared bio-composite films, compared to A3-0, led to a reduction of the elongation at break, which is attributed to the tough network structure formed between the cellulose micro/nanofibrils so thoroughly restricting the polymer chain activity.[167,326] These results illustrated that the elongation at break were found in the range of 316.60%-482.36%, decreased from A3-0 around 21-48%. The reinforcing potential of modified defibrillated celluloses from water hyacinth on mechanical properties of PVA matrix blended with glycerol could be partly explained by the crosslinks between micro/nanofibrils and PVA functional groups but also by the even distribution of the modified cellulose nanofibers in the PVA matrix.[247]

Table 24 Tensile properties of as-prepared A3 film series

Film series A3	Tensile strength (MPa)	Elongation at break (%)
A3-0	31.49 ± 0.29	609.54 ± 7.98
A3-1	38.56 ± 0.55	482.36 ± 7.48
A3-2	40.77 ± 0.77	316.60 ± 6.955
A3-3	43.96 ± 0.74	440.06 ± 8.69
A3-4	45.25 ± 0.26	359.82 ± 8.02

Larger improvements in the mechanical properties have been reported for A3 series made from WH-B2-H1 treated with an alkaline solution and by bleaching, subsequently homogenisation for 15 min, compared with those formed from WH-MW-H fibers.[9]

The tensile properties of as-prepared films (A3 series) were also shown in **Fig. 74**. Nanoscale fibers as reinforcement or reinforcing agent have the large special surface which may form a high adhesion interface with the polymer matrix.[328] Thus, these properties can not only improve the mechanical performance of the bio-composite films, but also reduce the light loss when the size of the nanomaterial is less than that of the wavelength of visible light.[249,329]

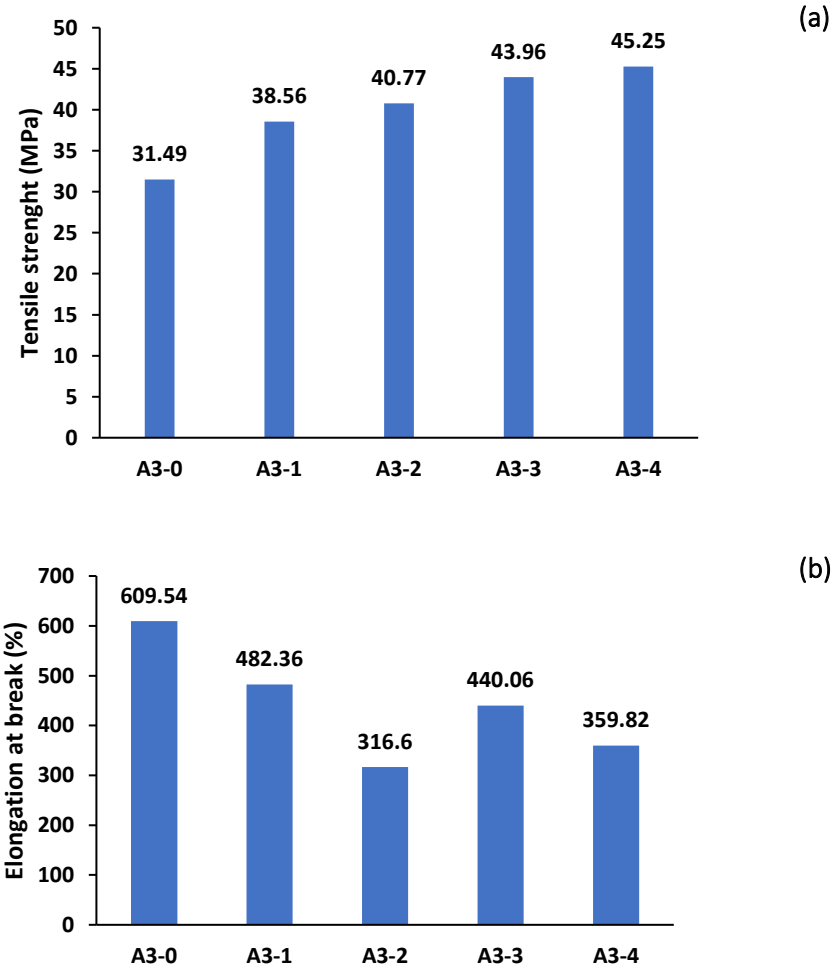

Fig. 74 Tensile strength (a) and elongation at break (b) of as-prepared A3 film series

3.2.2.3 Film preparation Series A4

Bio-derived films preparation from WH-C added into film preparation (series A4). Cellulose nanofibrils (CNFs) as the smallest fibrous unit of plant fiber, has attracted considerable interest because of their surprising properties such as high specific surface area.[125] Bio-derived films obtained from CNC and CNF derived from water hyacinth through acid hydrolysis with containing 0%, 1%, 2%, 3% and 5% (v/v) for film preparation denoted as A4-0, A4-1, A4-2, A4-3 and A4-4, respectively.

Both cellulose nanocrystals (CNCs) and cellulose nanofibers (CNFs) have numerous intermolecular and intramolecular hydrogen bonds. Moreover, CNCs and CNFs offer many advantages such as lightweight, low cost, high aspect ratio, nontoxicity, and surface modification.

Due to the superior optical transparency of the neat PVA films, the morphology of nanocellulose and its distribution in the PVA matrix play a dominant role in the visible light transmission of the nanocomposites.[326] Optical property of bio-composite films obtained from the optimum content of glycerol was 1% (v/v) due to higher content of glycerol can cause negative effect for increasing the film permeability as mentioned in previous section. The optimum content of glycerol was 1% (v/v) represents the highest light transmittance of 98.7% at wavelength of 500 nm. The results for A4 film series show that the light transmittance was slightly decreased from 99.0%, 96.8%, 95.0% and 91.2% for A4-1, A4-2, A4-3 and A4-4 bio-composite films, respectively. However, A4-1 obtained from 1% v/v WH-C addition in film preparation was found to be the slightly higher light transmittance than A4-0 due to the penetration behavior of water molecules, the dense structures of CNCs and CNFs can provide a longer path length. Therefore, the optical properties of the material can be increased.[319]

These film A4 series exhibit the highest value of light transmittance which is a clear benefit for a transparent packaging.[327] It was found the same trend of series A3 films that the excess amount of glycerol of 5% (v/v) effected in the negative effect for increasing the film permeability and A4-4 exhibited the greasy film. A poor UV shielding property was also found in A4 series which can be seen that %transmittance was slightly decreased from 80% (A4-0) to 45% (A4-4) in UV region.

It should be noted that the bio-composite films obtained from CNC and CNF exhibited the best optical transmittance compared with the other bio-composite films (series A2 and series A3). The increasing of addition of WH-C in the film preparation, the transmittance declined slightly. As can be seen in **Fig 75**.

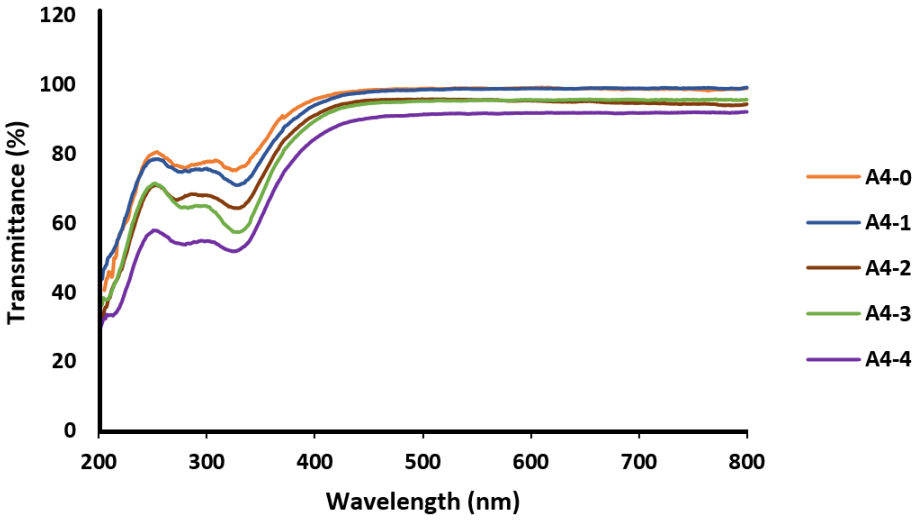

Fig. 75 Optical properties of bio-composite films in UV and visible light wavelength range prepared from WH-C

Due to the mechanical properties of the nanocellulose-based nanocomposites, the addition of nanocellulose as a reinforcement phase in the polymer matrices can improve the mechanical performance of the as-prepared films.[326]

The mechanical properties of the PVA and modified WH-C reinforced PVA composite films (series A4) were determined by tensile testing as illustrated in Table 25. In this study, nano-structure of cellulose from WH-C was expected to increase the tensile strength of the PVA films through chemical cross-linking.[247] Bio-composite films with different WH-C contents as filler or reinforcing agent adding in the matrix were determined. The addition of 1% v/v increased the tensile strength of as-prepared A4-1 film and also led to the same trend with 2%, 3% and 5% v/v of A4-2, A4-3 and A4-4, respectively. The increasing of % WH-C added in bio-composite film preparation caused an increase in tensile strength in the range of 27.31-60.75%. This result suggests that tensile strength increased significantly with the percentage of the WH-C. It is the likely tensile strength increased with increasing intermolecular forces of the hydrogen bonds between the substrate and filler.[319] The homogeneous dispersion of the filler is necessary for promoting the development of hydrogen bonds between the substrate and reinforcing agent and

enhancing the mechanical properties of bio-composites films, which means that homogeneous dispersion of the filler assists the formation of hydrogen bonds to transfer stress more effectively.[319]

Table 25 Tensile properties of as-prepared A4 film series

Film series A4	Tensile strength (MPa)	Elongation at break (%)
A4-0	31.49 ± 0.29	609.54 ± 7.98
A4-1	40.09 ± 0.13	481.20 ± 5.65
A4-2	45.91 ± 0.72	351.96 ± 5.98
A4-3	47.08 ± 0.70	447.34 ± 7.36
A4-4	50.62 ± 0.43	462.58 ± 5.63

The results of strain at break for these series suggested that no significant reduction was noted with the increasing WH-C content. Even though the reduction of elongation at break were found in all samples, they all demonstrated better mechanical performance than those in the A2 and A3 series.

The tensile strength and elongation at break of bio-composite films (series A4) shown in Fig. 76. Compared to the PVA film, the tensile strength of bio-composite film increased gradually with the increasing of WH-C content addition – in good agreement with the report by Miri *et al.*[144] described that the increase of adding CNC in film preparation led to increasing of tensile strength. This suggested that the bio-composite films obtained from CNC and CNF exhibited the best mechanical properties compared with the other bio-composite films (series A2 and series A3) which could be explained by the interactions between the cellulose fibers surface and the adjacent PVA chains.[330]

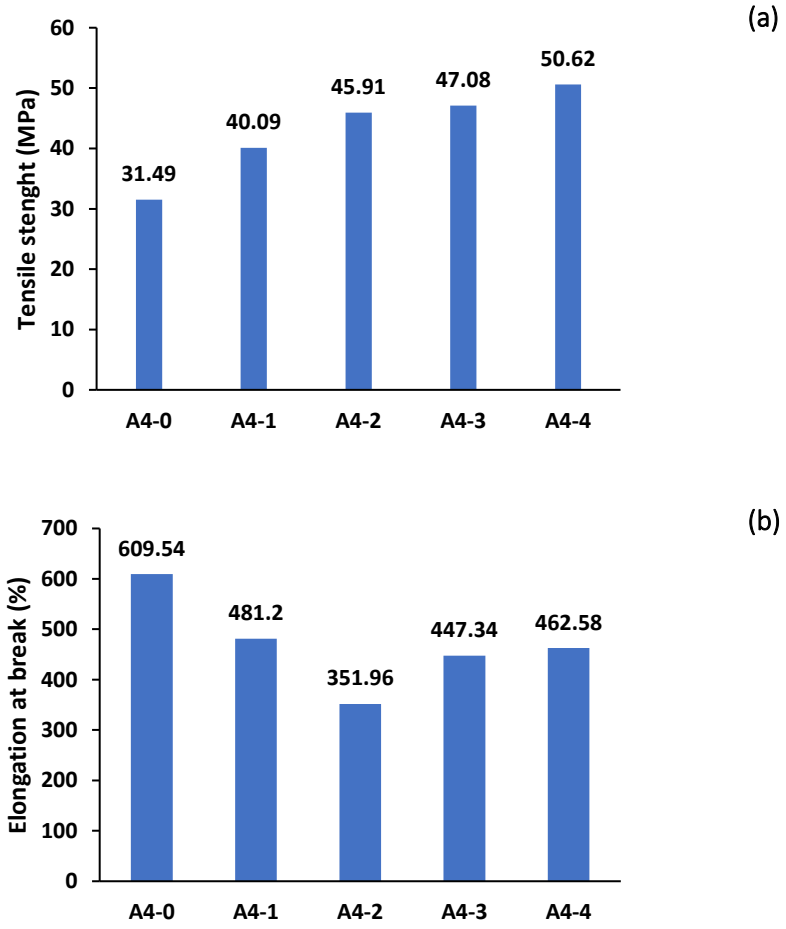

Fig. 76 Tensile strength (a) and elongation at break (b) of as-prepared A4 film series

3.3 Conclusion

From this part, it could be concluded that bio-composite films reinforced with cellulose microfibrils and cellulose nanofibrils were successfully prepared. The better dispersion of the modified WH-B2-H1 and WH-C in the PVA matrix blended with glycerol (compared to series A1) led to improved tensile strength. The bio-composite films obtained from cellulose nanofibrils from acid hydrolysis step exhibited the best optical and mechanical properties compared with the other bio-composite films (series A2 and series A3).

Chapter 4

Materials and Methodology

4.1 Materials

4.1.1 Rice husk

Rice husk was collected from a local farm (Chiang Mai, Northern Thailand), then washed with deionized water and dried at 110 ^{O}C overnight. Then ground rice husks were prepared then the acquired powder was separated using sieve machine and particles (size <100 μm) were collected for further experiment.

4.1.2 Water hyacinth

Water hyacinth fibers (Eichornia crassipes) were collected from Phayao lake in Phayao province, Thailand. In this research, the stems of water hyacinth were used for experimental due to it contains the highest cellulose content, compared to the plant roots and leaves.[10]

4.2 Chemicals

All chemicals and reagents were used as received without further purification.

Deionized water was applied for all treatment processes. Sodium hydroxide (NaOH: ≥ 99.7%, Sigma-Aldrich), glycerol (99%, Sigma-Aldrich), hydrochloric acid (HCl: 36%, Sigma-Aldrich), sulfuric acid (H_2SO_4: 99.99%, Sigma-Aldrich), hydrogen peroxide (H_2O_2: 36%, Sigma-Aldrich), Iron(II) chloride tetrahydrate ($FeCl_2.4H_2O$: ≥99%, Sigma-Aldrich), Iron(III) chloride hexahydrate ($FeCl_3.6H_2O$: ≥99%, Sigma-Aldrich), ammonium hydroxide solution (NH_4OH: ≥30%, Sigma-Aldrich), sodium hypochlorite solution (Reagent grade, Honeywell), polyvinyl alcohol (PVA) (Approx. Mw 13,000 g mol^{-1}, 98% hydrolyzed, Thermo Scientific), cetyltrimethyl ammonium bromide ((CTAB, $C_{16}H_{33}$ $(CH_3)_3NBr$), Sigma-Aldrich) was used as a template, methylene blue ($C_{16}H_{18}ClN_3S$, Merck), acetic acid (98%, Sigma-Aldrich), ethanol (99%, Fisher Chemical) and acetone (≥ 99%, Fisher Chemical).

4.3 Methodology for Chapter 2: Synthesis of bio-derived porous materials from rice husk for methylene blue adsorption in aqueous solutions

4.3.1 Silica extraction

Silica powders were extracted from rice husk through a simple acid pretreatment (chemical pretreatment) by conventional method and microwave-assisted method.[207]

4.3.1.1 Pretreatment by conventional method

Rice husk (RH) (10.00 g) was refluxed at 100 ^{O}C for 3 h in 1 M hydrochloric acid (HCl) (100 ml) solution (solid-to-liquid ratio (SLR) 1:10) to eliminate the impurities, washed with deionized water several times until pH~7. Then, it was dried over night at 100 ^{O}C. After that, a white powder was obtained by calcination with the heating rate of 5 ^{O}C/min and then held at 700 ^{O}C for 3 h to remove organic content.[266]

4.3.1.2 Pretreatment by microwave-assisted method

RH (5.00 g) was heated under microwave radiation at 80 ^{O}C for 30-50 min in 1 M hydrochloric acid (HCl) solution (50 ml) (solid-to-liquid ratio (SLR) 1:10) carried out in CEM MAR 6 with One Touch^{TM} microwave, using EasyPrep^{TM} Plus Easy Prep Teflon 100 ml closed vessels with ramp rate of 15 ^{o}C/min followed by holding time of 30 min, 45 min and 50 min at 80 ^{o}C, to eliminate the impurities, washed with deionized water several times, dried in oven, and calcined at 700 ^{O}C for 3 h, as described in **4.3.1.1**. A white solid powder was obtained after calcination for further analysis.[266]

4.3.2 Preparation of silicate solution

The resulting white powders (2.00 g) after calcination were dissolved in 1 M sodium hydroxide (NaOH) solution (10 ml) (solid-to-liquid ratio = 2:10). The mixture was vigorously stirred at 80 ^{O}C until white powder was completely dissolved. Finally, a clear solution of sodium silicate solution was obtained.[89] A Schematic diagram of silicate solution preparation from rice husk is given in **Fig. 77**.

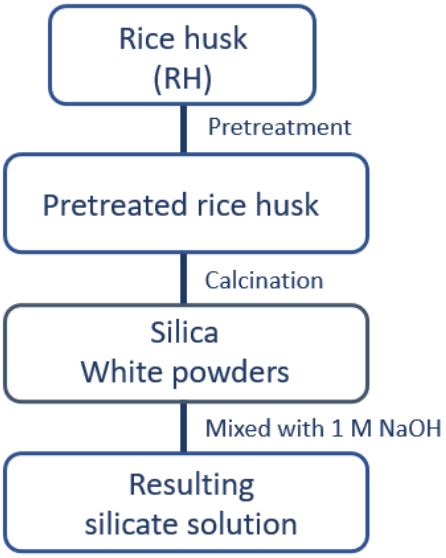

Fig. 77 A Schematic diagram of silicate solution preparation from rice husk

4.3.3 Synthesis of MCM-41 mesoporous materials

The synthesis of MCM-41 in this work based on sodium silicate solution as alternative precursor (commercial silicate solution and bio-derived silicate solution from rice husk) with using CTAB as cationic surfactant via both using conventional method and microwave-assisted method. Moreover, the influence of different ratios of CTAB:Si were also investigated.

4.3.3.1 Conventional method using commercial sodium silicate solution

MCM-41 was prepared by dissolving CTAB (9.60 g) in 200 ml of deionized water. CTAB was used as a template. Then, sodium silicate solution was slowly added to CTAB solution with vigorous stirring for 20 h (molar ratio, CTAB:Si = 0.5:1).[189] The solution pH was adjusted to 11 by 1 M sulfuric acid and 1 M sodium hydroxide. After that, the mixed solution was further stirred for 20 h. Then, the resulting solution was aged at 100 ^{O}C for 4 h. The precipitates were filtered, washed with deionized water, and dried at 100 ^{O}C for 24 h. Finally, the as-obtained product was obtained for characterization by calcination heating rate of 1 ^{O}C/min and then held at 550 ^{O}C for 5 h.

Finally, the as-prepared MCM-41-S was prepared for further analysis.

4.3.3.2 Conventional method using sodium silicate solution derived from rice husk

MCM-41-C was prepared by conventional method (see **4.3.3.1**). Typically, MCM-41 was prepared by dissolving CTAB (9.60 g) in 200 ml of deionized water. The sodium silicate extraction procedure was conducted based on the early part (see **4.3.2**). Then, sodium silicate solution was slowly added to CTAB solution with vigorous stirring for 20 h (CTAB:Si = 0.5:1).[189] Finally, the as-prepared MCM-41-C was characterized as can be seen in **2.3.2**.

4.3.3.3 Microwave-assisted method using sodium silicate solution derived from rice husk

MCM-41-MW was prepared by dissolving CTAB (9.60 g) in 200 ml of deionized water. The sodium silicate extraction procedure was conducted based on the procedure described earlier (see **4.3.2**). Then, sodium silicate solution was slowly added to CTAB solution with vigorous stirring for 5 h (CTAB:Si = 0.5:1).[189] The solution pH was adjusted to 11 by 1 M sulfuric acid and 1 M sodium hydroxide solution. After that, the mixed solution was further stirred for 20 h. Then, the resulting solution was aged in hydrothermal step of synthesis using microwave radiation carried out in CEM MAR 6 with One Touch^{TM} microwave, using EasyPrep^{TM} Plus Easy Prep Teflon 100 ml closed vessels with ramp rate of 15 ^{o}C/min followed by holding time of 30 min at 100 ^{O}C.[187] Then, the procedure was performed based on the procedure described earlier (see **4.3.3.1**). Finally, the as-prepared MCM-41-MW product was obtained.

4.3.3.4 Microwave-assisted method using sodium silicate solution derived from rice husk with varying ratios of CTAB:Si

MCM-41 was prepared by dissolving a desired amount of CTAB (3.84 g, 1.92 g, 0.96 g, and 0.38 g for CTAB:Si of 0.2, 0.1, 0.05 and 0.02, respectively) in 200 ml of deionized water. Then, rice husk derived solution was slowly added to CTAB solution with vigorous stirring for 5 h using various molar ratio of CTAB:Si (0.02-0.2:1).[189] The solution pH was adjusted

to 11 by 1 M sulfuric acid and 1 M sodium hydroxide solution. After that, the mixed solution was further stirred for 20 h. Then, the resulting solution was aged in hydrothermal step of synthesis using microwave radiation carried out in CEM MAR 6 with One Touch™ microwave, using EasyPrep™ Plus Easy Prep Teflon 100 ml closed vessels with ramp rate of 15 °C/min followed by holding time of 30 min at 100 °C.[187] Then, the procedure was performed based on the procedure described earlier (see **4.3.3.1**). Finally, the as-prepared MCM-41 products was obtained and further characterization.

4.3.4 Synthesis of silica particles via acid precipitation

In brief, calcination of rice husk was carried out to provide the resulting white powders (2.00 g) (from the earlier part, section **4.3.1**) which were dissolved in 1 M sodium hydroxide (NaOH) solution (10 ml) (solid-to-liquid ratio = 2:10). The mixture was vigorously stirred at 80 °C until white powders were completely dissolved. Silica particles were prepared via acid precipitation technique from sodium silicate solution derived from rice husk. Methods were slightly modified from the literature as reported elsewhere.[223,230] In this study, 1 M H_2SO_4 and 1 M HCl were used to adjusted the mixed solution until pH = 2 for silica precipitation. In this study simple wet chemical method and the sonication assisted method in aging step at 60 °C for 30 min was used for silica precipitation. Sonication assisted method was carried out using ultrasonic bath (60 kHz) with using 1 M H_2SO_4 to provide SC-H1 and 1 M HCl to provide SC-H4. Whereas, conventional heating was used for wet chemical method with using 1 M HCl to provide SC-H2 and using 1 M H_2SO_4 to provide SC-H3, respectively. The precipitates were filtered, washed with deionized water, and dried at 100 °C for 24. Then, the resulting silica particles under the influence of low frequency ultrasonic irradiation was also studied in this project. Finally, the as-prepared products were obtained for further analysis.

4.3.5 Synthesis of MCM-41 magnetite composite materials

MCM-41 magnetite composite materials were prepared by using $FeCl_2.4H_2O$ (0.80 g) and $FeCl_3.6H_2O$ (2.00 g) were dissolved in 10 ml DI water. Then, 1 M NH_4OH (5 ml) and CTAB

(9.60 g) were mixed in 185 ml DI water. Then, the first solution was added to the second solution to form a colloidal solution of Fe_3O_4. Then, the sodium silicate solution was added to the Fe_3O_4 colloidal solution.[23] The pH of the solution was adjusted to 11 by 1 M sulfuric acid and 1 M sodium hydroxide. After that, the mixed solution was further stirred for 20 h. Then, the resulting solution was aged at 100 ^{O}C for 4 h (the same procedure as described in section **4.3.3.1**). The precipitates were filtered, washed with deionized water, and dried at 100 ^{O}C. Finally, composite material was obtained for characterization by calcination with a heating rate of 1 ^{O}C/min and then held at 550 ^{O}C for 5 h. In this research the effect of different ratio of CTAB:Si at 0.5, 0.2 and 0.02 by using 9.60 g, 3.84 g and 0.38 g of CTAB were also investigated (see section **4.3.3.4**) for the as-obtained CM1, CM2 and CM3 composite materials, respectively.

4.3.6 Application for MB dye adsorption in aqueous solution using as-synthesised mesoporous materials as adsorbent

The maximum adsorption peak of MB in water was shown in the visible region. Its absorption determined at maximum wavelengths of the dye (λ_{max} = 664 nm) and calibration curve was prepared by the plot of absorbance *vs* concentration of MB at λ_{max}. Beer's Law (A = εbc) is observed in the concentration range (0–10 ppm) and a straight line with high regression coefficient value was obtained. For this research $R^2 > 0.9995$ were obtained for MB adsorption study.

4.3.6.1 Removal efficiency

The adsorption capacity at equilibrium q_e (mg g^{-1}) was calculated as follows:

$$q_e = \frac{C_0 - C_e}{W} \times V$$

where C_0 and C_e (mg g^{-1}) are the initial and equilibrium concentrations of methylene blue (MB),

W is the mass of mesoporous silica (g), and

V is the volume of the aqueous solution (L).

In addition, the removal rate of MB was calculated by the following equation:

$$Removal\ (\%) = \frac{C_0 - C_e}{C_0} \times 100\%$$

4.3.6.2 Kinetic study

Adsorption kinetic studies of MB adsorption on mesoporous materials have been studied.

The linear adsorption kinetics models pseudo-first-order and pseudo-second-order were used to analyze the kinetic data. Pseudo-first order kinetics can be defined by the following equation:

$$\log(q_e - q_t) = \log q_e - \frac{k_1}{2.303} k_1 t$$

The pseudo second order kinetic equation is given as:

$$\frac{t}{q_t} = \frac{1}{k_2 q_e^2} + \frac{1}{q_e}\ t$$

where q_e and q_t ($mg \cdot g^{-1}$) are the amount of dye absorbed on adsorbent at equilibrium and at time t (min), respectively. k_1 and k_2 are the rate constant of the pseudo first order (min^{-1}) and pseudo second order ($g\ mg^{-1}\ min^{-1}$), respectively.[331] The straight line can examine the pseudo-second order rate constant (k_2) by the intercept and adsorption capacity ($q_{e,cal}$) by slope.[201,332]

4.3.6.3 Isotherm study

Methylene blue adsorption on mesoporous materials been studied using adsorption isotherm models including the Langmuir and Freundlich models, which can identify the adsorption layer on the surface of materials.

Langmuir isotherm predicts that adsorption occurs at specific sites within the adsorbent by forming a homogenous monolayer of adsorbate. Langmuir isotherm can be expressed as follows:

$$\frac{C_e}{q_e} = \frac{1}{(q_{max})b} + \frac{C_e}{q_{max}}$$

where C_e is the equilibrium concentration of dye (mg L^{-1}), q_e is the amount of adsorbate adsorbed (dye) per unit of mass of adsorbent (mg g^{-1}) at equilibrium, q_{max} is the monolayer adsorption capacity (mg g^{-1}), and b or k_L is the Langmuir constant. In addition, the separation factor (R_L) is an important Langmuir adimensional constant which expresses the feasilibility of adsorption and can be expressed by the following equation:

$$R_L = \frac{1}{bC_0 + 1}$$

where C_0 is the initial adsorbate concentration (mg L^{-1}) and R_L is the value that indicates the nature of isotherm to be unfavorable ($R_L > 1$), linear ($R_L = 1$), favorable ($0 < R_L < 1$), and irreversible ($R_L = 0$), respectively.[66]

While the Langmuir isotherm requires that the adsorbate forms a monolayer on the surface, the Freundlich isotherm is able to deal with multilayer adsorption of MB on the surface of materials. The Freundlich isotherm is represented as follows:

$$\log q_e = \log K_f + \frac{1}{n} \log C_e$$

where K_f is the Freundlich parameter which is related to adsorption capacity (mg g^{-1}), n is the heterogeneity factor, indicating the adsorption intensity. This factor (1/n) indicates the type of isotherm which are irreversible (1/n = 0), favorable ($0 < 1/n < 1$) and unfavorable ($1/n > 1$), respectively for this Freundlich parameter as can be seen from the Freundlich isotherm.[60]

4.3.6.4 Thermodynamic study

The effect of temperature was studied over the range (25-65 ^{O}C). The equilibrium constant (k_c) was calculated using the following equation.[287]

$$k_c = \frac{q_e}{C_e}$$

Thermodynamic parameters of MB adsorption from aqueous solution give a great deal of information concerning the type and mechanism of the adsorption process onto materials. The thermodynamic parameters, Gibbs free energy change ($\Delta G°$), enthalpy change ($\Delta H°$), and entropy change ($\Delta S°$) were calculated by presenting ln k_c vs. *1/T* as presented by equation.

The adsorption free energy change $\Delta G°$ of MB using bio-derived adsorbents was calculated using equation below:

$$\Delta G° = -RT\ lnk_c$$

where R is the universal gas constant (8.314 J mol^{-1} K^{-1}). T is the absolute temperature (K). A negative Gibbs free energy value indicates the feasibility and spontaneous nature of the adsorption process.

The relationship of (ΔG°) to enthalpy change (ΔH°) and entropy change (ΔS°) of adsorption is represented as:

$$\Delta G° = \Delta H° - T\Delta S°$$

Finally, the values of ΔH° and ΔS° are determined from the slope and intercept of the linear plot of (ln k) versus (1/T).

$$lnk = -\frac{\Delta H°}{RT} + \frac{\Delta S°}{R}$$

The positive value of enthalpy change (ΔH°) indicates that the adsorption is an endothermic process, whereas positive value of entropy change (ΔS°) implies the increased randomness at the solid/solution interface adsorption process. The negative value of Gibbs free energy change ($\Delta G°$) also indicates that the adsorption reaction was spontaneous.[62]

4.4 Methodology for Chapter 3: Production of cellulose microfibrils/nanofibrils from water hyacinth for bio-composite films preparation

4.4.1 Production of defibrillated celluloses from water hyacinth

Water hyacinth is lignocellulosic biomass which composed of a cellulose, hemicellulose and lignin so it requires pretreatment to remove noncellulosic components prior to easier defibrillated celluloses generation. In this part, microwave-assisted hydrothermal treatment, chemical treatments including alkaline pretreatment and bleaching steps (chlorine and chlorine-free), acid hydrolysis, and mechanical treatment as well as the effect of different pretreatments on the as-obtained products were investigated which were describes as following part.

4.4.1.1 Microwave-assisted pretreatment method

The microwave-assisted pretreatment of water hyacinth was carried out using a Milestone Synthwave (Maximum power 1500 W, Maximum volume 700 ml, Maximum temperature 300 ^{O}C and Maximum pressure 190 bar). Ground water hyacinth (10 g) was mixed with deionized water (350 ml) at solid-to-liquid ratio of 1:35 (w/v) in a PTFE vessel (700 ml), and microwaved at different temperatures (160 ^{O}C, 180 ^{O}C, 200 ^{O}C and 220 ^{O}C) for a total time of 30 min (15 min ramp time and 15 holding time). After microwave-assisted pretreatment, the pellet was washed sequentially with hot water (80 ^{O}C) 150 ml, 2 times of hot ethanol (65 ^{O}C) 150 ml, cold ethanol (20 ^{O}C) 150 ml and acetone (20 ^{O}C) 150 ml, followed by air-drying at ambient temperature for 24 h to provide WH 160, WH 180, WH 200 and WH 220, respectively.

4.4.1.2 Alkaline pretreatment

Cellulose extraction from lignocellulosic biomass was carried out through different processes depending on the materials available, scale of production and quality of product. A variety of processes for cellulose extraction were studied in the following parts.

Raw water hyacinth was rinsed and sun-dried before using. Then water hyacinth was manually cut into small pieces of 1 cm in length, then further ground to provide the raw water hyacinth powders and sieved to 100 µm before alkaline treatment step.

In brief, ground water hyacinth powders were treated with 5 %w/v NaOH solution (fiber: liquor ratio = 1:20 w/v) at 80 ^{o}C for 30 min for microwave- assisted method denoted as WH-A, then alkaline-treat fibers were filtrated and washed with DI water until neutral fibers were obtained (pH ~ 7) to remove the remaining extractive and impurities.

4.4.1.3 Bleaching step (Chlorine and chlorine-free bleaching method)

The alkaline-treat fibers (10.00 g) were bleached in 2 wt% $NaClO_2$ solution (200 ml) acidified by acetic acid (fiber: liquor ratio = 1:20 w/v) under the vigorously stirred at 80 ^{o}C for 3 h. Then, the as-obtained white fibers were filtered by vacuum filtration and washed with DI water to remove the residue of bleaching agent.

The alkaline-treat fibers were bleached in H_2O_2 acidified by acetic acid under the vigorous stirred at 80 ^{o}C for 3 h for chlorine-free process. Then, the as-obtained white fibers were filtered by vacuum filtration and washed with DI water to remove the residue. Both steps were slightly modified from the literature as reported elsewhere.[117]

4.4.1.4 Acid hydrolysis

Typically, the preparation of nanocellulose from cellulose requires two main stages. The first stage focuses on the pretreatments of feedstocks to obtain pure cellulose, whereas the second stage is dedicated to the transformation of cellulose to nanocellulose. A typical method starts with alkali and bleaching pretreatments followed by acid hydrolysis.

The resulting fibers from bleaching step (1.00 g) were mixed with 50% wt sulfuric acid (10 ml) (fiber: liquor ratio = 1:10 w/v) under vigorous stirring at 45 ^{o}C for 30 min. The as-obtained fibers were centrifuged and washed with DI water until the pH is neutral and then nanocellulose was produced.

4.4.1.5 Mechanical treatment

The as-obtained WH fibers from microwave-assisted pretreatment method and from bleaching step (chlorine-free method), were diluted with DI water. Subsequently, the mechanical treatment was applied to the chemical-treated fibers to disintegrate micro/nanofibers.[9] The mechanical treatment of homogenisation is known to modify the original cellulose fibers by defibrillation resulting in releasing microfibrils and microfibril bundles in the water suspension.[312] This part was described the methodology of mechanical treatment by homogenisation.[125]

Two different methods were carried out which including MW-assisted pretreatment to produce defibrillated celluloses, subsequently homogenisation (referred to as method MW-M) and WH-B2 obtained by chemical treatment after bleaching step with using chlorine free method was then subsequent mechanical treatment through homogenisation (denoted as method C-M).

For Method MW-M, the resulting fibers from MW-assisted pretreatment to produce defibrillated celluloses, were subsequently subjected to a 60 min-treatment time using the high-speed homogenisation. Following the homogenisation process, mixed solution of MW-M suspension in deionized water in vial and subjected to homogenisation with probe which was immersed in the middle of the mixture to get defibrillated cellulose.

For method C-M, the resulting WH-B2 from chemical treatment after bleaching step with using chlorine free method was subsequently subjected to a 15 min-treatment time using the homogenisation process to get WH-B2-H1 and 20 min-treatment time to get WH-B2-H2. A mixture solution of desired amount of WH-B2 suspension in deionized water in vial

and subjected to homogenisation with probe which was immersed in the middle of the mixture to get defibrillated cellulose in micro/nano scale.[313]

4.4.2 Application for film preparation

PVA was used for films preparation due to its biodegradability, good mechanical strength, thermal stability, high hydrophilic properties and water solubility, nontoxicity.[250,293,314] Blending with glycerol to improve its flexibility. Then, defibrillated nanocellulose was expected to be used as a substitute and filler as nanofiller to provide new materials of bio-composite materials with specific properties such as mechanical properties described in this part. Various conditions for film preparation including, optimization condition for film preparation of PVA films blended with glycerol (denoted as series A1), bio-composite film preparation from WH-MW-H (denoted as series A2), bio-composite film preparation from WH-B2 after homogenisation for 15 min (denoted as series A3) and bio-composite film preparation from WH-C (denoted as series A4), respectively.

4.4.2.1 Optimisation conditions for film preparation

In brief, PVA was dissolved in distilled water at 80 °C for 30 min with constant stirring until complete dissolution to obtain PVA solution. To study the optimum condition for film preparation, glycerol was used for mixing solution.

Film preparation series A1 was prepared by the following procedure. PVA was dissolved in deionised water by heating to 80 ^{O}C and vigorously stirred to create well-defined solutions at 2–20 wt % solution.[258,316] This section developed from previous reports PVA film prepared by 5% (w/v) of PVA solution studied by Fong *et al*.[316], and Bahrami *et al.*[293] The mixture was casted in the petri dish, then the mixture was dried at 25 ^{O}C for 24 h for further characterization.

To study the effect of plasticizer on properties of films, a desired aqueous solution of PVA blended with glycerol were prepared. The suspension was vigorously stirred and mixed with various content of glycerol of 1%-5% v/v., then the solution was casted onto the Petri

dishes and dried at 25 ^{O}C for 24 h for further analysis. Various conditions were prepared for film preparation series A1 of 0%, 1%, 2%, 3% and 5% (v/v) of glycerol adding in bio-composite films to provide A1-0, A1-1, A1-2, A1-3 and A1-4, respectively.

4.4.2.2 Bio-composite film preparation

PVA was dissolved in deionised water by heating to 80 ^{O}C and the vigorously stirred to create well-defined solutions at 2–20 wt % solution. The procedure was conducted based on the early part (see **4.4.2.1**). Similar aqueous solutions of plasticizers were prepared with a desired ratio of mixture. Films were solution cast into petri dishes under the atmospheric condition and subsequently dried in a vacuum oven at 25 ^{O}C for 24 h.[316]

Film preparation series A2 was prepared by the following procedure. PVA was dissolved in deionised water by heating to 80 ^{O}C and vigorously stirred to create well-defined solution at 5 wt % solution. Then PVA solution was mixed with a desired quantity of MW-M (1%-5%) at ambient temperature and then glycerol (2% v/v) was added into a mixed solution under vigorously stirring.

This part the 2% v/v of glycerol were prepared for this series A2 due to this condition was an optimum condition for MW-M addition in bio-composite films preparation. Finally, the solution was casted onto the petri dish and dried at 25 ^{O}C for 24 h for further analysis. Various conditions were prepared for film preparation series A2 of 0%, 1%, 2%, 3% and 5% of MW-M suspension adding in bio-composite films to provide A2-0, A2-1, A2-2, A2-3 and A2-4, respectively.

In terms of film preparation Series A3 can be prepared by the following step. Firstly, PVA was dissolved in deionised water by heating to 80 ^{O}C and vigorously stirred to create well-defined solution at 5 wt % solution. Then PVA solution was mixed with a desired quantity of WH-B2-H1 at ambient temperature and then glycerol was added into a mixed solution under vigorously stirring and followed by glycerol (1% v/v) was added into a mixed solution under vigorously stirring. Finally, the solution was casted onto the petri dish and

dried at 25 ^{O}C for 24 h for further analysis. Various conditions were prepared for film preparation series A3 of 0%, 1%, 2%, 3% and 5% of WH-B2-H1 suspension adding in bio-composite films to provide A3-0, A3-1, A3-2, A3-3 and A3-4, respectively.

For film preparation Series A4 PVA, this part can be prepared the same procedure with series A3 but using the different type of cellulose fibers. Firstly, PVA was dissolved in distilled water at 80 °C for 30 min with constant stirring until complete dissolution to obtain PVA solution. Then PVA solution was mixed with a desired quantity of micro-fibrillated/ nano-fibrillated cellulose at ambient temperature and then glycerol was added into a mixed solution under vigorously stirring. The mixture was poured into a petri dish and oven-dried at 25 ^{O}C for 24 h to ensure slow evaporation of the excess moisture. The as-obtained films were peeled off the dish and stored in a desiccator for further analysis.[121] These series A4 were prepared of 0%, 1%, 2%, 3% and 5% of WH-C suspension to provide A4-0, A4-1, A4-2, A4-3 and A4-4, respectively.

4.5 Techniques for characterization and analysis

4.5.1 X-Ray Powder Diffraction (XRD)

To investigate the important factors including crystalline structure and degree of crystallinity of the crystalline and semi-crystalline materials and define the impurities. Identification of phases is achieved by comparison of the acquired data to that in reference databases. X-ray diffraction is useful for evaluating minerals, corrosion products, polymers, and unknown materials. XRD patterns of the materials were investigated using X-ray diffractometers (XRD; Aeris Malvern Panalytical) and were recorded as a function of diffraction angle (2θ) from 5 to 40° with a step size of 0.01° and step time of 0.5 s.[117]

4.5.2 Crystallinity Index (CI)

The crystallinity index (crystallinity percentage), which governs the mechanical and physical properties of nanocellulose is calculated employing an X-ray diffractometer (XRD)

with Cu Kα radiation at 0.154 nm operating at 40 kV and 40 mA. Crystallinity index (CI) was estimated using an empirical method according to the Segal's equation:

$$CI\ (\%) = (I_{200} - I_{am}/I_{200}) \times 100$$

where I_{200} is the maximum intensity of 200 plane in crystalline region, whereas I_{am} is the intensity presenting amorphous region.

4.5.3 Small-angle X-ray Scattering (SAXS)

Small Angle X-ray Scattering (SAXS) is an X-ray technique which allows the non-destructive investigation of nanoscale particle size, distribution and morphology. The Xeuss 2.0 SAXS system is equipped with two microfocus sources; Cu for standard measurements and Mo for more absorbing samples. It has a q range of 0.025 to 30 nm^{-1}, giving a maximum measurable particle diameter up to roughly 250 nm.

4.5.4 Ultraviolet–Visible Spectroscopy (UV-Vis)

The ultraviolet and visible light barrier properties of the film was measured via a UV–Vis spectrophotometer at wavelength from 200 to 800 nm using transmittance mode at 2 nm intervals in UV–VIS regions. The transparency of the films was calculated from the percent transmittance of light at 500 nm.

4.5.5 Fourier-Transform Infrared Spectroscopy (FTIR)

A Fourier transform infrared spectrophotometer (FTIR) in attenuated total reflectance (ATR) mode was used for identifying the functional groups of the samples. The background was recorded at the beginning of the measurement. The spectra were collected from 600- 4000 cm^{-1} with data acquisition of 16 scans at a resolution of 4 cm^{-1}. Analysis was carried out using Bruker OPUS software. Attenuated Total Reflection Infrared Spectroscopy (ATR-IR). Functional group of material was determined by Attenuated Total Reflection Infrared Spectroscopy (ATR-IR). Attenuated Total Reflection Infrared Spectroscopy was carried out using a Perkin Elmer FTIR/FTNIR Spectrum 400

Spectrophotometer. The measurement was achieved between 650 cm^{-1} and 4000 cm^{-1} with a total of 16 scans and a resolution of 4 cm^{-1}.

4.5.6 Porosimetry, N_2 adsorption/desorption analysis

Nitrogen at 77 K is considered to be a standard adsorbate for surface area and pore size analysis. Three parameters can be analysed by porosimetry, including specific surface area, pore size distribution and pore volume. Brunauer-Emmett-Teller (BET) Surface Area Analysis was used for determining the specific surface area of porous materials which is based on a kinetic model of Langmuir model adsorption process.

A micromeritics TriStar II plus (at liquid nitrogen temperature (77K)) porosimeter was used for investigation of the specific surface area and total pore volume can be obtained through the specific surface area, pore volume and pore size of nanocellulose samples. The desired sample (80-100 mg) was added into the porosimeter tube and weight of tube and samples were recorded. Prior to the measurement, a degas step was performed at 120 ^{O}C for 8 h, after that the degassed sample was weighted again before analysis.

4.5.7 Thermogravimetric Analysis (TGA)

Thermal stability, which signifies the thermal decomposition and impurities of nanocellulose, can be investigated by differential scanning calorimetry (DSC), thermogravimetric analysis (TGA), and differential thermogravimetry (DTG).

Thermal stability and degradation behavior of each sample were investigated using a thermogravimetric analyzer (PL Thermal Sciences STA 625). In brief, approximately 10 mg of each sample was heated from 25^{O}C to 625 ^{O}C at a constant heating rate of 10 $^{O}C\ min^{-1}$ under a constant nitrogen flow of 50 ml/min.[131]

4.5.8 Morphological structure

The morphology and dimensional evaluation of nanocellulose can be carried out by using a Scanning Electron Microscope (SEM) operated at 15 kV and Transmission Electron

Microscopy (TEM). Prior to characterization by SEM, the as-obtained samples were sputtered-coated with a few conductive gold layers to compromise the image charging.

4.5.8.1 Scanning Electron Microscopy (SEM)

Morphology of high surface area porous materials from rice husk and morphology of water hyacinth cellulose microfibrils/nanofibrils (microcrystals and nanocrystals) were investigated by scanning electron microscopy (SEM) at Department of Biology, University of York. High surface area porous materials were dispersed in absolute ethanol (0.01% wt/v) before being dropped onto the sample stub. Water hyacinth cellulose (microfibrils/nanofibrils) microcrystals and nanocrystals samples were homogenised and diluted to form 0.01 wt% solution before being dropped on a freshly cleaved mica that was attached on stub. The surface morphology of samples was characterised using scanning electron microscopy (SEM- JEOL JSM-6490LV) at an accelerated voltage of 15–20 kV after gold or platinum coating by a JEOL JFC–1100 E sputtering device for 85 seconds prior to SEM observation.

4.5.8.2 Transmission Electron Microscopy (TEM)

TEM Tecnai 12 BioTWIN with a SIS Megaview 3 camera at a 76-acceleration voltage of 120 kV (manufactured by FEI) at the accelerating voltage of 120 kV was used to observe morphology and size of samples. Briefly, samples were suspended in absolute ethanol in microcentrifuge tubes and were deposited onto 200 mesh grids with a carbon support film for 2 h, allowing them to air-dry for 2 h. The diameter of TEM images was measured using an imageJ software.

4.8.9 X-Ray Fluorescence spectroscopy (XRF)

Elemental analyses of solid samples and quantitative analysis was performed on a Horiba XGT 7000 X-ray analytical microscope. Samples were coated on a holder and analysed using a standardless independent parameters method. Each measurement was repeated the average was taken.

4.8.10 Mechanical testing

The tensile analysis of the PVA film, PVA blended with glycerol and micro/nanocellulose reinforced PVA composite films or bio-composite films were carried out using an Instron® 3367 Universal Testing machine. The tensile measurements were conducted following by the Standard Test Method for Tensile Properties of Thin Plastic Sheeting (ASTM D882) at 25 ^{O}C.[254,333] Each sample was investigated for five times under the same condition and the average value were reported which includes tensile strength (MPa) and elongation at break (%).[334,335]

Chapter 5

Conclusions and future work

5.1 Conclusions

In conclusion, this study successfully demonstrated the valorisation of rice husk for synthesis of high surface area porous silica materials, MCM-41 and its composite through the microwave-assisted method which offer the shorter reaction time for preparation. Rice husk can be used as sustainable source from agricultural waste for the silica extraction and then can be used for preparation of silicate solution for the synthesis of silica particles, MCM-41 and MCM-41 magnetite composite materials. These as-synthesised products also provide the high surface area mesoporous materials that exhibited remarkable adsorption performance for methylene dye in aqueous solution by almost 100% removal within an hour for using MCM-41 magnetite composite as adsorbent. This suggests that this bio-based mesoporous magnetite composite prepared through microwave-assisted route could be a promising material with outstanding environment benefits for methylene blue (cationic dye) adsorption and easy for separation process after wastewater treatment. Hence, the study of anionic dyes adsorption model, pesticides or even heavy metals in wastewater from industrial processes and agricultural waste could be further studied for potential applications.

Water hyacinth is a floating plant and an invasive species that pollutes and clogs waterways, has been a problem in Thailand for over a decade, apart from the conversion of this plant into bioethanol with a source of renewable energy. In this study, the design of method for production of cellulose microfibrils and cellulose nanofibrils from water hyacinth was also successfully prepared for using as reinforcing agent for bio-composite films preparation. Owing to WH has high content of cellulose, abundance and biocompatibility. Nanocellulose produced from water hyacinth are gaining in the research field that can be used as reinforcing agent for biodegradable films from polyvinyl alcohol based which could be a candidate to replace conventional plastic films from petroleum-based. This study demonstrated the simple method for biodegradable film preparation which can be prepared by mixing with the optimum ratio of PVA, cellulose micro/nanofibrils and glycerol at controlled temperature, and finally the bio-composite

films were successfully prepared by simple solution casting technique. The enhancing of tensile strength was significantly increased from cellulose nanofibrils addition in films preparation process and the best optical properties also obtained from this bio-composite film. Due to its good mechanical and optical properties (transparency), this film could be used as food and non-food packaging with high quality of product. Moreover, this practical technique for producing bio composite films could be used for a large-scale production. Fabricating cellulose microfibrils and cellulose nanofibrils from cellulose wastes would be an alternative route for efficiently valorising water hyacinth wastes and developed for use in a variety of additional applications, including aerogels, hydrogels, coatings, and smart materials such as film protection, coating materials and etc.

Overall, the waste biomass (rice husk and water hyacinth) has been valorised to generate value-added products which can be developed a greener procedure for production through microwave-assisted method and avoid to use harsh conditions for producing sustainable materials for waste water treatment generated from many industries and smart materials with possess high quality which is necessary to be an alternative material for biodegradation and sustainability.

5.2 Future work

5.2.1 Future work- Project 1: Rice husk

Synthesis of bio-derived mesoporous materials from rice husk for methylene blue adsorption in aqueous solutions

It is necessary that waste is reduced and that materials are not to be disposed of after their first use for waste water treatment. Although, the removal efficiency of adsorbent for methylene blue adsorption may decrease in many cycles but it is still benefit for cost-effective if it can be reused for waste water treatment in the several times. Reusability of the as-synthesized MCM-41, silica nanoparticles and MCM-41 magnetite composite materials for MB dye adsorption will be investigated for reusing as adsorbent. Due to porous silica materials could be recycle for waste water treatment by calcination to obtain the materials. Moreover, MCM-41 magnetite composite materials could also be easily

separated from aqueous solutions which could be useful process for cost saving and time saving for water purification and also reduce waste disposal.

The investigation of the methylene blue dye adsorption was studied for the cationic dye adsorption models. The other types of organic dyes which are classified into anionic dyes (e.g. methyl orange (MO), Congo red (CR) and methyl blue) and other cationic dyes (e.g. crystal violet), widely used in printing and textile industries that can cause the negative effect for aquatic organisms and human health when discharged into the environment without the proper treatment. So, these adsorbents could be used for wastewater remediation for other organic dyes in wastewater from industrial processes. In addition, water contaminated with heavy metals (such as Pb^{2+}, Cd^{2+}, Cr^{6+}, etc.) and pesticides wastewater from agricultural waste that can also cause a danger to ecosystems and living organisms also require the proper approach to remove them from water. To meet the growing emission of water contaminants, high surface area MCM-41 mesoporous material and its composite both have hexagonal structures with average pore diameter of 2.8-6.3 nm that can provide the properties that might enhance the performance for materials concerning adsorption/catalysis capability, and stability. The physical remediation is based mostly on the adsorption process can apply on a large scale that can also further studied for a broad range of potential applications which relating to solid waste management (SDG 11) in Thailand.

5.2.2 Future work- Project 2: Water hyacinth

Production of cellulose microfibrils/nanofibrils from water hyacinth for bio-composite films preparation

In this work, bio-composite films were successfully prepared with improved mechanical properties by addition of cellulose microfibrils and cellulose nanofibrils as reinforcing agent. In addition, food packaging could be improved its properties such as quality maintenance with aims for enhancing and improving food quality and safety by reduction of pathogen growth or to prevent microbial growth and extension of shelf life by adding some small amount of silver that may enhance the shelf-life of stored food.

The production of bio composite films though simple solution casting technique also has a beneficial to explore the process of scaling up from lab-scale to pilot-scale that might be useful for sustainable packaging derived from renewable resources that are entirely biodegradable.

Abbreviations

ATR-IR	Attenuated total reflection infrared spectroscopy
BET	Brunauer-Emmett-Teller
BJH	Barrett Joyner and Halenda
CHN	Carbon, Hydrogen and Nitrogen
CMF	Cellulose microfibril
CNC	Cellulose nanocrystal
CNF	Cellulose nanofibril
CTAB	Cetyltrimethylammonium bromide
CI	Crystallinity Index
DSC	Differential Scanning Calorimetry
DTG	Differential Thermogravimetric Analysis
FTIR	Fourier Transform Infrared Spectroscopy
IL	Ionic liquid
IUPAC	International Union of Pure and Applied Chemistry
NMR	Nuclear Magnetic Resonance
MB	Methylene blue
MCM-41	Mobil Composition of Matter No. 41

MW	Microwave
ppm	Parts per million
RH	Rice husk
SAXS	Small-Angle X-ray Scattering
SDGs	Sustainable Development Goals
SEM	Scanning Electron Microscopy
STA	Simultaneous Thermal Analysis
TEOS	Tetraethylorthosilicate
TEM	Transmission Electron Microscopy
TGA	Thermogravimetric Analysis
UN	United Nations
UV-Vis	Ultraviolet–Visible Spectroscopy
WH	Water Hyacinth
XPS	X-ray photoelectron spectroscopy
XRD	X-ray Diffraction
XRF	X-Ray Fluorescence

References

1 M. O. S. Dias, T. L. Junqueira, C. D. F. Jesus, C. E. V. Rossell, R. Maciel Filho and A. Bonomi, *Energy*, 2012, **43**, 246–252.

2 K. Im-orb, W. Wiyaratn and A. Arpornwichanop, *Energy*, 2018, **153**, 592–603.

3 M. Monção, P. P. Thoresen, T. Wretborn, H. Lange, U. Rova, P. Christakopoulos and L. Matsakas, *Sustain Energy Fuels*, 2023, **7**, 3902–3918.

4 E. Calcio Gaudino, G. Cravotto, M. Manzoli and S. Tabasso, *Green Chem*, 2019, **21**, 1202–1235.

5 K. Aroonrat and S. Wongwises, *Renew Sustain Energy Rev*, 2015, **46**, 70–78.

6 T. Silalertruksa and S. H. Gheewala, *Energ Policy*, 2010, **38**, 7476–7486.

7 T. Silalertruksa, S. H. Gheewala and P. Pongpat, *Appl Energy*, 2015, **160**, 603–609.

8 X. Zhang, K. Rajagopalan, H. Lei, R. Ruan and B. K. Sharma, *Sustain Energy Fuels*, 2017, **1**, 1664–1699.

9 S. Tanpichai, S. K. Biswas, S. Witayakran and H. Yano, *ACS Sustain Chem Eng*, 2019, **7**, 18884–18893.

10 P. Pantamanatsopa, W. Ariyawiriyanan and S. Ekgasit, *J Nat Fibers*, 2023, **20**, 1-14.

11 M. Asrofi, H. Abral, A. Kasim, A. Pratoto, M. Mahardika, J. W. Park and H. J. Kim, *Fiber Polym*, 2018, **19**, 1618–1625.

12 J. H. Clark, R. Luque and A. S. Matharu, *Annu Rev Chem Biomol Eng*, 2012, **3**, 183–207.

13 P. Morone, A. Koutinas, N. Gathergood, M. Arshadi and A. Matharu, *J Clean Prod*, 2019, **221**, 10–16.

14 K. L. Ong, G. Kaur, N. Pensupa, K. Uisan and C. S. K. Lin, *Bioresour Technol*, 2018, **248**, 100–112.

15 S. Chaijamrus and B. Mouthung, *Songklanakarin J Sci Technol*, 2011, **33**, 163–170.

16 G. Smagulova, A. Imash, A. Baltabay, B. Kaidar and Z. Mansurov, *C-J Carbon res*, 2022, **8**, 55.

17 N. Na chat, S. Sangsuradet, P. Tobarameekul and P. Worathanakul, *Mater Chem Phys*, 2022, **282**, 125933.

18 Y. Shen, *Glob Chall*, 2018, **2**, 1800043.

19 Y. Gao, M. Z. Ozel, T. Dugmore, A. Sulaeman and A. S. Matharu, *J Hazard Mater*, 2021, **401,** 123400.

20 T. Silalertruksa, P. Pongpat and S. H. Gheewala, *J Clean Prod*, 2017, **140**, 906–913.

21 C. Sakdaronnarong, W. Pipathworapoom, T. Vichitsrikamol, T. Sema, P. Posoknistakul, W. Koo-amornpattana and N. Laosiripojana, *Process Saf Environ Prot*, 2018, **116**, 1–13.

22 T. J. Bondancia, J. De Aguiar, G. Batista, A. J. G. Cruz, J. M. Marconcini, L. H. C. Mattoso and C. S. Farinas, *Ind Eng Chem Res*, 2020, **59**, 11505–11516.

23 S. Kamari and F. Ghorbani, *Biomass Convers Biorefin*, 2021, **11**, 3001-3009.

24 J. J. Bozell, S. K. Black, M. Myers, D. Cahill, W. P. Miller and S. Park, *Biomass Bioenerg*, 2011, **35**, 4197–4208.

25 S. Tanpichai and J. Wootthikanokkhan, *IEEE J Sel Top Quant*, 2018, **25**, 395–401.

26 J. U. Hernández-Beltrán, I. Hernández-De Lira, M. Cruz-Santos, A. Saucedo-Luevanos, F. Hernández-Terán and N. Balagurusamy, *Appl Sci*, 2019, **9**, 1-29.

27 L. J. Jönsson and C. Martín, *Bioresour Technol*, 2016, **199**, 103–112.

28 M. J. Taherzadeh and K. Karimi, *Int J Mol Sci*, 2008, **9**, 1621-1651.

29 H. Chen, J. Liu, X. Chang, D. Chen, Y. Xue, P. Liu, H. Lin and S. Han, *Fuel Process Technol*, 2017, **160**, 196–206.

30 J. D. McMillan, *Pretreatment of Lignocellulosic Biomass*, American Chemical Society, Washington DC, 1994.

31 I. K. M. Yu, H. Chen, F. Abeln, H. Auta, J. Fan, L. Vitaly, J. H. Clark, S. Parsons, C. J. Chuck, G. Luo, *Crit Rev Environ Sci Technol*, 2020, **51**, 1479-1532.

32 N. Samsalee, J. Meerasri and R. Sothornvit, *Carbohydr. Polym.*, 2023, **6**, 100353.

33 Z. Zhu, D. J. Macquarrie, R. Simister, L. D. Gomez and S. J. McQueen-Mason, *Sustain Chem Process*, 2015, **3**, 1–13.

34 M. R. Zakaria, S. Hirata, S. Fujimoto and M. A. Hassan, *Bioresour Technol*, 2015, **193**, 128–134.

35 N. Mosier, C. Wyman, B. Dale, R. Elander, Y. Y. Lee, M. Holtzapple and M. Ladisch, *Bioresour Technol*, 2005, **96**, 673–686.

36 A. Kruse and E. Dinjus, *J Supercrit Fluids*, 2007, **39**, 362–380.

37 W. Dedsuksophon, K. Faungnawakij, V. Champreda and N. Laosiripojana, *Bioresour Technol*, 2011, **102**, 2040–2046.

38 C. Tangsathitkulchai, N. Punsuwan and P. Weerachanchai, *Processes*, 2019, **7**, 1-20.

39 C. Rodriguez Correa, T. Hehr, A. Voglhuber-Slavinsky, Y. Rauscher and A. Kruse, *J Anal Appl Pyrolysis*, 2019, **140**, 137–147.

40 M. J. C. van der Stelt, H. Gerhauser, J. H. A. Kiel and K. J. Ptasinski, *Biomass Bioenerg*, 2011, **35**, 3748–3762.

41 A. Toptas, Y. Yildirim, G. Duman and J. Yanik, *Bioresour Technol*, 2015, **177**, 328–336.

42 W. Kajina, P. Rousset, W. H. Chen, T. Sornpitak and J. M. Commandré, *Renew Energy*, 2018, **118**, 113–121.

43 P. Buapeth, W. Watcharin, D. Dechtrirat and L. Chuenchom, *IOP Conf Ser Mater Sci Eng*, 2019, **515**, 1-7.

44 H. M. Liu, B. Feng and R. C. Sun, *J Agric Food Chem*, 2011, **59**, 10524–10531.

45 J. Yang, Q. (Sophia)He and L. Yang, *Appl Energy*, 2019, **250**, 926–945.

46 A. Koriakin, S. Moon, D. W. Kim and C. H. Lee, *Fuel*, 2017, **208**, 184–192.

47 D. J. Macquarrie, J. H. Clark and E. Fitzpatrick, *Biofuel Bioprod Bior*, 2012, **6**, 549–560.

48 V. L. Budarin, J. H. Clark, B. A. Lanigan, P. Shuttleworth and D. J. Macquarrie, *Bioresour Technol*, 2010, **101**, 3776–3779.

49 F. P. Bouxin, J. H. Clark, J. Fan and V. Budarin, *Green Chem*, 2019, **21**, 1282–1291.

50 P. Alvira, E. Tomás-Pejó, M. Ballesteros and M. J. Negro, *Bioresour Technol*, 2010, **101**, 4851–4861.

51 Z. Zhu, Y. Liu, X. Yang, S. J. McQueen-Mason, L. D. Gomez and D. J. Macquarrie, *Biomass Convers Biorefin*, 2021, **11**, 2681-2693.

52 D. Klein-Marcuschamer, P. Oleskowicz-Popiel, B. A. Simmons and H. W. Blanch, *Biotechnol Bioeng*, 2012, **109**, 1083–1087.

53 S. Suwannarangsee, B. Bunterngsook, J. Arnthong, A. Paemanee, A. Thamchaipenet, L. Eurwilaichitr, N. Laosiripojana and V. Champreda, *Bioresour Technol*, 2012, **119**, 252–261.

54 S. Prasertwasu, D. Khumsupan, T. Komolwanich, T. Chaisuwan, A. Luengnaruemitchai and S. Wongkasemjit, *Bioresour Technol*, 2014, **163**, 152–159.

55 P. F. Siqueira, S. G. Karp, J. C. Carvalho, W. Sturm, J. A. Rodríguez-León, J. L. Tholozan, R. R. Singhania, A. Pandey and C. R. Soccol, *Bioresour Technol*, 2008, **99**, 8156–8163.

56 A. Di Paola, E. García-López, G. Marcì and L. Palmisano, *J Hazard Mater*, 2012, **211–212**, 3–29.

57 J. Wang, L. Qin, J. Lin, J. Zhu, Y. Zhang, J. Liu and B. Van der Bruggen, *Chem Eng J*, 2017, **323**, 56–63.

58 C. Santasnachok, W. Kurniawan and H. Hinode, *J Environ Chem Eng*, 2015, **3**, 2115–2126.

59 C. Santasnachok, W. Kurniawan and H. Hinode, *J Life Sci*, 2015, **10**, 127–130.

60 H. I. Meléndez-Ortiz, B. Puente-Urbina, J. A. Mercado-Silva and L. García-Uriostegui, *Int J Appl Ceram Technol*, 2019, **16**, 1533–1543.

61 H. Iván, M. Ortiz, L. G. Uriostegui, B. Puente, U. Jesus and A. Mercado, *Int J Appl Ceram*, 2019, **16**, 1533–1543.

62 M. N. Sahmoune, *Environ Chem Lett*, 2019, **17**, 697–704.

63 T. Qiang, Y. Song, J. Zhao and J. Li, *J Alloys Compd*, 2019, **770**, 792–802.

64 T. Suwunwong, N. Hussain, S. Chantrapromma and K. Phoungthong, *Mater Res Express*, 2020, **7**, 15518.

65 M. Rafatullah, O. Sulaiman, R. Hashim and A. Ahmad, *J Hazard Mater*, 2010, **177**, 70–80.

66 S. Chandrasekhar and P. N. Pramada, *Adsorption*, 2006, **12**, 27–43.

67 P. T. Dang, H. T. H. Nguyen, C. D. Dao, G. H. Le, Q. K. Nguyen, K. T. Nguyen, H. T. K. Tran, T. V. Nguyen and T. A. Vu, *Adv Mater Sci Eng*, 2016, **2016**, 1-9.

68 X. Sun, W. Yu, J. Yan, J. Li, G. Jin, J. Feng, Z. Guo and X. Liang, *RSC Adv*, 2018, **8**, 27207–27215.

69 Y. Dong, B. Lu, S. Zang, J. Zhao, X. Wang and Q. Cai, *J Chem Technol Biotechnol*, 2011, **86**, 616–619.

70 W. Zhu, J. Wang, D. Wu, X. Li, Y. Luo, C. Han, W. Ma and S. He, *Nanoscale Res Lett*, 2017, **12**, 1-9.

71 V. Zeleňák, J. Magura, A. Zeleňáková and R. Smolková, *Pure Appl Chem*, 2017, **89**, 493–500.

72 K. Siriworarat, V. Deerattrakul, P. Dittanet and P. Kongkachuichay, *J Clean Prod*, 2017, **142**, 1234–1243.

73 P. Fu, T. Yang, J. Feng and H. Yang, *J Ind Eng Chem*, 2015, **29**, 338–343.

74 G. Yang, Y. Deng, H. Ding, Z. Lin, Y. Shao and Y. Wang, *Appl Clay Sci*, 2015, **111**, 61–66.

75 M. S. Abdel Salam, M. A. Betiha, S. A. Shaban, A. M. Elsabagh, R. M. Abd El-Aal and F. Y. El kady, *Egypt J Pet*, 2015, **24**, 49–57.

76 S. Bhattacharyya, G. Lelong and M. L. Saboungi, *J Exp Nanosci*, 2006, **1**, 375–395.

77 E. P. Favvas, K. L. Stefanopoulos, A. C. Mitropoulos and N. K. Kanellopoulos, *Micropor Mesopor Mat*, 2015, **209**, 122–125.

78 A. Zukal, M. Thommes and J. Čejka, *Micropor Mesopor Mat*, 2007, **104**, 52–58.

79 E. B. Celer and M. Jaroniec, *J Am Chem Soc*, 2006, **128**, 14408–14414.

80 S. Varshney, V. Mulpuru, N. Mishra and M. K. Gupta, *Mater Technol*, 2022, **37**, 2608–2622.

81 J. Remón, J. Randall, V. L. Budarin and J. H. Clark, *Green Chem*, 2019, **21**, 284–299.

82 Z. Zhu, C. A. Rezende, R. Simister, S. J. McQueen-Mason, D. J. Macquarrie, I. Polikarpov and L. D. Gomez, *Biomass Bioenerg*, 2016, **93**, 269–278.

83 E. Saksornchai, J. Kavinchan, S. Thongtem and T. Thongtem, *Nanoscale Res Lett*, 2017, **12**, 1-10.

84 B. L. Newalkar, J. Olanrewaju and S. Komarneni, *J Phys Chem B*, 2001, **105**, 8356–8360.

85 D. Schneider, R. Kircheis, S. Wassersleben, W. D. Einicke, R. Gläser and D. Enke, *Front Chem*, 2019, **7**, 1-13.

86 Y. Shen, P. Zhao and Q. Shao, *Micropor Mesopor Mat*, 2014, **188**, 46–76.

87 A. Bazargan, Z. Wang, J. P. Barford, J. Saleem and G. McKay, *J Clean Prod*, 2020, **260**, 1-12.

88 L. A. Pfaltzgraff, M. De Bruyn, E. C. Cooper, V. Budarin and J. H. Clark, *Green Chem*, 2013, **15**, 307–314.

89 W. Roschat, T. Siritanon, B. Yoosuk and V. Promarak, *Energy Convers Manag*, 2016, **119**, 453–462.

90 V. C. Niculescu, *Front Mater*, 2020, **7**, 1-14.

91 R. Ryoo, S. H. Joo, M. Kruk and M. Jaroniec, *Adv Mater*, 2001, **13**, 677–681.

92 D. Battegazzore, S. Bocchini, J. Alongi and A. Frache, *RSC Adv*, 2014, **4**, 54703–54712.

93 X. G. Chen, S. S. Lv, S. T. Liu, P. P. Zhang, A. B. Zhang, J. Sun and Y. Ye, *Sep Sci Technol*, 2012, **47**, 147–156.

94 J. R. Dodson, E. C. Cooper, A. J. Hunt, A. Matharu, J. Cole, A. Minihan, J. H. Clark and D. J. MacQuarrie, *Green Chem*, 2013, **15**, 1203–1210.

95 Y. Shen, *J Agric Food Chem*, 2017, **65**, 995–1004.

96 S. Schacht, M. Janicke and F. Schü, *Micropor Mesopor Mater*, 1998, **22**, 485-493.

97 J. Fan, M. De bruyn, Z. Zhu, V. Budarin, M. Gronnow, L. D. Gomez, D. Macquarrie and J. Clark, *Chem Eng Process*, 2013, **71**, 37–42.

98 A. Banka, T. Komolwanich and S. Wongkasemjit, *Cellulose*, 2015, **22**, 9–29.

99 J. P. Dhal, T. Dash and G. Hota, *J Porous Mater*, 2020, **27**, 205–216.

100 A. de N. de Oliveira, R. da S. Cardoso, I. M. Ferreira, L. S. da Silva, A. A. F. da Costa, L. H. de O. Pires, G. N. da Rocha Filho, R. Luque, R. C. R. Noronha and L. A. S. do Nascimento, *Micropor Mesopor Mater*, 2023, **354**, 1-50.

101 A. A. Sabri, T. M. Albayati and R. A. Alazawi, *Korean J Chem Eng*, 2015, **32**, 1835–1841.

102 M. A. Hubbe, P. Tayeb, M. Joyce, P. Tyagi, M. Kehoe, K. Dimic-Misic and L. Pal, *Bioresources*, 2017, **12**, 9556–9661.

103 M. Y. Khalid, A. Al Rashid, Z. U. Arif, W. Ahmed and H. Arshad, *J Mater Res Technol*, 2021, **14**, 2601–2623.

104 Z. Shi, G. O. Phillips and G. Yang, *Nanoscale*, 2013, **5**, 3194–3201.

105 Q. Zhang, C. Weng, H. Huang, V. Achal and D. Wang, *Front Microbiol*, 2016, **6**, 1–9.

106 P. Phanthong, P. Reubroycharoen, X. Hao, G. Xu, A. Abudula and G. Guan, *Carbon Resour Convers*, 2018, **1**, 32–43.

107 J. Gröndahl, K. Karisalmi and J. Vapaavuori, *Soft Matter*, 2021, **17**, 9842–9858.

108 H. V. Lee, S. B. A. Hamid and S. K. Zain, *Sci World J*, 2014, **1**, 1-20.

109 C. Zinge and B. Kandasubramanian, *Eur Polym J*, 2020, **133**, 1-20.

110 D. Iqbal, Y. Zhao, R. Zhao, S. J. Russell and X. Ning, *Polymers (Basel)*, 2022, **14**, 1-36.

111 V. Nang An, H. T. Chi Nhan, T. D. Tap, T. T. T. Van, P. Van Viet and L. Van Hieu, *J Polym Environ*, 2020, **28**, 1465–1474.

112 E. Lam and U. D. Hemraz, *Nanomaterials*, 2010, **11**, 1-32.

113 S. Tanpichai, S. Mekcham, C. Kongwittaya, W. Kiwijaroun, K. Thongdonsun, C. Thongdeelerd and A. Boonmahitthisud, *J Nat Fibers*, 2022, **19**, 5676–5696.

114 J. Sugiyama, R. Vuong and H. Chanzy, *Macromolecules*, 1991, **24**, 4168–4175.

115 P. Lenihan, A. Orozco, E. O'Neill, M. N. M. Ahmad, D. W. Rooney and G. M. Walker, *Chem Eng J*, 2010, **156**, 395–403.

116 Y. C. Lin, S. Shangdiar, S. C. Chen, F. C. Chou, Y. C. Lin and C. A. Cho, *Renew Energy*, 2018, **125**, 511–517.

117 K. Pakutsah and D. Aht-Ong, *Int J Biol Macromol*, 2020, **145**, 64–76.

118 D. A. Laroque, G. M. F. de Aragão, P. H. H. de Araújo and B. A. M. Carciofi, *Packag Technol Sci*, 2021, **34**, 463–474.

119 L. An, J. Chen, J. W. Heo, J. H. Bae, H. Jeong and Y. S. Kim, *Carbohydr Polym*, 2021, **274**, 1-11.

120 P. Cazón, M. Vázquez and G. Velazquez, *Carbohydr Polym*, 2018, **195**, 432–443.

121 H. C. Oyeoka, C. M. Ewulonu, I. C. Nwuzor, C. M. Obele and J. T. Nwabanne, *Journal of Bioresources and Bioproducts*, 2021, **6**, 168–185.

122 Y. Pan, Y. Xie and P. Cai, *Cellulose*, 2022, **29**, 9375–9391.

123 R. Tan, F. Li, Y. Zhang, Z. Yuan, X. Feng, W. Zhang, T. Liang, J. Cao, C. F. De Hoop, X. Peng and X. Huang, *J Nanomater*, 2021, **2021**, 1-9.

124 M. Mahardika, H. Abral, A. Kasim, S. Arief and M. Asrofi, *Fibers*, 2018, **6**, 1–12.

125 M. Dilamian and B. Noroozi, *Cellulose*, 2019, **26**, 5831–5849.

126 Z. Yan, L. Meng, X. Huang, Q. Wei, J. Liu, Z. Sun and S. Ding, *J Text Inst*, 2023, **114**, 1881-1886.

127 E. C. Peres, N. Favarin, J. Slaviero, A. R. F. Almeida, M. P. Enders, E. I. Muller and G. L. Dotto, *Mater Lett*, 2018, **231**, 72–75.

128 P. N. Amaniampong, A. Karam, Q. T. Trinh, K. Xu, H. Hirao, F. Jérôme and G. Chatel, *Sci Rep*, 2017, **7**, 1–8.

129 W. Laumer, L. Andreu, G. Helle, G. H. Schleser, T. Wieloch and H. Wissel, *Rapid Commun Mass Sp*, 2009, **23**, 1934–1940.

130 H. Wang, M. Zuo, N. Ding, G. Yan, X. Zeng, X. Tang, Y. Sun, T. Lei and L. Lin, *ACS Sustain Chem Eng*, 2019, **7**, 9378–9386.

131 D. Sun, A. J. Onyianta, D. O'Rourke, G. Perrin, C. M. Popescu, L. H. Saw, Z. Cai and M. Dorris, *Cellulose*, 2020, **27**, 3727–3740.

132 M. Yuttitham, S. H. Gheewala and A. Chidthaisong, *J Clean Prod*, 2011, **19**, 2119–2127.

133 C. Sakdaronnarong, N. Srimarut and N. Laosiripojana, *Key Eng Mater*, 2015, **659**, 527–532.

134 S. Imman, N. Laosiripojana and V. Champreda, *Appl Biochem Biotechnol*, 2018, **184**, 432-443.

135 P. Boonchuay, C. Techapun, N. Leksawasdi, P. Seesuriyachan, P. Hanmoungjai, M. Watanabe, S. Takenaka and T. Chaiyaso, *Bioresour Technol*, 2018, **256**, 399–407.

136 A. Saning, S. Herou, D. Dechtrirat, C. Ieosakulrat, P. Pakawatpanurut, S. Kaowphong, C. Thanachayanont, M. M. Titirici and L. Chuenchom, *RSC Adv*, 2019, **9**, 24248–24258.

137 X. Sun, Q. Wu, X. Zhang, S. Ren, T. Lei, W. Li, G. Xu and Q. Zhang, *Cellulose*, 2018, **25**, 1103–1115.

138 K. K. Packiam, B. Murugesan, P. M. Kaliyannan Sundaramoorthy, H. Srinivasan and K. Dhanasekaran, *J Nat Fibers*, 2022, **19**, 7424–7435.

139 A. Xia, J. Cheng, W. Song, C. Yu, J. Zhou and K. Cen, *Energy*, 2013, **61**, 158–166.

140 J. Cai, J. Chen, Q. Zhang, M. Lei, J. He, A. Xiao, C. Ma, S. Li and H. Xiong, *Carbohydr Polym*, 2016, **140**, 238–245.

141 S. Chen, M. Chen, H. Huang, X. Liu, B. Qu, R. Wang, K. Liu, Y. Zheng and D. Zhuo, *Appl Compos Mater*, 2022, **29**, 1597–1619.

142 K. J. Nagarajan, M. R. Sanjay, K. Sathick Basha, G. R. Raghav, R. Ashok Kumar, S. Siengchin, B. Surya Rajan, P. Sabari Nath and A. Khan, *Polym Compos*, 2022, **43**, 4942–4958.

143 K. Pacaphol and D. Aht-Ong, *Surf Coat Technol*, 2017, **320**, 70–81.

144 N. El Miri, K. Abdelouahdi, M. Zahouily, A. Fihri, A. Barakat, A. Solhy and M. El Achaby, *J Appl Polym Sci*, 2015, **132**, 1-13.

145 Anastas, P.T. and Warner, J.C. (1998) Green Chemistry: Theory and Practice. Oxford University Press, New York, 29-56.

146 The Sustainable Development Goals Report (2023): Special Edition is the only UN official report that monitors global progress on the 2030 Agenda for Sustainable Development.

147 J. Zhang, Y. S. Choi, C. G. Yoo, T. H. Kim, R. C. Brown and B. H. Shanks, *ACS Sustain Chem Eng*, 2015, **3**, 293–301.

148 M. Z. H. Kazmi, A. Karmakar, V. K. Michaelis and F. J. Williams, *Tetrahedron*, 2019, **75**, 1465–1470.

149 N. I. Abdo, Y. M. Tufik and S. M. Abobakr, *Curr Res Green Sustain Chem*, 2023, **6**, 1-7.

150 C. J. Chirayil, J. Joy, L. Mathew, M. Mozetic, J. Koetz and S. Thomas, *Ind Crops Prod*, 2014, **59**, 27–34.

151 S. El-Din Al-Mofty, N. H. Elghazawy and H. M. E. Azzazy, *RSC Sustainability*, 2023, **1**, 1743-1750.

152 S. Rani, K. Gulati, N. Raghav and S. Arora, *ChemistrySelect*, 2022, **7**, 1-8.

153 X. Kang, S. Kuga, C. Wang, Y. Zhao, M. Wu and Y. Huang, *ACS Sustain Chem Eng*, 2018, **6**, 2954–2960.

154 D. Trache, A. F. Tarchoun, M. Derradji, T. S. Hamidon, N. Masruchin, N. Brosse and M. H. Hussin, *fchem*, 2020, **8**, 1-33.

155 M. N. Tousignant, N. A. Rice, A. Peltekoff, C. Sundaresan, C. Miao, W. Y. Hamad and B. H. Lessard, *Langmuir*, 2020, **36**, 3550–3557.

156 P. Kumar, D. M. Barrett, M. J. Delwiche and P. Stroeve, *Ind Eng Chem Res*, 2009, **48**, 3713–3729.

157 P. A. Larsson, A. V. Riazanova, G. Cinar Ciftci, R. Rojas, H. H. Øvrebø, L. Wågberg and L. A. Berglund, *Cellulose*, 2019, **26**, 1565–1575.

158 D. Trache, M. H. Hussin, C. T. Hui Chuin, S. Sabar, M. R. N. Fazita, O. F. A. Taiwo, T. M. Hassan and M. K. M. Haafiz, *Int J Biol Macromol*, 2016, 93, 789–804.

159 D. Miyashiro, R. Hamano and K. Umemura, *Nanomaterials*, 2020, **10**, 1-23.

160 Y. Wang, S. Liu, Q. Wang, X. Fu and P. Fatehi, *Cellulose*, 2020, **27**, 8725–8743.

161 D. Tian, J. Hu, J. Bao, R. P. Chandra, J. N. Saddler and C. Lu, *Biotechnol Biofuels*, 2017, **10**, 1-11.

162 R. Katahira, T. J. Elder and G. T. Beckham, *RSC Energy and Environment Series*, 2018, **2018**, 1–20

163 J. Dai, A. F. Patti and K. Saito, *Tetrahedron Lett*, 2016, **57**, 4945–4951.

164 H. Yang, R. Yan, H. Chen, D. H. Lee and C. Zheng, *Fuel*, 2007, **86**, 1781–1788.

165 Y. V. Larichev, P. M. Yeletsky and V. A. Yakovlev, *J Phys Chem Solids*, 2015, **87**, 58–63.

166 V. B. Carmona, R. M. Oliveira, W. T. L. Silva, L. H. C. Mattoso and J. M. Marconcini, *Ind Crops Prod*, 2013, **43**, 291–296.

167 Z. Wang, X. Qiao and K. Sun, *Carbohydr Polym*, 2018, **197**, 442–450.

168 D. F. Hincapié Rojas, P. Pineda Gómez and A. Rosales Rivera, *Adv Mater Lett*, 2019, **10**, 67–73.

169 R. A. Bakar, R. Yahya and S. N. Gan, *Procedia Chem*, 2016, **19**, 189–195.

170 N. Bisht, P. C. Gope and N. Rani, *J Mech Behav Mater*, 2020, **29**, 147–162.

171 N. Shahi, E. Lee, B. Min and D. J. Kim, *Sensors*, 2021, **21**, 1-16.

172 U. Zulfiqar, T. Subhani and S. Wilayat Husain, *J Non Cryst Solids*, 2015, **429**, 61–69.

173 Q. Wang, S. Kudo, S. Asano and J. I. Hayashi, *ACS Omega*, 2022, **7**, 27638–27648.

174 L. Y. Jaramillo, K. Arango-Benítez, W. Henao, E. Vargas, G. Recio-Sánchez and M. Romero-Sáez, *Mater Lett*, 2019, **257**, 126749.

175 G. Martínez-Edo, A. Balmori, I. Pontón, A. M. Del Rio and D. Sánchez-García, *Catalysts*, 2018, **8**, 1-62.

176 F. Adam, J. N. Appaturi and A. Iqbal, *Catal Today*, 2012, **190**, 2–14.

177 S. Rashid and H. Dutta, *Ind Crops Prod*, 2020, 154, 1-12.

178 W. Wang, J. C. Martin, R. Huang, W. Huang, A. Liu, A. Han and L. Sun, *RSC Adv*, 2012, **2**, 9036–9041.

179 T. Y. Chiou, T. L. Neoh, T. Kobayashi and S. Adachi, *Biosci Biotechnol Biochem*, 2012, **76**, 1535–1539.

180 G. K. Gaurav, T. Mehmood, L. Cheng, J. J. Klemeš and D. K. Shrivastava, *J Clean Prod*,2020, **277**, 1-17.

181 B. T. N. Thi, L. H. V. Thanh, T. N. P. Lan, N. T. D. Thuy and Y.-H. Ju, *J Clean Energy Technol*, 2017, **5**, 274–279.

182 P. Pantamanatsopa, W. Ariyawiriyanan and S. Ekgasit, *J Nat Fibers*, 2022, **20**, 1-14.

183 W. Ben Bakrim, A. Ezzariai, F. Karouach, M. Sobeh, M. Kibret, M. Hafidi, L. Kouisni and A. Yasri, *Front Pharmacol*, 2022, **13**, 1-21.

184 M. Akkoç, N. Buğday, S. Altın and S. Yaşar, *Appl Organomet Chem*, 2021, **35**, 1-21.

185 V. Chaudhary and S. Sharma, *Journal of Porous Materials*, 2017, **24**, 741–749.

186 R. Kueasook, N. Rattanachueskul, N. Chanlek, D. Dechtrirat, W. Watcharin, P. Amornpitoksuk and L. Chuenchom, *Microporous Mesoporous Mater*, 2020, **295**, 1-15.

187 A. N. Ergün, Z. Ö. Kocabaş, M. Baysal, A. Yürüm and Y. Yürüm, *Chem Eng Commun*, 2013, **200**, 1057–1070.

188 Y. Zhao, H. Wang, Y. Liu, J. Ye and S. Shen, *Mater Lett*, 2008, **62**, 4254–4256.

189 K. Siriworarat, V. Deerattrakul, P. Dittanet and P. Kongkachuichay, *J Clean Prod*, 2017, **142**, 1234–1243.

190 M. Bhagiyalakshmi, L. J. Yun, R. Anuradha and H. T. Jang, *J Porous Mater*, 2010, **17**, 475–484.

191 C. T. Kresge and W. J. Roth, *Chem Soc Rev*, 2013, **42**, 3663–3670.

192 R. Ryoo, C. H. Ko and I. S. Park, *Chem Commun*, 1999, **15**, 1413–1414.

193 A. F. Hassan, S. A. Helmy and A. Donia, *J Braz Chem Soc*, 2015, **26**, 1367–1378.

194 S. Wu, W. Zhang, S. Jia, Y. Liu, J. Ran, H. Ren and J. Hou, *Mater Lett*, 2013, **98**, 138–141.

195 E. V. Vyshegorodtseva, Y. V. Larichev and G. V. Mamontov, *J Solgel Sci Technol*, 2019, **92**, 496–505.

196 E. Gianotti, G. Berlier, K. Costabello, S. Coluccia and F. Meneau, *Catal Today*, 2007, **126**, 203–210.

197 J. Rathousky, A. J. Zukal Heyrovsky and G. Schulz-Ekloff, *J Chem Soc*, 1994, **90**, 2821-2826.

198 W. Y. Sang and O. P. Ching, *J Adv Res Fluid Mech Therm Sci*, 2018, **42**, 46–56.

199 T. Prasomsri, W. Jiao, S. Z. Weng and J. Garcia Martinez, *Chem Commun*, 2015, **51**, 8900–8911.

200 M. R. Oliveira, J. A. Cecilia, J. F. De Conto, S. M. Egues and E. Rodríguez-Castellón, *J Solgel Sci Technol*, 2023, **105**, 370–387.

201 M. K. Seliem, S. Komarneni and M. R. Abu Khadra, *Micropor Mesopor Mater*, 2016, **224**, 51–57.

202 S. H. Abbas, F. Adam and L. Muniandy, *Micropor Mesopor Mater*, 2020, **305**, 1-10.

203 C. Gonzalez-Arellano, A. M. Balu, R. Luque and D. J. Macquarrie, *Green Chem*, 2010, **12**, 1995–2002.

204 S. B. Bhaduri, *Mater Manuf Process*, 1993, **8**, 391–392.

205 D. Singh, R. Kumar, A. Kumar and K. N. Rai, *Ceramica*, 2008, **54**, 203–212.

206 M. Huang, J. Cao, X. Meng, Y. Liu, W. Ke, J. Wang and L. Sun, *Chem Phys Lett*, 2016, **662**, 42–46.

207 S. Sankar, S. K. Sharma, N. Kaur, B. Lee, D. Y. Kim, S. Lee and H. Jung, *Ceram Int*, 2016, **42**, 4875–4885.

208 U. Zulfiqar, T. Subhani and S. Wilayat Husain, *J Non Cryst Solids*, 2015, **429**, 61–69.

209 I. Made Joni, Rukiah and C. Panatarani, *AIP Conf Proc*, 2020, **2219**, 80018.

210 D. An, Y. Guo, B. Zou, Y. Zhu and Z. Wang, *Biomass Bioenerg*, 2011, **35**, 1227–1234.

211 I. A. Rahman, P. Vejayakumaran, C. S. Sipaut, J. Ismail, M. A. Bakar, R. Adnan and C. K. Chee, *Colloids Surf A Physicochem Eng Asp*, 2007, **294**, 102–110.

212 M. Abdollahi-Alibeik and Z. Ramazani, *Main Group Metal Chemistry*, 2022, **45**, 190–201.

213 A. Ulu, S. A. A. Noma, S. Koytepe and B. Ates, *Artif Cells Nanomed Biotechnol*, 2018, **46**, 1035–1045.

214 M. Abdollahi-Alibeik and A. Rezaeipoor-Anari, *J Magn Magn Mater*, 2016, **398**, 205–214.

215 N. A. Fellenz, S. G. Marchetti, J. F. Bengoa, R. C. Mercader and S. J. Stewart, *J Magn Magn Mater*, 2006, **306**, 30–34.

216 E. Saksornchai, J. Kavinchan, S. Thongtem and T. Thongtem, *Mater Lett*, 2018, **213**, 138–142.

217 J. S. Kim, Y. Y. Lee and T. H. Kim, *Bioresour Technol*, 2016, **199**, 42–48.

218 G. Bali, X. Meng, J. I. Deneff, Q. Sun and A. J. Ragauskas, *ChemSusChem*, 2015, **8**, 275–279.

219 A. P. Sulaeman, Y. Gao, T. Dugmore, J. Remón and A. S. Matharu, *Cellulose*, 2021, **28**, 7687–7705.

220 A. H. Tayeb, E. Amini, S. Ghasemi and M. Tajvidi, *Molecules*, 2018, **23**, 1-24.

221 M. Mariano, N. El Kissi and A. Dufresne, *J Polym Sci B Polym Phys*, 2014, **52**, 791–806.

222 H. M. Ng, L. T. Sin, T. T. Tee, S. T. Bee, D. Hui, C. Y. Low and A. R. Rahmat, *Compos B Eng*, 2015, **75**, 176–200.

223 G. K. Gupta and P. Shukla, *Front Chem*, 2020, **8**, 601256.

224 W. Guo, G. Li, Y. Zheng and K. Li, *RSC Adv*, 2021, **11**, 34915–34922.

225 N. Johar, I. Ahmad and A. Dufresne, *Ind Crops Prod*, 2012, **37**, 93–99.

226 X. Wu, C. Lu, Z. Zhou, G. Yuan, R. Xiong and X. Zhang, *Environ Sci Nano*, 2014, **1**, 71–79.

227 N. A. Rosli, I. Ahmad and I. Abdullah, *Cellulose nanocrystals from agave*, 2013, **8**, 1893-1908.

228 X. Qiao, Z. Wang and K. Sun, *Mater Chem Phys*, 2022, **292**, 126879.

229 Z. Wang, Y. Ding and J. Wang, *Nanomaterials*, 2019, **9**, 1-17.

230 B. Sun, H. Y. Yu, Y. Zhou, Z. Huang and J. M. Yao, *Ind Crops Prod*, 2016, **89**, 66–77.

231 K. Yuwawech, J. Wootthikanokkhan, S. Wanwong and S. Tanpichai, *J Appl Polym Sci*, 2017, **134**, 1-12.

232 X. Yu, Y. Jiang, Q. Wu, Z. Wei, X. Lin and Y. Chen, *Front Energy Res*, 2021, **9**, 774783.

233 W. Zhang, X. He, C. Li, X. Zhang, C. Lu, X. Zhang and Y. Deng, *Cellulose*, 2014, **21**, 485–494.

234 K. Choi, J. Do Nam, S. H. Kwon, H. J. Choi, M. S. Islam and N. Kao, Polymers (Basel), 2019, **11**, 1-11.

235 S. Nuchdang, V. Thongtus, M. Khemkhao, S. Kirdponpattara, E. J. Moore, H. D. B. Setiabudi and C. Phalakornkule, *Biomass Convers Biorefin*, 2020, **11**, 2471-2483.

236 M. Raita, N. Denchokepraguy, V. Champreda and N. Laosiripojana, *3 Biotech*, 2017, **7**, 1–10.

237 N. Khat-udomkiri, B. S. Sivamaruthi, S. Sirilun, N. Lailerd, S. Peerajan and C. Chaiyasut, *AMB Express*, 2018, **8**, 1–10.

238 T. S. Ng, Y. C. Ching, N. Awanis, N. Ishenny and M. R. Rahman, *Mater Res Innov*, 2014, **18**, 400-404.

239 S. C. Shi and G. T. Liu, *Cellulose*, 2021, **28**, 6147–6158.

240 T. Wang and Y. Zhao, *Carbohydr Polym*, 2021, **253**, 117225.

241 T. Zhong, G. S. Oporto, J. Jaczynski and C. Jiang, *Biomed Res Int*, 2015, **2015**, 456834-456838.

242 A. A. Ebnalwaled, A. H. Sadek, S. H. Ismail and G. G. Mohamed, *Opt Quantum Electron*, 2022, **54**, 1-31.

243 T. Kittikorn, W. Chaiwong, E. Stromberg, R. M. Torro, M. Ek and S. Karlsson, *Journal of Plastic Film and Sheeting*, 2020, **36**, 368–390.

244 L. Meng, J. Li, X. Fan, Y. Wang, Z. Xiao, H. Wang, D. Liang and Y. Xie, *Compos Sci Technol*, 2023, **232**, 109885.

245 A. Mandal and D. Chakrabarty, *J Ind Chem Eng*, 2014, **20**, 462–473.

246 H. P. S. Abdul Khalil, A. H. Bhat and A. F. Ireana Yusra, *Carbohydr Polym*, 2012, **87**, 963–979.

247 S. Virtanen, S. Vuoti, H. Heikkinen and P. Lahtinen, *Cellulose*, 2014, **21**, 3561–3571.

248 T. V. Panova, A. A. Efimova, A. K. Berkovich and A. V. Efimov, *RSC Adv*, 2020, **10**, 24027–24036.

249 J. Cai, J. Chen, Q. Zhang, M. Lei, J. He, A. Xiao, C. Ma, S. Li and H. Xiong, *Carbohydr Polym*, 2016, **140**, 238–245.

250 H. Tian, L. Yuan, D. Zhou, J. Niu, H. Cong and A. Xiang, *Polym Adv Technol*, 2018, **29**, 2612–2618.

251 P. Cazón, G. Velazquez and M. Vázquez, *Food Hydrocoll*, 2019, **89**, 481–491.

252 A. Abdulkhani, E. Hojati Marvast, A. Ashori, Y. Hamzeh and A. N. Karimi, *Int J Biol Macromol*, 2013, **62**, 379–386.

253 A. Briddick, P. Li, A. Hughes, F. Courchay, A. Martinez and R. L. Thompson, *Langmuir*, 2016, **32**, 864–872.

254 R. Santi, A. Cigada, B. Del Curto and S. Farè, *J Appl Biomater Funct Mater*, 2019, **17**, 1-7.

255 S. Lal, V. Kumar and S. Arora, *Polymers and Polymer Composites*, 2021, **29**, 1505–1514.

256 W. Li, Q. Wu, X. Zhao, Z. Huang, J. Cao, J. Li and S. Liu, *Carbohydr Polym*, 2014, **113**, 403–410.

257 Z. Feng, D. Xu, Z. Shao, P. Zhu, J. Qiu and L. Zhu, *Carbohydr Polym*, 2022, **296**, 119886.

258 D. Rahmadiawan, H. Abral, R. M. Railis, I. C. Iby, M. Mahardika, D. Handayani, K. D. Natrana, D. Juliadmi and F. Akbar, *J Compos Sci*, 2022, **6**, 1-15.

259 S. Suganthi, S. Vignesh, J. Kalyana Sundar and V. Raj, *Appl Water Sci*, 2020, **10**, 1-11.

260 I. J. Fernandes, D. Calheiro, A. G. Kieling, C. A. M. Moraes, T. L. A. C. Rocha, F. A. Brehm and R. C. E. Modolo, *Fuel*, 2016, **165**, 351–359.

261 P. P. Nayak, S. Nandi and A. K. Datta, *Engineering Reports*, 2019, **1**, 1-13.

262 S. Azat, A. V. Korobeinyk, K. Moustakas and V. J. Inglezakis, *J Clean Prod*, 2019, **217**, 352–359.

263 W. Wang, J. C. Martin, X. Fan, A. Han, Z. Luo and L. Sun, *ACS Appl Mater Interfaces*, 2012, **4**, 977–981.

264 E. Mily, A. González, J. J. Iruin, L. Irusta and M. J. Fernández-Berridi, *J Solgel Sci Technol*, 2010, **53**, 667–672.

265 F. Adam, J. N. Appaturi, Z. Khanam, R. Thankappan and M. A. M. Nawi, *Appl Surf Sci*, 2013, **264**, 718–726.

266 C. Kongmanklang and K. Rangsriwatananon, *J Spectrosc*, 2015, **2015**, 2–7.

267 X. Li, X. Xu, Y. He, Y. Jiang, Y. Teng, Q. Wang and K. Lin, *Mater Lett*, 2015, **146**, 84–86.

268 F. Guo, N. N. Wei, Z. L. Xiu and Z. Fang, *Fuel*, 2012, **93**, 468–472.

269 X. Yang, P. Roonasi and A. Holmgren, *J Colloid Interface Sci*, 2008, **328**, 41–47.

270 N. K. Renuka, A. K. Praveen and K. Anas, *Mater Lett*, 2013, **109**, 70–73.

271 M. R. Alves, M. F. Paiva, P. T. A. Campos, E. F. de Freitas, M. C. H. Clemente, G. A. V. Martins, A. T. Silveira, L. C. C. da Silva, M. C. A. Fantini, S. C. L. Dias and J. A. Dias, *J Porous Mater*, 2021, **28**, 323–335.

272 L. López Pérez, M. J. Ortiz-Iniesta, H. Jan Heeres and I. Melián-Cabrera, *Mater Lett*, 2014, **118**, 51–54.

273 E. A. Gorrepati, P. Wongthahan, S. Raha and H. S. Fogler, *Langmuir*, 2010, **26**, 10467–10474.

274 F. Adam, T. S. Chew and J. Andas, *J Solgel Sci Technol*, 2011, **59**, 580–583.

275 M. Abdollahi-Alibeik and A. Rezaeipoor-Anari, *J Magn Magn Mater*, 2016, **398**, 205–214.

276 P. Parthasarathy and S. K. Narayanan, *Environ Prog Sustain Energy*, 2014, **33**, 676–680.

277 M. Zirak, A. Abdollahiyan, B. Eftekhari-Sis and M. Saraei, *Cellulose*, 2018, **25**, 503–515.

278 W. E. Rashwan, K. S. Abou-El-Sherbini, M. A. Wahba, S. A. Sayed Ahmed and P. G. Weidler, *Silicon*, 2020, **12**, 2017–2029.

279 M. Zirak, A. Abdollahiyan, B. Eftekhari-Sis and M. Saraei, *Cellulose*, 2018, **25**, 503–515.

280 P. Sharma, R. Kaur, C. Baskar and W. J. Chung, *Desalination*, 2010, **259**, 249–257.

281 Y. Tong, P. J. McNamara and B. K. Mayer, *Environ Sci (Camb)*, 2019, **5**, 821–838.

282 M. Sharma, S. Hazra and S. Basu, *J Colloid Interface Sci*, 2017, **504**, 669–679.

283 Y. Miyah, A. Lahrichi, M. Idrissi, A. Khalil and F. Zerrouq, *Surf Interfaces*, 2018, **11**, 74–81.

284 Y. S. Ho, *Water Res*, 2006, **40**, 119–125.

285 F. Subhan, S. Aslam, Z. Yan, M. Khan, U. J. Etim and M. Naeem, *J Porous Mater*, 2019, **26**, 1465–1474.

286 A. A. Nada, M. F. Bekheet, S. Roualdes, A. Gurlo and A. Ayral, *J Mol Liq*, 2019, **274**, 505–515.

287 M. Abboud, T. Sahlabji, M. A. Haija, A. A. El-Zahhar, S. Bondock, I. Ismail and S. M. A. S. Keshk, *New J Chemistry*, 2020, **44**, 2291–2302.

288 Y. Gao, H. Xia, A. P. Sulaeman, E. M. De Melo, T. I. J. Dugmore and A. S. Matharu, *ACS Sustain Chem Eng*, 2019, **7**, 11861–11871.

289 S. H. Osong, S. Norgren and P. Engstrand, *Cellulose*, 2016, **23**, 93–123.

290 A. E. Karaca, C. Özel, A. C. Özarslan and S. Yücel, *Polym Compos*, 2022, **43**, 6838–6853.

291 N. Aggarwal, P. Pal, N. Sharma and S. Saravanamurugan, *ACS Omega,* 2021, **6**, 27247-27258.

292 Y. Ma, H. Zhang, H. Yang and Y. Zhang, *Cellulose*, 2019, **26**, 8465–8474.

293 A. Bahrami and R. Fattahi, *Food Sci Nutr*, 2021, **9**, 4974–4985.

294 P. Cazón, M. Vázquez and G. Velazquez, *Carbohydr Polym*, 2018, **195**, 432–443.

295 S. Imman, J. Arnthong, V. Burapatana, V. Champreda and N. Laosiripojana, *Chem Eng J*, 2015, **278**, 85–91.

296 F. L. Zitzmann, E. Ward and A. S. Matharu, *Gels*, 2022, **8**, 1-9.

297 V. Nang An, H. T. Chi Nhan, T. D. Tap, T. T. T. Van, P. Van Viet and L. Van Hieu, *J Polym Environ*, 2020, **28**, 1465–1474.

298 S. Imman, J. Arnthong, V. Burapatana, N. Laosiripojana and V. Champreda, *Appl Biochem Biotechnol*, 2013, **170**, 1982–1995.

299 S. S. Nair and N. Yan, *Cellulose*, 2015, **22**, 3137–3150.

300 R. A. Fenner and J. 0 Lephardt, *Food Chem*, 1981, **29**, 846-849.

301 N. Zhang, P. Tao, Y. Lu and S. Nie, *Cellulose*, 2019, **26**, 7823–7835.

302 J. K. Singh, B. Chaurasia, A. Dubey, A. M. F. Noguera, A. Gupta, R. Kothari, C. P. Upadhyaya, A. Kumar, A. Hashem, A. A. Alqarawi and E. F. A. Allah, *Sustainability*, 2021, **13**, 1–16.

303 P. Asawaworarit, P. Daorattanachai, W. Laosiripojana, C. Sakdaronnarong, A. Shotipruk and N. Laosiripojana, *Chem Eng J*, 2019, **356**, 461–471.

304 E. Pinto, W. N. Aggrey, P. Boakye, G. Amenuvor, Y. A. Sokama-Neuyam, M. K. Fokuo, H. Karimaie, K. Sarkodie, C. D. Adenutsi, S. Erzuah and M. A. D. Rockson, *Sci Afr*, 2022, **15**, 1-14.

305 G. Bali, X. Meng, J. I. Deneff, Q. Sun and A. J. Ragauskas, *ChemSusChem*, 2015, **8**, 275–279.

306 A. R. Martin, M. A. Martins, O. R. R. F. Da Silva and L. H. C. Mattoso, *Thermochim Acta*, 2010, **506**, 14–19.

307 F. L. Zitzmann, E. Ward, X. Meng and A. S. Matharu, *Molecules*, 2021, **26**, 1-13.

308 K. Yuwawech, J. Wootthikanokkhan and S. Tanpichai, *Mater Renew Sustain Energy*, 2018, **7**, 1-13.

309 R. Agrawal, N. Saxena, K. Sharma, S. Thomas and M. Sreekala, *Mater Sci Eng A*, 2000, **277**, 77-82.

310 K. K. Packiam, B. Murugesan, P. M. Kaliyannan Sundaramoorthy, H. Srinivasan and K. Dhanasekaran, *J Nat Fibers*, 2022, **19**, 7424–7435.

311 P. Senthamaraikannan, M. R. Sanjay, K. S. Bhat, N. H. Padmaraj and M. Jawaid, *Journal of Natural Fibers*, 2019, **16**, 1124–1131.

312 N. Quiévy, N. Jacquet, M. Sclavons, C. Deroanne, M. Paquot and J. Devaux, *Polym Degrad Stab*, 2010, **95**, 306–314.

313 S. Ang, V. Haritos and W. Batchelor, *Cellulose*, 2019, **26**, 4767–4786.

314 P. Jia, M. Zhang, C. Bo, L. Hu and Y. Zhou, *Pol J Chem Technol*, 2015, **17**, 29–33.

315 B. Liu, J. Zhang and H. Guo, *Membranes (Basel)*, 2022, **12**, 1-13.

316 R. J. Fong, A. Robertson, P. E. Mallon and R. L. Thompson, *Polymers (Basel)*, 2018, **10**, 1-15.

317 M. Mohsin, A. Hossin and Y. Haik, *J Appl Polym Sci*, 2011, **122**, 3102–3109.

318 P. Cazón, G. Velazquez and M. Vázquez, *Food Hydrocoll*, 2020, **99**, 1-12.

319 C. T. Chou, S. C. Shi, T. H. Chen and C. K. Chen, *Sci Prog*, 2023, **106**, 1-15.

320 B. Hararak, C. Winotapun, J. Inyai, P. Wannid and C. Prahsarn, *J Nanoparticle Res*, 2021, **23**, 1-15.

321 X. He, F. Luzi, X. Hao, W. Yang, L. Torre, Z. Xiao, Y. Xie and D. Puglia, *Int J Biol Macromol*, 2019, **127**, 665–676.

322 W. Yang, X. He, F. Luzi, W. Dong, T. Zheng, J. M. Kenny, D. Puglia and P. Ma, *Int J Biol Macromol*, 2020, **161**, 617–626.

323 X. Z. Yuan, C. Nayoze-Coynel, N. Shaigan, D. Fisher, N. Zhao, N. Zamel, P. Gazdzicki, M. Ulsh, K. A. Friedrich, F. Girard and U. Groos, *J Power Sources*, 2021, **491**, 1-9.

324 M. Rouhi, S. H. Razavi and S. M. Mousavi, *Materials Science and Engineering C*, 2017, **71**, 1052–1063.

325 Mahadevaiah, L. R. Shivakumara, T. Demappa and S. Vasudev, *J Food Process Preserv*, 2017, **41**, 1-10.

326 M. Wang, X. Miao, H. Li and C. Chen, *Polymers (Basel)*, 2021, **14**, 1-16.

327 M. Imran, A. M. Revol-Junelles, N. René, M. Jamshidian, M. J. Akhtar, E. Arab-Tehrany, M. Jacquot and S. Desobry, *Food Hydrocoll*, 2012, **29**, 407–419.

328 E. M. Abdel Bary, Y. A. Soliman, A. Fekri and A. N. Harmal, *Int J Environ Stud*, 2018, **75**, 750–762.

329 H. Yano, J. Sugiyama, A. N. Nakagaito, M. Nogi, T. Matsuura, M. Hikita and K. Handa, *Adv Mater*, 2005, **17**, 153–155.

330 S. Virtanen, J. Vartianen, H. Setälä, T. Tammelin and S. Vuoti, *RSC Adv*, 2014, **4**, 11343–11350.

331 Y. Long, L. Xiao and Q. Cao, *Powder Technol*, 2017, **310**, 24–34.

332 Y. Huang and A. A. Keller, *Water Res*, 2015, **80**, 159–168.

333 W. Yang, G. Qi, J. M. Kenny, D. Puglia and P. Ma, *Polymers (Basel)*, 2020, **1364**, 1-15.

334 H. Chen, R. Li, X. Xu, P. Zhao, D. S. H. Wong, X. Chen, S. Chen and X. Yan, *J Mater Sci*, 2019, **54**, 1236–1247.

335 J. A. Sirviö, M. Visanko, J. P. Heiskanen and H. Liimatainen, *J Mater Chem A Mater*, 2016, **4**, 6368–6375.